AN ABSTRACT OF THE DISSERTATION OF

Jeremy D. Shakun for the degree of Doctor of Philosophy in Geology presented on May 21, 2010.

Title: Analyzing Large Paleoclimate Datasets: Implications for Past and Future Climate Change.

Abstract approved: _____

Peter U. Clark

This dissertation presents the results of statistical analyses of large climate datasets from two time intervals – the 20th century instrumental record and the proxy record of the last deglaciation – in order to understand the forcings and mechanisms of past climate variability.

A longstanding question in climate dynamics concerns the origin of Pacific decadal variability (PDV). This issue is addressed by calculating the Southern Hemisphere equivalent of the Pacific Decadal Oscillation (PDO) index from Pacific sea surface temperature (SST) anomalies over the 20th century, which is found to be similar to its Northern Hemisphere counterpart. The Northern and Southern PDO indices both exhibit pronounced seasonality in autocorrelation with interannual persistence of winter SST anomalies despite their absence during the intervening summer, suggesting a role for reemergence. These two indices can be reasonably well reproduced using a first-order autoregressive model forced by the El Niño-Southern Oscillation, suggesting that Pacific decadal variability on both sides of the equator may largely be a reddened response to tropical forcing.

Over 100 high-resolution proxy climate time series spanning parts or all of the Last Glacial Maximum (LGM) to Holocene interval are analyzed to characterize spatiotemporal patterns of glacial-interglacial climate change. Peak glacial and

interglacial conditions occurred statistically synchronously between the Northern (22.1 ± 4.3 ka and 8.0 ± 3.2 ka) and Southern (22.3 ± 3.6 ka and 7.4 ± 3.7 ka) Hemispheres, suggesting that the hemispheres were synchronized by greenhouse gases, local insolation, and/or ocean circulation. Global cooling during the LGM was likely ≥4.9°C, but only ~0.6°C during the Younger Dryas. Younger Dryas climate anomalies exhibit a general hemispheric seesaw pattern with the largest negative anomalies in the high northern latitudes, mixed sign anomalies in the low latitudes, and modest positive anomalies in the high southern latitudes, consistent with an ocean circulation driver of this event. Empirical Orthogonal Function analysis of 71 records from 19-11 ka indicates that 72% of deglacial climate variability can be explained by two modes. The first mode (61% of the variance) shows a globally near-uniform signal and its associated principal component is strongly correlated with ice-core records of atmospheric CO_2. The second mode (11% of the variance) displays a more variable spatial pattern and its principal component parallels variations in Atlantic Meridional Overturning Circulation (AMOC) strength.

Averaging 77 calibrated proxy temperature records over the last deglaciation indicates that global mean temperature was highly correlated and varied nearly in phase with the rise in CO_2, which differs from ice-core studies suggesting Antarctic temperature led CO_2. This result thus suggests a primary role for CO_2 in driving deglacial warming and the global deglaciation. Northern and Southern Hemisphere mean temperature time series both bear the imprint of CO_2 forcing, but differ largely in response to the millennial-scale seesawing of heat between the hemispheres related to AMOC variability. An analysis of deglacial temperature variability by latitude indicates that deglacial warming began near-synchronously throughout the Southern Hemisphere and tropics at ~19 ka and was coeval with abrupt cooling in the northern extratropics. These worldwide temperature changes may have been driven by a collapse of the AMOC related to the 19-kyr meltwater pulse. As this meltwater event has been tied to initial melting of Northern Hemisphere ice sheets in response to

boreal summer insolation forcing, a classic Milankovitch trigger is implicated for the last deglaciation.

ANALYZING LARGE PALEOCLIMATE DATASETS: IMPLICATIONS FOR PAST AND FUTURE CLIMATE CHANGE

by

Jeremy D. Shakun

A DISSERTATION

submitted to

Oregon State University

in partial fulfillment of
the requirements for the
degree of

Doctor of Philosophy

Presented May 21, 2010
Commencement June 2011

Doctor of Philosophy dissertation of Jeremy D. Shakun presented May 21, 2010.

APPROVED:

Major Professor, representing Geology

Chair of the Department of Geosciences

Dean of the Graduate School

I understand that my dissertation will become part of the permanent collection of Oregon State University libraries. My signature below authorizes release of my dissertation to any reader upon request.

Jeremy D. Shakun, Author

ACKNOWLEDGMENTS

First and foremost, I am greatly indebted to my advisor, Peter Clark. I came to Oregon State because I wanted to 'work on everything' related to climate (which is only a mild exaggeration). Peter provided me with not one, but several fascinating research projects, and critically, the intellectual freedom to pursue my interests as they developed. He has also been an absolutely dependable, loyal supporter in anything I have needed. I have worked in amazing field locations, laboratories, and with many world-class scientists, all due to Peter. Any ability I have developed to be an independent, creative scientist is in no small part attributable to Peter and the experience he has provided me with over the past several years.

My committee members – Ed Brook, Alan Mix, Steve Hostetler, and Jeff Shaman – have also been very helpful mentors, with regard to my dissertation as well as climate science at large. Each has provided me with different but complementary insights into what makes for a successful scientist. I particularly appreciate Jeff's interest and willingness to essentially take me on as a student of his own and develop a research project with me. I also benefited considerably from interaction with Nick Pisias – some of the most interesting results of my doctoral research came about simply by following in his footsteps. I thank Steve Sharrow for serving as my external committee member.

Andy Ross, June Padman, Andy Ungerer, and Hai Cheng all provided essential assistance in the lab and were a pleasure to work with.

I was fortunate enough to start my Ph.D. at the same time as Shaun Marcott, and so had someone in the trenches with me through all the ups and downs of the doctoral process. I have learned a great deal about both science and life from Shaun, more than I knew there was to know about either, and have thoroughly enjoyed his friendship. A whole other cast of characters enriched my experience both inside and outside of Wilkinson including Barbara Burkholder, Mo Davies, Bre Craig, Summer Praetorius, Thomas Bauska, Jon Hornung, Elina Lin, Anders Carlson, Faron Anslow, Lica Ersek, Brent Goehring, and Jay Alder.

I owe my family for instilling in me the values of science – a love of thinking analytically and independently and arguing for hours on end. My parents have been endlessly supportive of everything I have ever done and have given me every advantage available – my successes are theirs.

CONTRIBUTION OF AUTHORS

Jeff Shaman oversaw every phase of the work presented in Chapter 2 and provided considerable guidance during the research and writing process. Anders Carlson aided in the experimental design, interpretation, presentation, and writing of the results presented in Chapter 3. Peter Clark collected many of the proxy records utilized in Chapter 4 and provided helpful input during the interpretation of the results.

TABLE OF CONTENTS

TABLE OF CONTENTS (continued)

Page

TABLE OF CONTENTS (continued)

Page

LIST OF FIGURES

LIST OF FIGURES (Continued)

LIST OF TABLES

For my folks, of course

Analyzing Large Paleoclimate Datasets: Implications for Past and Future Climate Change

Chapter 1

Introduction

1.1 Context

The paleoclimate record informs our understanding of future climate change associated with anthropogenic forcings in at least two critical ways: 1) it can reveal the dynamics of internal climate variability upon which anthropogenic warming will be superimposed, and 2) it shows how the climate system responded to past forcings, providing insight into climate sensitivity. This dissertation addresses both of these issues through statistical analyses of large datasets from two time intervals – the 20th century instrumental record and the proxy record of the last deglaciation. A recurrent theme in this work is determining spatial and temporal patterns of climate variability in order to elucidate the underlying physical mechanisms.

1.2 Motivating Questions and Approaches

1.2.1 Chapter 2: Tropical origins of North and South Pacific decadal variability

The Pacific Decadal Oscillation (PDO) is defined as the leading mode of sea surface temperature variability in the North Pacific (Mantua et al., 1997). As its name suggests, the PDO is dominated by decadal-scale variability and exerts an important control on North American climate and ecosystems (Mantua et al., 1997) and possibly the interdecadal structure of the global mean temperature record as well (Swanson and Tsonis, 2009). A long-standing question concerns the origin of the PDO: is it an independent climate mode driven by low frequency processes in the North Pacific or instead a reddened response to interannual climate variability initiated elsewhere, such as the El Niño-Southern Oscillation (ENSO) in the tropical Pacific? This question is addressed by calculating the South Pacific-equivalent of the PDO index over the 20th

century and statistically evaluating its relationship to its North Pacific counterpart as well as ENSO.

1.2.2 Chapter 3: A global perspective on Last Glacial Maximum to Holocene Climate Change

While many forcings potentially responsible for climate change during the last glacial-interglacial transition have been identified – e.g., insolation, greenhouse gases, ice sheets, freshwater, etc. – the relative role and expression of each remains to be satisfactorily parsed out (e.g., Alley and Clark, 1999; Liu et al., 2009). For example, the abrupt climate changes of the last deglaciation, such as the Younger Dryas, have been variously attributed to changes in ocean circulation (Broecker and Denton, 1985; Clark et al., 2002), the mean state of the tropical coupled ocean-atmosphere system (e.g., ENSO) (Clement et al., 2001; Broecker, 2003), and most recently, a bolide impact (Firestone, 2007). A large number of proxy records spanning this time interval have been developed over the past decade or so, which may permit evaluation of these various hypotheses. Here, 104 paleoclimate records covering parts or all of the Last Glacial Maximum to Holocene interval are synthesized to address several questions. When were peak glacial and interglacial conditions reached in the polar hemispheres? What was the magnitude and spatial pattern of climate anomalies during the Last Glacial Maximum and the Younger Dryas, and how do they compare? What were the most common spatiotemporal modes of climate variability during the last deglaciation, and what forcing mechanisms, if any, do they reflect?

1.2.3 Chapter 4: The role of CO_2 during the last deglaciation

Following on the results in Chapter 3, 77 calibrated, proxy temperature records spanning the last deglaciation (19-6.5 ka) are synthesized and averaged to determine how temperature varied globally and among various regions over this interval. This work explores the following questions. How important were greenhouse gases in driving global warming during the last deglaciation? What was the phasing of global

temperature and atmospheric CO_2 during this time? Did AMOC variations produce massive redistributions of heat between the hemispheres? And lastly, can spatiotemporal patterns of temperature variability be used to decipher the trigger of global deglaciation?

1.3 Current Publication Status

As of this writing, Chapters 2 has been published in *Geophysical Research Letters*, Chapter 3 has been published in *Quaternary Science Reviews*, and Chapter 4 is in preparation for submission to *Science*.

1.4 References

Alley, R. B., and Clark, P. U. 1999. The deglaciation of the northern hemisphere: A global perspective. Annual Reviews of Earth and Planetary Sciences, 27**,** 149-182.

Broecker, W. S. 2003. Does the trigger for abrupt climate change reside in the ocean or in the atmosphere? Science, 300**,** 1519-1522.

Clement, A. C., Cane, M. A., and Seager, R. 2001. An orbitally driven tropical source for abrupt climate change. Journal of Climate, 14**,** 2369-2375.

Firestone, R. B., West, A., Kennett, J. P., Becker, L., Bunch, T. E., Revay, Z. S., Schultz, P. H., Belgya, T., Kennett, D. J., Erlandson, J. M., Dickenson, O. J., Goodyear, A. C., Harris, R. S., Howard, G. A., Kloosterman, J. B., Lechler, P., Mayewski, P. A., Montgomery, J., Poreda, R., Darrah, T., Que Hee, S. S., Smith, A. R., Stich, A., Topping, W., Wittke, J. H., and Wolbach, W. S. 2007. Evidence for an extraterrestrial impact 12,900 years ago that contributed to the megafaunal extinctions and the Younger Dryas cooling. Proceedings of the National Academy of Sciences, 104, 16016-16021.

Liu, Z., Otto-Bliesner, B., He, F., Brady, E., Thomas, R., Clark, P.U., Carlson, A.E., Lynch-Stieglitz, J., Curry, W., Brook, E., Erickson, D., Jacob, R., Kutzbach, J., and Chen, J. 2009. Transient Climate Simulation of Last Deglaciation with a New Mechanism for Bølling-Allerød Warming. Science, 325, 310-314.

Mantua, N. J., Hare, S. R., Zhang, Y., Wallace, J. M., and Francis, R. 1997. A Pacific interdecadal climate oscillations with impacts on salmon production. Bulletin of the American Meteorological Society, 78, 1069-1079.

Swanson, K. L., and Tsonis, A. A. 2009. Has the climate recently shifted? Geophysical Research Letters, 36, doi:10.1029/2008GL037022.

Chapter 2

Tropical origins of North and South Pacific variability

Jeremy D. Shakun[1] and Jeffrey Shaman[2]

[1]Department of Geosciences, Oregon State University
Corvallis, OR 97331

[2]College of Oceanic and Atmospheric Sciences, Oregon State University
Corvallis, OR 97331

Geophysical Research Letters, 36, L19711, doi:10.1029/2009GL040313, 2009

2.1 Abstract

The origin of the Pacific Decadal Oscillation (PDO), the leading mode of sea surface temperature variability for the North Pacific, is a matter of considerable debate. One paradigm views the PDO as an independent mode centered in the North Pacific, while another regards it as a largely reddened response to El Niño-Southern Oscillation (ENSO) forcing from the tropics. We calculate the Southern Hemisphere equivalent of the PDO index based on the leading mode of sea surface temperature variability for the South Pacific and find that it adequately explains the spatial structure of the PDO in the North Pacific. A first-order autoregressive model forced by ENSO is used to reproduce the observed PDO indices in the North and South Pacific. These results highlight the strong similarity in Pacific decadal variability on either side of the equator and suggest it may best be viewed as a reddened response to ENSO.

2.2 Introduction and Approach

The origin of Pacific decadal variability (PDV) remains an outstanding question in climate dynamics. This issue has received considerable attention over the past 15 years and numerous hypotheses have been advanced concerning the mechanisms responsible for generating PDV. These hypotheses lie along a spectrum based on the geographic region held accountable for driving PDV. At one end of the spectrum emphasis is placed on the tropical Pacific, on the other the extratropical North Pacific is seen as the driver, and in between tropical-extratropical interactions are called upon. In reality, these hypotheses should be seen as representing a continuum of possibilities, with perhaps several processes in play.

Much evidence favors a tropical source for PDV. Newman et al. (2003) developed a simple statistical model to show that North Pacific decadal variability can be well represented as a reddened response to the El Niño-Southern Oscillation (ENSO). Deser et al. (2004) showed that the North Pacific Index (NPI; a measure of the strength of the Aleutian Low) was coherent with numerous climate variables in the

tropical Indo-Pacific on decadal timescales over the 20th century. Kidson and Renwick (2002) found that large scale South Pacific SST variability from 1981-1999 is almost entirely related to ENSO and coherent extratropical modes do not appear to be significant. Observations and modeling indicate that El Niño anomalies can persist for over a decade in the extratropical ocean as they propagate westward as Rossby waves (Jacobs et al., 1994). The regime shift in 1976/77 from a negative to a positive phase of PDV was concurrent with a deepening of the eastern tropical Pacific thermocline recorded in Galapagos corals (Guilderson and Schrag, 1997), while modeling suggests this thermocline shift can be explained solely by equatorial wind forcing and does not require a link to the extratropics (Karspeck and Cane, 2002).

At the same time, there is notable support for a North Pacific driver of PDV, particularly from modeling. One hypothesis is that ocean-atmosphere coupling involving the subtropical gyre and the Aleutian Low gives rise to a decadal oscillation in the North Pacific, with the timescale of the oscillation set by the spin-up time of the gyre (Latif and Barnett, 1994; White and Cayan, 1998; Barnett et al., 1999). In essence, the meridional gradient of SST is amplified by atmospheric feedbacks, but as SST anomalies propagate around the gyre, wind stress curl anomalies reverse and the opposite phase of the oscillation is reached. Also, observations indicate that North Pacific wintertime ocean-atmosphere variability may be largely independent of ENSO on both interannual and interdecadal timescales (Zhang et al., 1996). While these results suggest North Pacific decadal variability is not driven from the tropics, several studies argue that the North Pacific instead modulates ENSO variability. For example, the seasonal footprinting mechanism posits that North Pacific SST anomalies generated by winter atmospheric variability can influence tropical and subtropical atmospheric circulation the following summer, including the zonal wind stress anomalies along the equator important for driving ENSO variability (Vimont et al., 2001; Vimont et al., 2003a; 2003b).

Tropical-extratropical interactions have also received considerable attention. A well-known example is the conceptual and numerical work of Gu and Philander

(1997), which modeled PDV as a self-sustaining oscillation involving exchanges between the tropical and extratropical oceans. In their model, a tropical warming, for example, strengthens the mid-latitude westerlies causing cooling there. An extratropical cold SST anomaly then subducts in the subtropical gyre along isopycnals and upwells at the equator approximately a decade later reversing the phase of the oscillation. Zhang et al. (1998) suggested such a process triggered the 1976/77 climate shift. Schneider et al. (1999), on the other hand, found extratropical thermal anomalies do not propagate equatorward of 18°N.

In addition to this debate over the geographic origin of PDV, a related question concerns the nature of PDV itself. Some paradigms view PDV as a true oscillatory mode, while others suggest it manifests from the superposition of several quasi-independent processes acting at various spatial and temporal scales. Examples of an oscillator include those involving the isopycnal subduction mechanism of Gu and Philander (1997) as well as the delayed gyre-atmosphere coupling first proposed by Latif and Barnett (1994). In contrast, several statistical approaches have decomposed PDV into a number of distinct phenomena. Schneider and Cornuelle (2005) were able to reconstruct North Pacific decadal variability over the latter half of the 20th century using a first-order autoregressive model forced by ENSO, the NPI, and zonal advection anomalies in the Kuroshio-Oyashio extension (KOE) region. The contribution of these processes to PDV was found to be frequency dependent with subannual timescales dominated by the NPI, interannual timescales by the NPI and ENSO, and decadal timescales by all three. Newman (2007) arrived at a similar conclusion in reconstructing PDV from a multivariate empirical model, which suggested PDV arises from several red noise processes each with their own decay timescale and spatial pattern. Lastly, Vimont (2005) showed that the SST pattern of PDV can be recovered using only interannual information, specifically, three leading patterns of variability corresponding to ENSO precursors, peak ENSO conditions, and ENSO ‘leftovers’. He concluded, therefore, that PDV may simply represent the long-term average of ENSO cycle variations.

A fundamental characteristic of PDV is its spatial signature, which is often described as "ENSO-like" with sea surface temperature (SST) anomalies of one sign in the central to eastern tropical Pacific and along eastern boundaries surrounded by a horseshoe of oppositely signed anomalies extending into the central North and South Pacific from the western tropical Pacific (Zhang et al., 1997; Garreaud and Battisti, 1999). This interhemispheric symmetry and similarity to ENSO has been taken as evidence that PDV is driven from the tropics (Garreaud and Battisti, 1999; Linsley et al., 2000). However, while ENSO anomalies are largest in the tropics and rather narrowly confined about the equator, tropical anomalies associated with PDV are broader and similar in magnitude to those in the extratropics, particularly the North Pacific (Vimont, 2005). Thus, the North Pacific is often seen as the center of action. Accordingly, a commonly used metric of PDV is the Pacific Decadal Oscillation (PDO) index, which is the leading mode of SST variability in the North Pacific. More specifically, the PDO is defined as the leading principal component (PC) of residual monthly SST anomalies in the North Pacific poleward of 20°N after removing global mean SST anomalies. While the domain of the PDO and the term itself implicitly suggest PDV arises from an oscillation centered in the North Pacific, the pan-Pacific nature and apparent symmetry about the equator of PDV argue against this more regionalized perspective.

A simple approach is taken here to address the geographic extent of the PDO and quantify the interhemispheric symmetry of PDV. We calculate the Southern Hemisphere equivalent of the PDO index for 1901-2007 AD based on the leading PC of residual monthly SST anomalies in the South Pacific poleward of 20°S using the HadISST1 dataset (Rayner et al., 2003). This "Southern Hemisphere PDO" is strongly correlated with its Northern Hemisphere counterpart strengthening the case for tropically-driven PDV.

2.3 Results

The leading PCs of monthly SST anomalies in the North and South Pacific are shown in Figure 2.1. Both account for 23% of the variance in their respective domains. The timing of positive and negative phases in the PCs are broadly similar; indeed, the two time series are significantly correlated at r=0.38 ($p<0.0001$, using Student's t-test, the 1284 monthly data points, and a conservative estimate of 128 df). In addition, the prominent regime shifts in North Pacific PC1 (i.e, the PDO index) appear to generally have South Pacific counterparts, particularly those in 1976/77 and 1998/99. These leading PCs were low-pass filtered with a 7-year cutoff to remove interannual variability associated with ENSO that is almost certainly in common in the North and South Pacific (Karoly, 1989). This increases their correlation to r=0.59. One modest difference between the PCs worth noting is that North Pacific PC1 is somewhat redder than South Pacific PC1 and exhibits slightly greater variability at decadal periods. Schneider and Cornuelle (2005) found that decadal variability in the North Pacific was due in approximately equal part to ENSO, NPI, and KOE zonal advection anomalies. While ENSO also directly affects the South Pacific, the latter two phenomena are confined to the North Pacific, which may explain the weaker low frequency variability in the South Pacific.

Regressing basinwide monthly SST anomalies onto the leading PCs from the North and South Pacific produces fields with high pattern correlation (r=0.75) (Figure 2.2). The correlation within the PDO domain (i.e., poleward of 20°N) is r=0.83. Repeating this regression onto the low pass filtered PCs increases the basinwide spatial correlation to r=0.87 (Figure 2.2). These observations indicate the spatial structure of the PDO in the North Pacific can be well explained by the leading mode of variability for the South Pacific. This result is particularly striking in light of the various fundamental differences between the North and South Pacific, such as basin geometry, a much stronger western boundary current (Kuroshio-Oyashio) and an isolated subpolar low pressure center (Aleutian Low) in the North Pacific, a subtropical atmospheric convergence zone in the South Pacific, and the equatorial

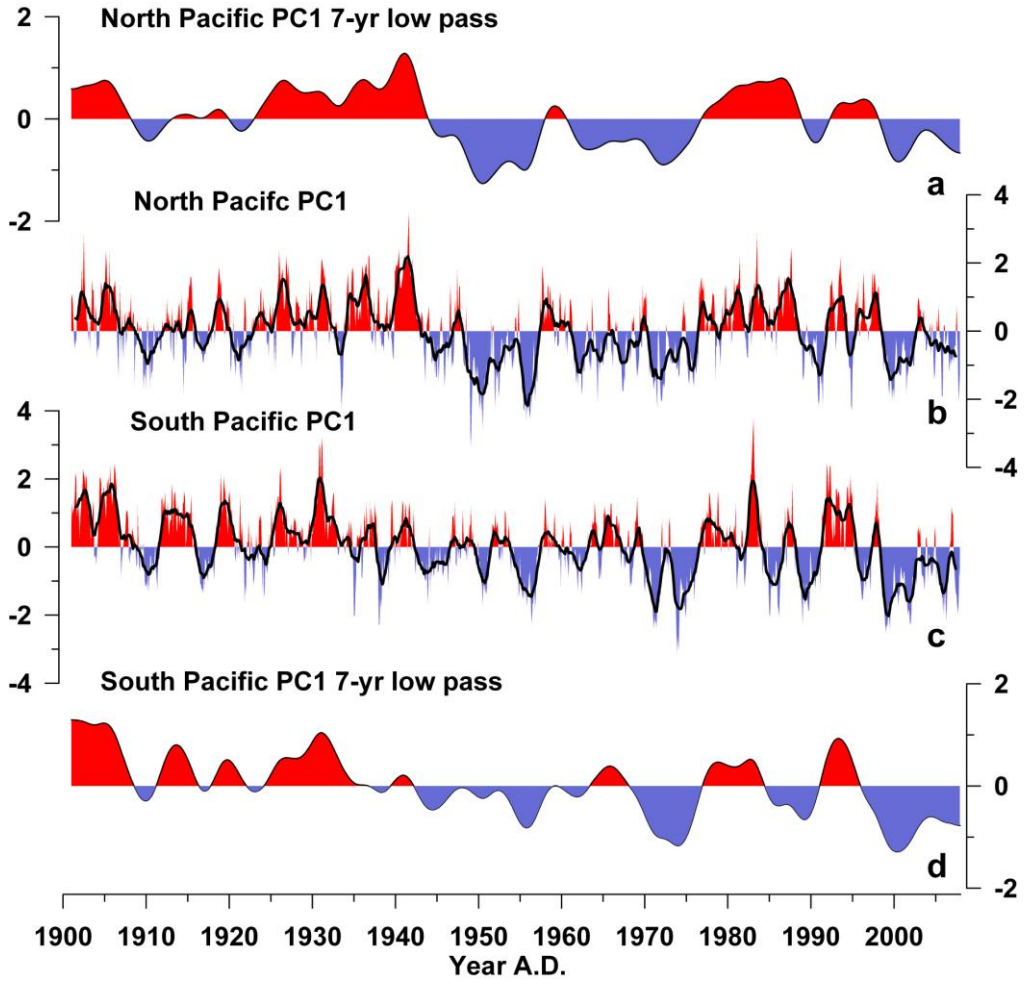

Figure 2.1: The leading PCs of (**b**) North and (**c**) South Pacific monthly SST anomalies, each poleward of 20° latitude. Both account for 23% of the variance in their respective domains. The time series have been standardized to unit variance. Also shown are the PCs after low pass filtering (**a** and **d**) with a 7 year cutoff to remove ENSO-band variability.

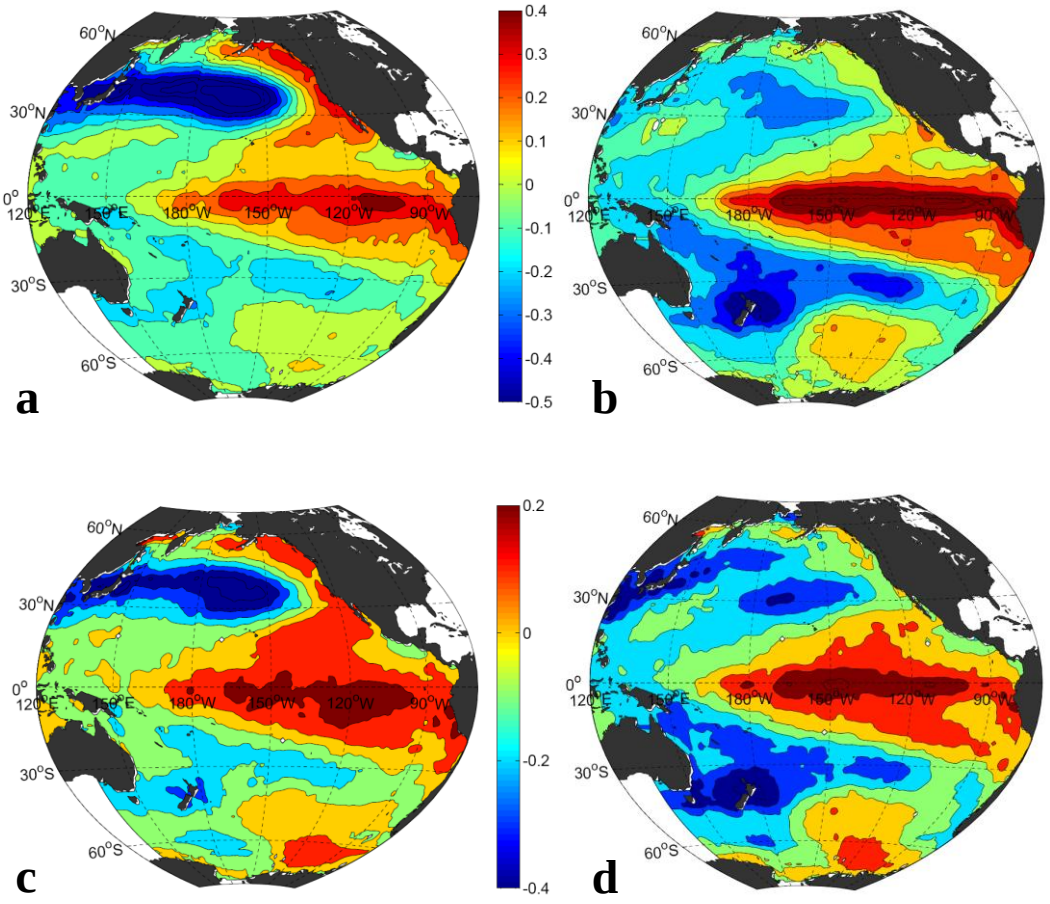

Figure 2.2: Basin-wide monthly SST anomalies regressed onto PC1 for the (**a**) North and (**b**) South Pacific. Regression parameters have been standardized such that they show the °C change per standard deviation of the PC. SST regressions onto the low pass filtered (**c**) North and (**d**) South Pacific are also shown. Contour intervals are 0.1°C.

asymmetry of ENSO SST anomalies in the eastern tropical Pacific. We also explored whether the reduced space optimal interpolation used to create the HadISST1 dataset may have corrupted this finding of interhemispheric symmetry, but found this unlikely (see Appendix A). It thus appears PDV is very similar on both sides of the equator implicating the tropics as the common forcing.

Plots of monthly lag autocorrelation for the North and South Pacific PC1s reveal an interesting similarity. In both cases, the annual cycle of lag autocorrelation exhibits considerable seasonality with maximum autocorrelation in the winter and minimum autocorrelation in the summer of each respective hemisphere (Figure 2.3). This reflects the interannual persistence of winter SST anomalies despite the lack of a relationship between SST anomalies from one summer to the next. This phenomenon has received considerable attention in the North Pacific and has been theorized to be a product of the reemergence mechanism in which winter SST anomalies are sequestered beneath a thin summer mixed layer only to reemerge the following winter as mixing increases and the mixed layer thickens (Alexander et al., 1999; Deser et al., 2003).

Based on the two observations made above, namely that tropical forcing and reemergence both appear to play important roles in Pacific SST variability, we model PDV as a first-order autoregressive process driven by ENSO as done by Newman et al. (2003). This AR-1 model is applied to the North and South Pacific separately.

$$PDO_n = \alpha PDO_{n-1} + \beta ENSO_n + \eta_n$$

The modeled PDO index at year *n* is a function of the modeled PDO index at *n-1* and the observed ENSO index (Niño 3.4) at *n*. These annually-averaged indices are centered on boreal winter (Jul-Jun) for the North Pacific and austral winter (Jan-Dec) for the South Pacific. Per Newman et al. (2003), the coefficients β and α are parameters derived, respectively, by regression of the PDO index on the ENSO index, then autoregression of the residual time series with a lag of one year. η is an

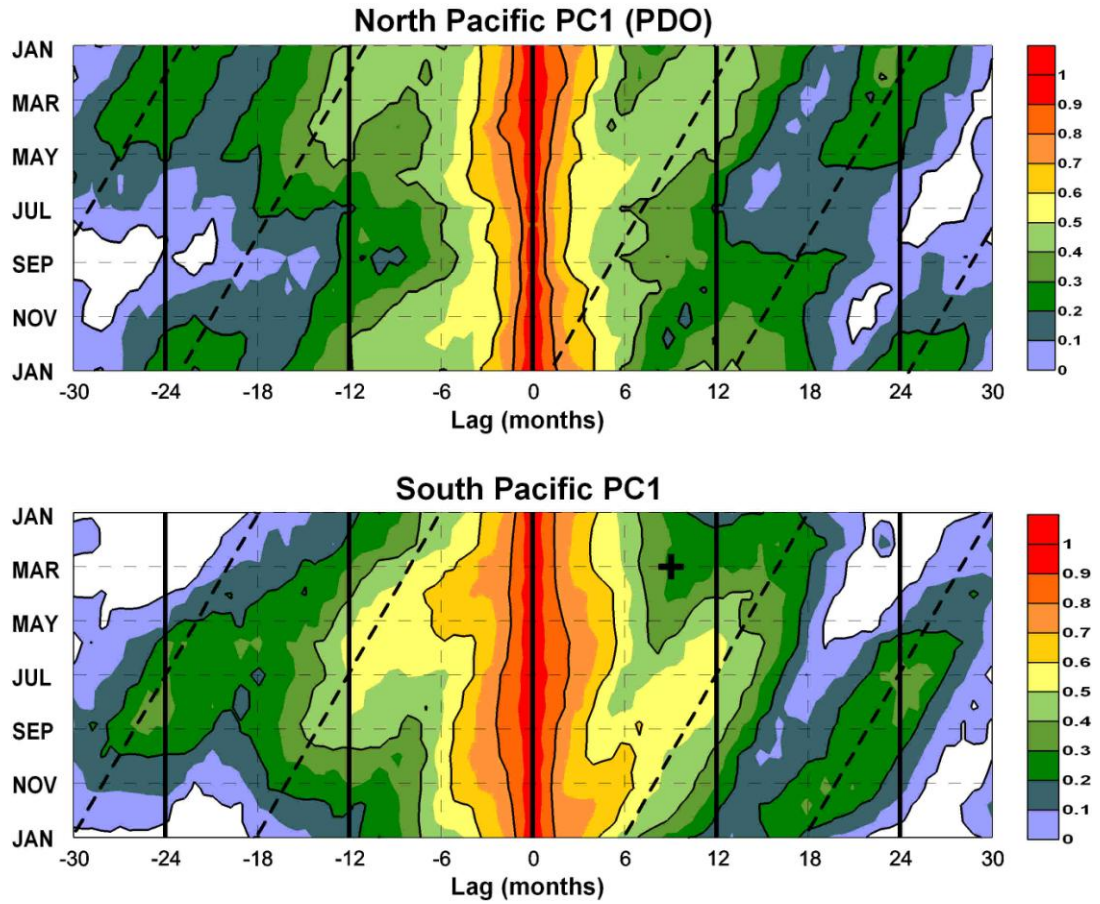

Figure 2.3: Plots of monthly lag autocorrelation for (**top**) North and (**bottom**) South Pacific PC1. Lag in months is given on the abscissa and month of the year is given on the ordinate. Correlations are represented by the color bar on the right and are contoured in intervals of 0.2. Lags of 0, 1, and 2 years are demarcated by the vertical black bars. The diagonal dashed lines highlight the seasonal cycle of lag autocorrelation, which is centered on February for North Pacific PC1 and July for South Pacific PC1. The black cross shows the correlation between South Pacific PC1 during March and the following December, as an example.

uncorrelated noise term not used in our analysis but shown for completeness. α and β are 0.51 and 0.56 for North Pacific PC1 and 0.62 and 0.71 for South Pacific PC1. While Newman et al. (2003) found this simple model did a remarkable job reproducing the observed 20th century PDO index in the North Pacific (r=0.63 in our study), it yields an even stronger fit to our Southern Hemisphere PDO index (r=0.71) (Figure 2.4). The greater success of the model in the South Pacific may be a function of its larger α and β terms, which indicate that the persistence of SST anomalies and ENSO forcing are more important. The stronger ENSO signal in the South Pacific may derive from the equatorial asymmetry of ENSO SST anomalies in the eastern tropical Pacific, which extend considerably further to the south than north. One implication of this finding is that the South Pacific may be a better place to develop paleo-ENSO records as it appears to contain a 'cleaner' ENSO signal.

2.4 Conclusions

Deriving a Southern Hemisphere equivalent of the PDO index shows that the spatial signature of the PDO can be well explained by the leading mode of SST variability for the South Pacific. Thus, PDV appears to be a basin-wide phenomenon most likely driven from the tropics. Moreover, while it was already known PDV north of the equator could be adequately modeled as a reddened response to ENSO, our results indicate this is true to an even greater extent in the South Pacific.

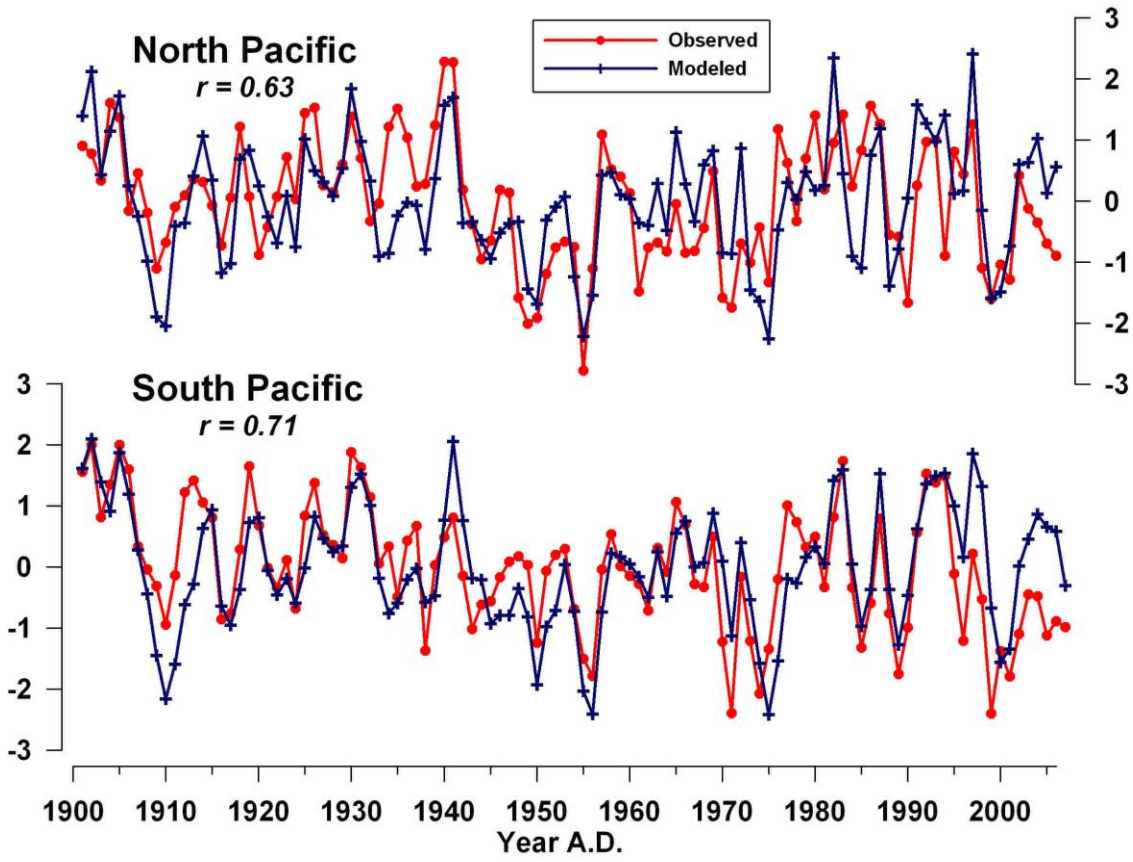

Figure 2.4: Observed (red) and modeled (blue) PC1s for the (top) North and (bottom) South Pacific. The model is of an AR-1 process forced by ENSO; see text for more details.

2.5 Acknowledgments

J. D. S. is funded by the NSF Paleoclimate Program. We would like to thank D. Battisti and A. Kaplan for helpful input. Two anonymous reviewers provided insightful comments.

2.6 References

Alexander, M. A., Deser, C. and Timlin, M. S. 1999. The reemergence of SST anomalies in the North Pacific Ocean. Journal of Climate, 12, 2419-2433.

Barnett, T. P., Pierce, D. W., Saravanan, R., Schneider, N., Dommenget, D. and Latif, M. 1999. Origins of the midlatitude Pacific decadal variability. Geophysical Research Letters, 26, 1453-1456.

Deser, C., Alexander, M.A. and Timlin, M. S. 2003. Understanding the persistence of sea surface temperature anomalies in midlatitudes. Journal of Climate, 16, 57-72.

Deser, C., Phillips, A. S. and Hurrell, J. W. 2004. Pacific interdecadal climate variability: Linkages between the Tropics and the North Pacific during boreal winter since 1900. Journal of Climate, 17, 3109-3124.

Garreaud, R. D. Battisti, D. S. 1999. Interannual (ENSO) and interdecadal (ENSO-like) variability in the Southern Hemisphere tropospheric circulation. Journal of Climate, 12, 2113-2123,

Gu, D., and Philander, S. G. H. 1997. Interdecadal climate fluctuations that depend on exchanges between the tropics and the extratropics. Science, 275, 805-807.

Guilderson, T., and Schrag, D. 1998. Abrupt shift in subsurface temperatures in the tropical Pacific associated with changes in El Niño. Science, 281, 240-243.

Jacobs, G. A., Hurlburt, H. E., Kindle, J. C., Metzger, E. J., Mitchell, J. L., Teague, W. J., and Wallcraft, A. J. 1994. Decade-scale trans-Pacific propagation and warming effects of an El Niño anomaly. Nature, 370, 360-363.

Karoly, D. J. 1989. Southern Hemisphere circulation features associated with El Niño-Southern Oscillation events. Journal of Climate, 2, 1239-1252.

Karspeck, A. R., and Cane, M. A. 2002. Tropical Pacific 1976-77 climate shift in a linear, wind-driven model. Journal of Physical Oceanography, 32, 2350-2360.

Kidson, J. W., and Renwick, J. A. 2002. The Southern Hemisphere evolution of ENSO during 1981-99. Journal of Climate, 15, 847-863.

Latif, M., and Barnett, T. P. 1994. Causes of decadal climate variability over the North Pacific and North America. Science, 266, 634-637.

Linsley, B. K., Wellington, G. M., and Schrag, D. P. 2000. Decadal sea surface temperature variability in the subtropical South Pacific from 1726-1997 A.D. Science, 290, 1145-1148.

Mantua, N. J., Hare, S. R., Zhang, Y., Wallace, J. M., and Francis, R. 1997. A Pacific interdecadal climate oscillations with impacts on salmon production. Bulletin of the American Meteorological Society, 78, 1069-1079.

Newman, M., Compo, G. P., and Alexander, M. A. 2003. ENSO-forced variability of the Pacific Decadal Oscillation. Journal of Climate, 16, 3853-3857.

Newman, M. 2007. Interannual to decadal predictability of tropical and North Pacific sea surface temperatures. Journal of Climate, 20, doi:10.1175/JCLI14165.1.

Rayner, N. A., Parker, D. E., Horton, E. B., Folland, C. K., Alexander, L. V., Rowell, D. P., Kent, E. C., and Kaplan, A. 2003. Global analyses of sea surface temperature, sea ice, and night marine air temperature since the late nineteenth century. Journal of Geophysical Research, 108, 4407, doi:10.1029/2002JD002670.

Rayner, N. A., Brohan, P., Parker, D. E., Folland, C. K., Kennedy, J. J., Vanicek, M., Ansell, T. J., and Tett, S. F. B. 2006. Improved analyses of changes and uncertainties in sea surface temperature measured in situ since the mid-nineteenth century: the HadSST2 dataset. Journal of Climate, 19, 446-469.

Schneider, N., and Cornuelle, B. D. 2005. The forcing of the Pacific Decadal Oscillation. Journal of Climate, 21, 4355-4373.

Schneider, N., Miller, A., Alexander, M., Deser, C., and Latif, M. 1999. Subduction of decadal North Pacific temperature anomalies: Observations and dynamics. Journal of Physical Oceanography, 29, 1056-1070.

Vimont, D. J. 2005. The contribution of the interannual ENSO cycle to the spatial pattern of decadal ENSO-like variability. Journal of Climate, 18, 2080-2092.

Vimont, D. J., Battisti, D. S., and Hirst, A. C. 2001. Footprinting: A seasonal connection between the Tropics and mid-latitudes. Geophysical Research Letters, 28, 3923-3926.

Vimont, D. J., Battisti, D. S., and Hirst, A. C. 2003a. The seasonal footprinting mechanism in the CSIRO general circulation models. Journal of Climate, 16, 2653-2667.

Vimont, D. J., Wallace, J. M., and Battisti, D. S. 2003b. The seasonal footprinting mechanism in the Pacific: Implications for ENSO. Journal of Climate, 16, 2668-2675.

White, W. B., and Cayan, D. R. 1998. Quasi-periodicity and global symmetries in interdecadal upper ocean temperature variaibility. Journal of Geophysical Research, 103, 21335-21354.

Zhang, R., Rothstein, L., and Busalacchi, A. 1998. Origin of upper-ocean warming and El Niño changes on decadal scales in the tropical Pacific Ocean. Nature, 391, 879-883.

Zhang, Y., Wallace, J., and Iwasaka, N. 1996. Is climate variability over the North Pacific a linear response to ENSO?. Journal of Climate, 9, 1468-1478.

Zhang, Y., Wallace, J., and Battisti, D. 1997. ENSO-like decade-to-century scale variability: 1900-93. Journal of Climate, 10, 1004-1020.

Chapter 3

A Global Perspective on Last Glacial Maximum to Holocene Climate Change

Jeremy D. Shakun[1] and Anders E. Carlson[2]

[1]Department of Geosciences, Oregon State University
Corvallis, OR 97331

[2]Department of Geology & Geophysics, University of Wisconsin
Madison, WI 53706

Quaternary Science Reviews, 29, 1801-1816, 2010

3.1 Abstract

While the abrupt climate events of the last deglaciation are well defined in ice core records from the polar regions of both hemispheres, their manifestation elsewhere is less well constrained. Here we compile 104 high-resolution paleoclimate records to characterize the timing and spatial pattern of climate change during the last deglaciation. This compilation indicates relatively concurrent timing of the Last Glacial Maximum (LGM; peak glacial conditions) and the Altithermal (peak interglacial conditions) in the Northern (22.1 ± 4.3 ka and 8.0 ± 3.2 ka) and Southern (22.3 ± 3.6 ka and 7.4 ± 3.7 ka) Hemispheres, suggesting the hemispheres were synchronized by greenhouse gases, local insolation, and/or Northern Hemisphere induced ocean circulation changes. The magnitude of the glacial-interglacial temperature change increases with latitude, reflecting the polar amplification of climate change, with a likely minimum global mean cooling of ~4.9 °C during the LGM relative to the Altithermal.

Empirical orthogonal function (EOF) analysis of 71 records spanning 19-11 ka indicates that two modes explain 72% of deglacial climate variability. EOF1 (61% of variance) shows a globally near-uniform pattern, with its principal component (PC1) strongly correlated with changes in atmospheric CO_2. EOF2 (11% of variance) exhibits a bipolar seesaw pattern between the hemispheres, with its principal component (PC2) resembling changes in Atlantic meridional overturning circulation strength. EOF analysis of 90 records from 15-11 ka indicates that northern and southern modes of climate variability characterize the Younger Dryas-Bølling/Allerød interval. These modes dominate at the higher latitudes of each hemisphere and exhibit a complex interaction in the tropics. The magnitude of the Younger Dryas climate anomaly (cooler/drier) increases with latitude in the Northern Hemisphere, with an opposite pattern (warmer/wetter) in the Southern Hemisphere reflecting a general bipolar seesaw climate response. Global mean temperature decreased by ~0.6 °C during the Younger Dryas. Therefore, our analysis supports the paradigm that while the Younger Dryas was a period of global climate change, it was not a major global

cooling event but rather a manifestation of the bipolar seesaw driven by a reduction in Atlantic meridional overturning circulation strength.

3.2 Introduction

The development over the past decade of many higher resolution paleoclimate records spanning the last deglaciation provides an unprecedented perspective on orbital and millennial-scale climate changes during this time period (Clement and Peterson, 2008). Nevertheless, vast areas of the planet that may be integral players in any given climate event remain undersampled. Moreover, there is a danger in relying on a few records to characterize hemispheric to global climate change. This is particularly evident when attempting to determine the spatial response of the climate system to the millennial-scale events of the last deglaciation.

The most prominent deglacial events of the Northern Hemisphere are Heinrich Event 1 (H1, ~17.5-16 ka) and the associated Oldest Dryas cold period (~18-14.7 ka), the Bølling/Allerød warm period (~14.7-12.9 ka) and the Younger Dryas cold event (~12.9-11.7 ka) (Figure 3.1) (Alley and Clark, 1999). In the Southern Hemisphere, the most noted deglacial event is the Antarctic Cold Reversal, which was originally defined in Antarctic ice cores as cooling or cessation of deglacial warming ~15-13 ka (Figure 3.1) (Jouzel et al., 1995). Proxy records suggest a so-called bipolar seesaw response during this deglacial interval, with antiphased temperature anomalies in the two polar hemispheres (Alley and Clark, 1999; Blunier and Brook, 2001; Broecker, 1998; Clark et al., 2002). Concurrent changes in Atlantic meridional overturning circulation (AMOC) strength in response to North Atlantic surface freshening may have redistributed heat and thus caused this bipolar seesaw behavior (Boyle and Keigwin, 1987; Broecker, 1998; Carlson et al., 2007a; Clark et al., 2002; Liu et al., 2009; McManus et al., 2004; Robinson et al., 2005; Stouffer et al., 2006). In contrast, arguments for global cooling during the Younger Dryas and Oldest Dryas, predominately based on Southern Hemisphere valley glacier records, would imply an atmospheric forcing mechanism rather than variability in AMOC strength (Ariztegui

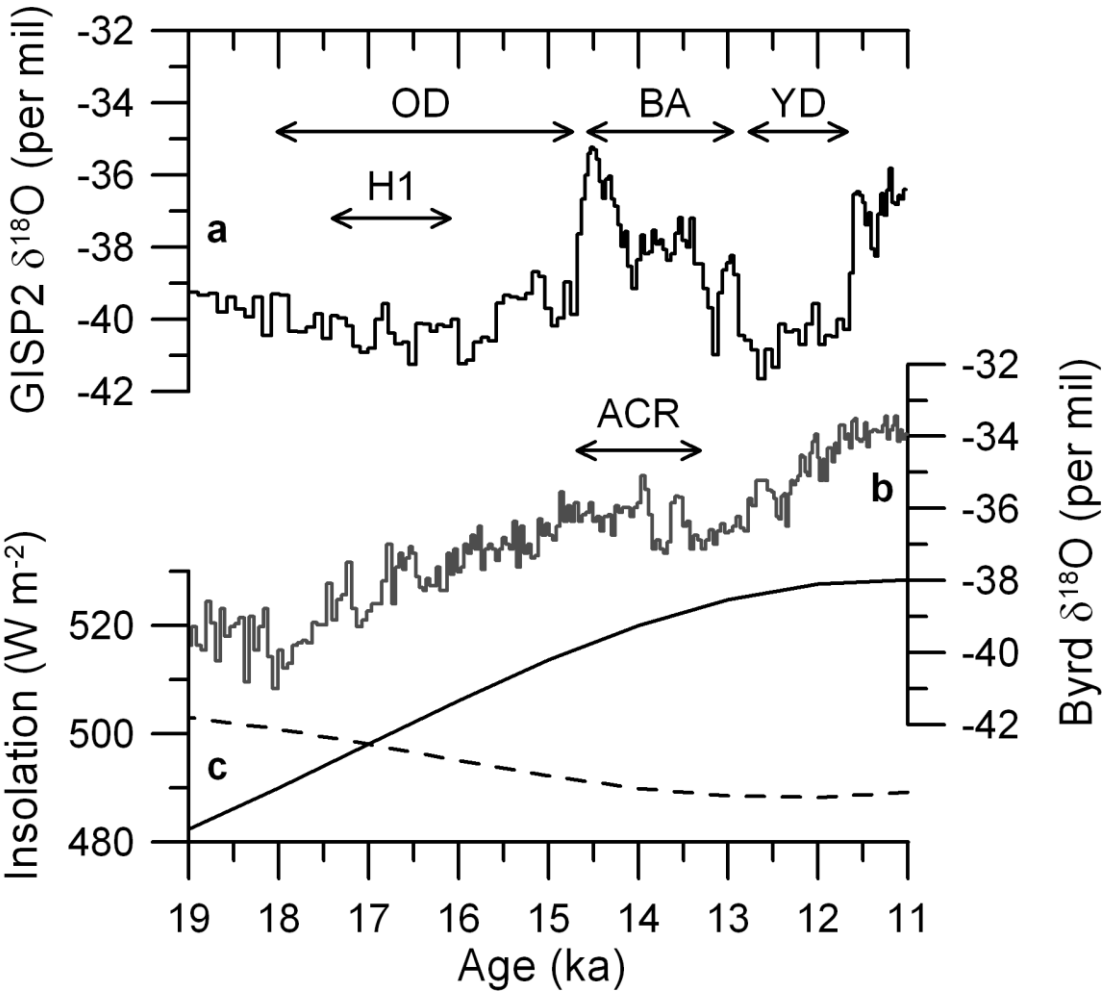

Figure 3.1: Deglacial ice core time series and insolation. (**a**) GISP2 $\delta^{18}O$ (black step plot) (Blunier and Brook, 2001). (**b**) Byrd $\delta^{18}O$ (grey step plot) (Blunier and Brook, 2001). (**c**) Insolation for 60 °N on June 21 (black line) and for 60 °S on December 21 (dashed black line) (Berger and Loutre, 1991). The timing of the Younger Dryas (YD), Bølling/Allerød (B/A), Heinrich Event 1 (H1), Oldest Dryas (OD) and Antarctic Cold Reversal (ACR) are denoted.

et al., 1997; Broecker, 2003; Denton and Hendy, 1994; Denton et al., 1999a; Huesser and Rabassa, 1987; Ivy-Ochs et al., 1999; Lowell et al., 1995; Moreno et al., 2001). These differing views on the impact of the Younger Dryas and Oldest Dryas thus imply profoundly different drivers of abrupt climate change (Clement and Peterson, 2008).

A more complete and accurate characterization of past climate events requires the integration of a large body of records, with sufficient resolution and dating control to adequately constrain the nature and behavior of different parts/regions of the climate system during an event. Here we compile 104 deglacial paleoclimate records to quantify the timing of the Last Glacial Maximum (LGM) and Holocene Altithermal, and perform time series analyses to identify patterns in deglacial climate variability, focusing on the Bølling/Allerød-Younger Dryas period. Our analyses indicate an interhemispheric synchronicity in the timing of the LGM and Altithermal. Similar to previous work with a smaller number of records (Clark et al., 2002), Empirical Orthogonal Function (EOF) analysis identifies two major modes of deglacial climate variability: a global pattern paralleling changes in atmospheric CO_2 concentration and a bipolar pattern resembling variations in AMOC strength. The Younger Dryas, as documented in 90 records, confirms this bipolar pattern with climate deterioration focused in northern high latitudes and climate amelioration in the Southern Hemisphere. We find that global cooling during the Younger Dryas was ~1/10 of LGM cooling.

3.3 Empirical Orthogonal Function Methodology

The database generated in this study is comprised of many of the highest-resolution and best-dated climate records currently available that cover the last 25 kyrs (Appendix B, Figure 3.2). We do not assign special consideration to the particular characteristics (e.g., geographic location, type of proxy, density of radiocarbon ages) of the climate records in forming the database, but rather simply attempt to include as many records as possible that are of sufficient temporal resolution to provide

meaningful information on deglacial climate changes. Figure 3.3 shows the resolution of the records; the median resolution is 130 years from 19-11 ka and 106 years from 15-11 ka. Approximately 80% of the records have resolutions higher than 250 years, corresponding to, for example, at least five datapoints during the Younger Dryas interval. The records are biased toward ocean margins due to the relative paucity of high-resolution time series from land as well as low sedimentation rates and carbonate dissolution in the deep ocean.

We use EOF analysis to compute objectively defined modes of variability from this database. EOF analysis identifies spatial-temporal patterns of variability in a dataset through a linear decomposition of the records into a series of independent basis functions (Mix et al., 1986a; 1986b). The EOFs are the eigenvectors of the temporal correlation matrix, which, as opposed to the covariance matrix, results in each dataset providing equal weight toward the EOFs. Such an approach is necessary because this database is comprised of many different proxies, which have different variances in their respective units and are thus not directly comparable.

Records were linearly interpolated to 100 yr resolution. Results are unaffected by factor-of-two changes in interpolated resolution. We find that the principal components (PCs) are relatively insensitive to the number of input records used through a jackknifing method in which 10, 20, 30,…90% of the records were randomly removed 100 times and the PCs recalculated. Monte Carlo simulations introducing random age model errors to the input records suggest the chronologies of the PCs are also relatively robust as these errors tend to be "averaged out" in the EOF analysis. Published chronologies were used for each record. Radiocarbon chronologies were calibrated when necessary. The chronologies were referenced to years before 1950 AD if the original author defined the "present" and left unchanged from the published version if not. Records were oriented so that "warm"/"wet" points upwards.

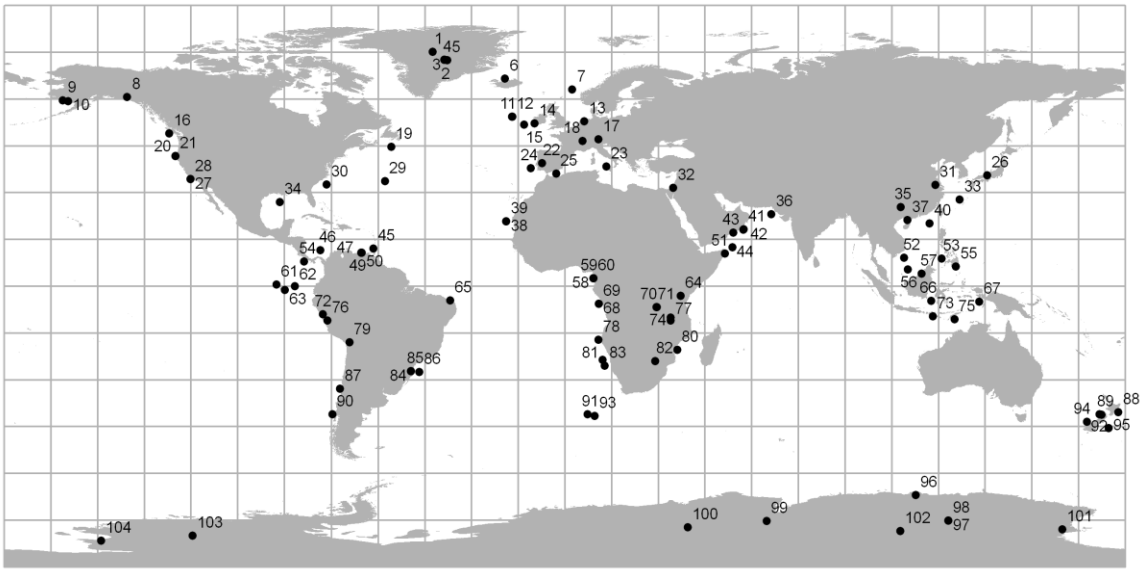

Figure 3.2: Map of the time series utilized in this chapter on a 15° grid. See Supplementary Data for specific time series locations and descriptions.

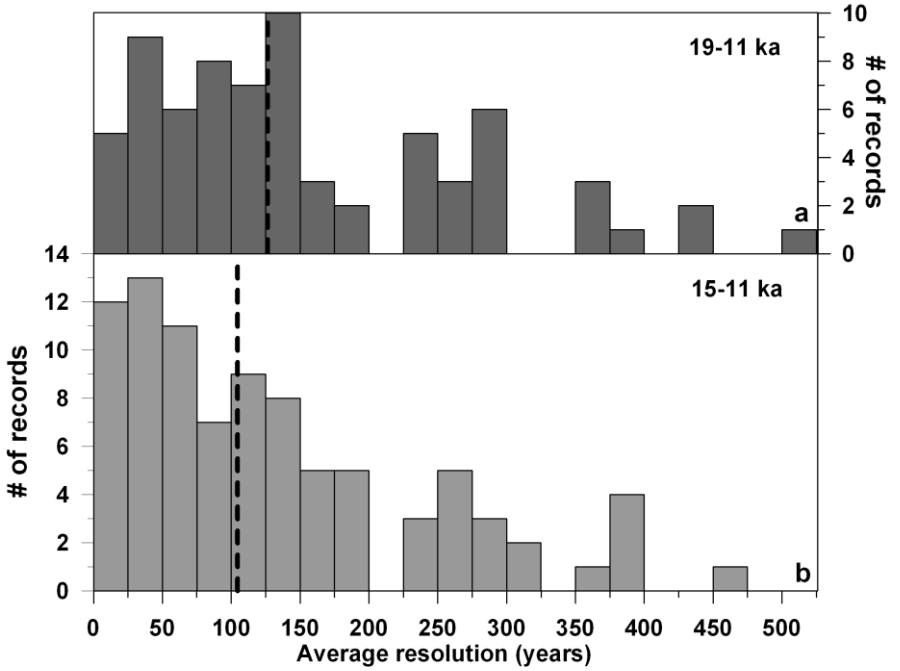

Figure 3.3: Histograms of the average resolution of the climate records used in this study over the intervals (**a**) 19-11 ka and (**b**) 15-11 ka. The vertical dashed lines show the median resolution of the records.

3.4 The Last Glacial-Interglacial Transition

3.4.1 Timing of the Last Glacial Maximum-Altithermal

We define the LGM (Altithermal) as the age of the lowest (highest) value in the 1 kyr running mean of the time series (Appendix B). A 1 kyr average was used in order to identify robust, persistent climate states and avoid anomalous outlying values. We use 56 records that cover at least 24-11 ka for the LGM and 78 records covering at least 10-2 ka for the Altithermal. Note that our use of existing terminology – 'LGM' and 'Altithermal' – for the most extreme climate periods is merely for convenience and not meant to imply our definition of these climate states is necessarily relevant to other definitions (e.g., maximum ice volume, sea-level lowstand, etc.).

There is considerable variation in the timing of these extreme climate states in different records with the LGM and Altithermal each spread over more than 10 kyr (Figure 3.4). Nevertheless, the timing of the LGM and Altithermal in the Northern (22.1 ± 4.3 ka, 8.0 ± 3.2 ka) and Southern (22.3 ± 3.6 ka, 7.4 ± 3.7 ka) Hemispheres is statistically indistinguishable and their mean ages differ by only a few centuries (Figure 3.4). Note that there is no latitudinal trend in the timing of the LGM (r^2=0.0036, p=0.66) or Altithermal (r^2=0.0085, p=0.43). These values are nearly unchanged when considering only the proxy temperature records.

3.4.2 Magnitude of the Glacial-Interglacial Temperature Change

Using just the proxy records of temperature (44 records), we calculate the glacial-interglacial temperature change at each site by taking the difference between the mean values during the global LGM (22.2 ± 4.0 ka) and Altithermal (7.8 ± 3.4 ka) (Appendix B). Note that not all records span these entire 1σ time intervals, but a mean value was still calculated from the data that lie within them. Glacial-interglacial temperature increases range from 0.4 to 17 °C (Figure 3.5). The magnitude of temperature changes increases poleward in both hemispheres, with

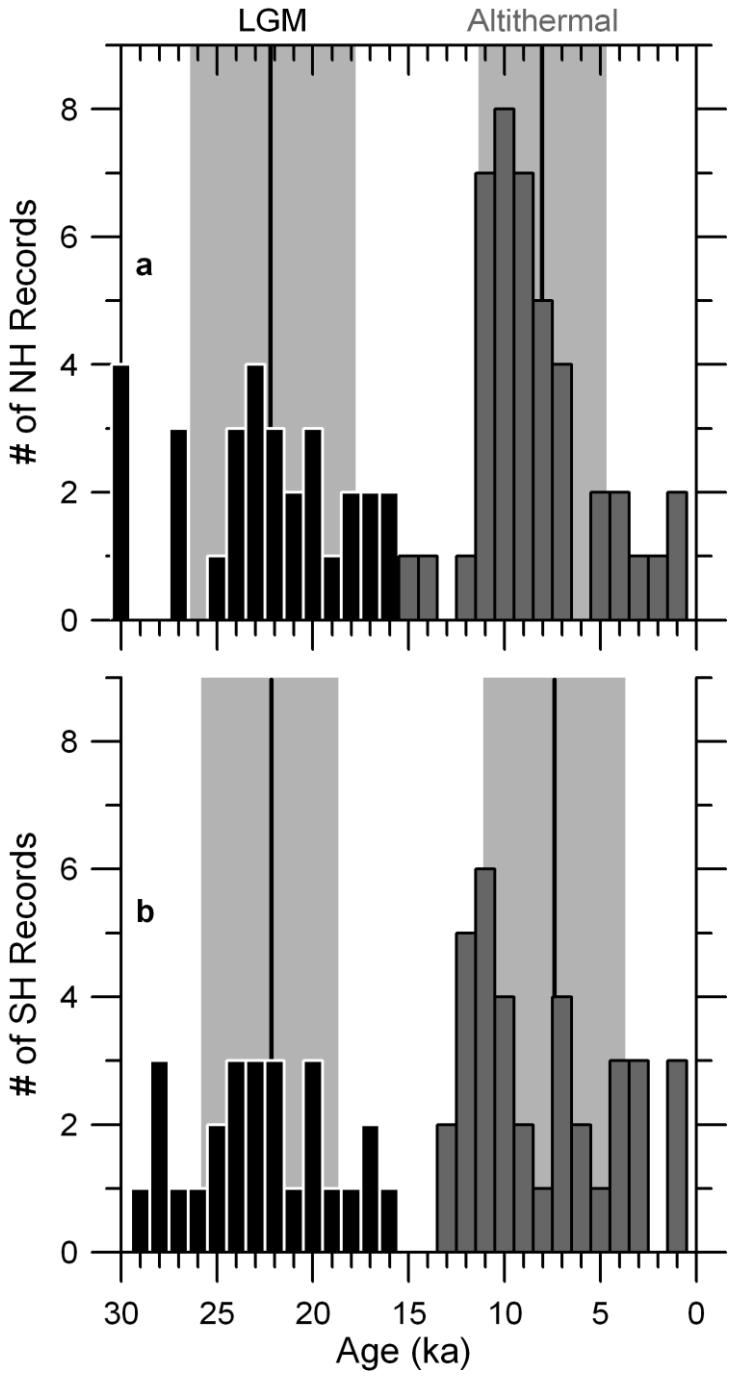

Figure 3.4: Timing of the LGM and Altithermal for the (**a**) Northern and (**b**) Southern Hemispheres. Bins are 1 kyr. Black line and gray box denote the average and standard deviation of LGM and Altithermal timing for each hemisphere. Northern Hemisphere LGM = 22.1 ± 4.3 ka; Southern Hemisphere LGM = 22.3 ± 3.6 ka; Northern Hemisphere Altithermal = 8.0 ± 3.2 ka; Southern Hemisphere Altithermal = 7.4 ± 3.7 ka.

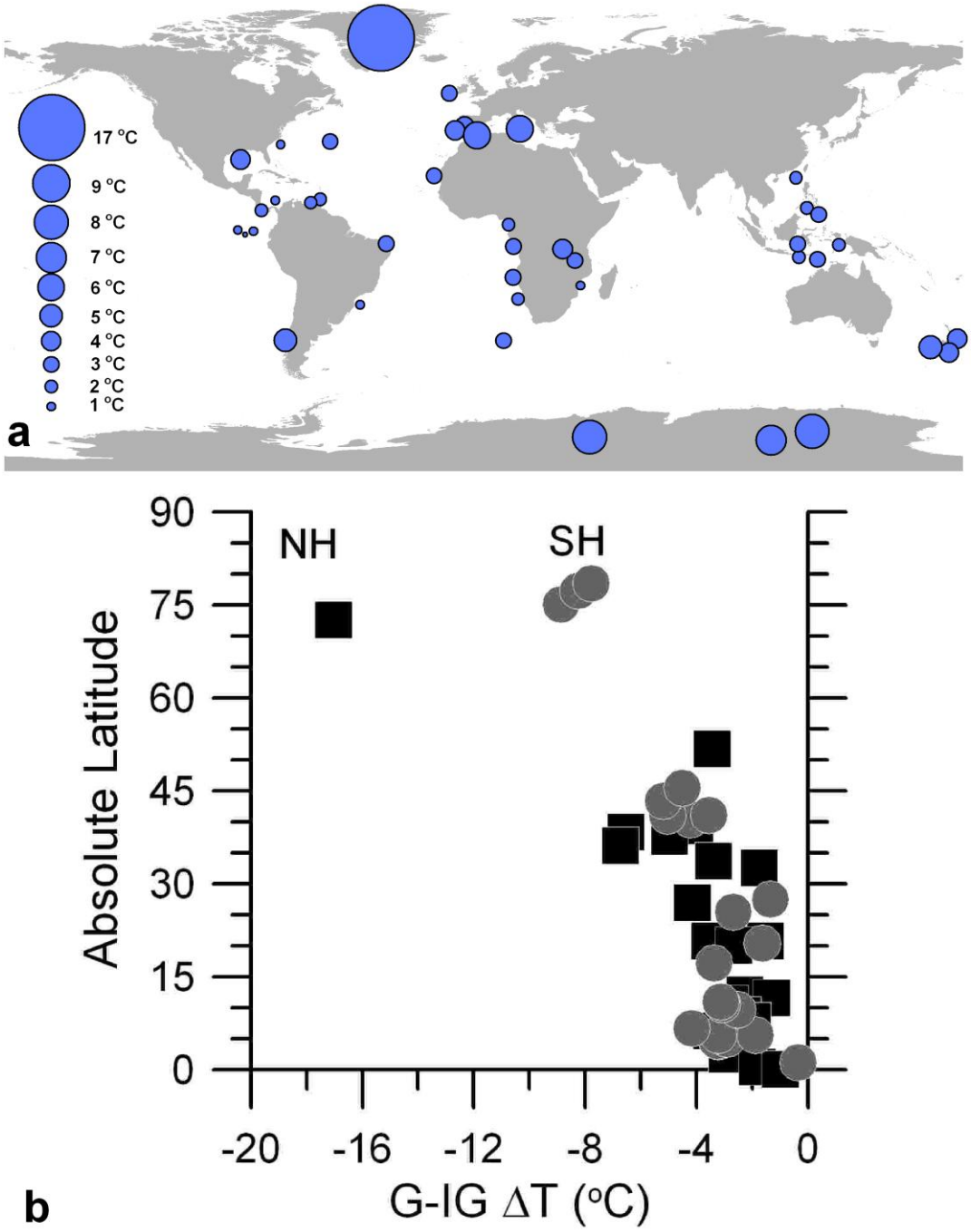

Figure 3.5: Magnitude of the glacial-interglacial temperature change relative to absolute latitude. Black squares are the Northern Hemisphere (NH), gray circles the Southern Hemisphere (SH).

significantly greater cooling in the northern relative to the southern high latitudes. However, the northern high latitudes are represented by only one point (GISP2 ice core) making this latter conclusion tenuous. At the same time, the GISP2 site has experienced relatively small changes in albedo and elevation since the LGM (Cuffey and Clow, 1997), so it is conceivable that northern high latitude regions formerly covered by sea ice or ice sheets cooled as much or more than GISP2 at the LGM. Nevertheless, there is a clear need for more high-resolution deglacial temperature records in the northern high latitudes.

We calculate a net global LGM cooling relative to the Altithermal with these data by fitting a 3rd order polynomial to the glacial-interglacial temperature changes as a function of latitude (r^2=0.80, $p<0.0001$) and then weighting by latitudinal area. The resulting global cooling at the LGM is ~4.9 °C, which should likely be considered a minimum estimate for several reasons. Most of the records used are from the oceans, which are less sensitive to climate change than the continents in climate models (e.g., Pinot et al., 1999; Otto-Bliesner et al., 2006). Furthermore, sea level lowering during the LGM effectively raised the continents by ~120 m (e.g., Clark and Mix, 2002), which would have resulted in an additional ~0.75 °C adiabatic cooling of marine air advected over land areas. Finally, proxy temperature records are absent from areas formerly covered by sea ice and ice sheets. These areas likely experienced the greatest cooling during the LGM due to their greatly altered albedo, and, in the case of the ice sheets, increased elevation. It should also be cautioned that our estimate for LGM cooling is limited by its relatively small sample size.

3.4.3 EOF Analysis of Deglacial Climate Variability

EOFs were computed for the last deglaciation (19-11 ka) using 71 records (Appendix 2). EOF1 dominates the variance in these datasets (61% of total) and shows strong positive factor loadings in nearly every record (Figure 3.6b), similar to the results of Clark et al. (2002). PC1 rises exponentially over this interval, although this pattern is interrupted by a plateau from ~14.5 to 12.5 ka. Rising boreal summer insolation as

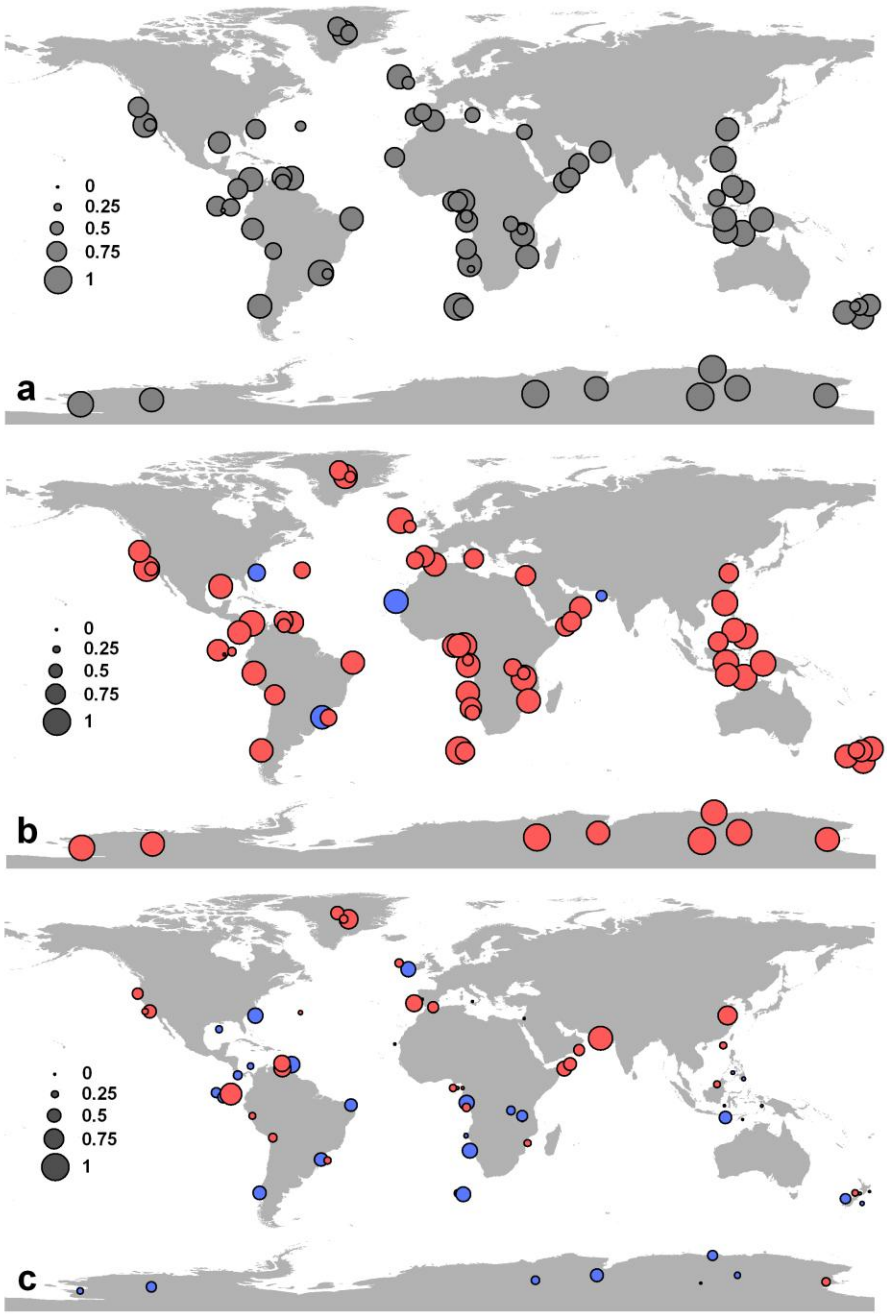

Figure 3.6: (**a**) Communality, (**b**) EOF1, and (**c**) EOF2 maps for the 19-11 ka analysis. EOF1 explains 61% of the deglacial variability; EOF2 explains 11% of the deglacial variability. Magnitude of each record's loading indicated by legend. Positive loadings are shown in red, negative loadings in blue. The square of the factor loading gives the fraction of variance in each record explained by the EOF. Communalities give the fraction of variance explained by the first two EOFs for each record.

well as decreasing global ice volume could potentially explain the deglacial trend seen in PC1 (Figure 3.7). However, these forcings likely had little effect on Southern Hemisphere climate (Broccoli, 2000; Manabe and Broccoli, 1985), and Southern Hemisphere records have equally high EOF1 loadings as those in the Northern Hemisphere. The largest deglacial climate forcing (or feedback) common to both hemispheres is the increase in atmospheric greenhouse gas concentration, particularly CO_2. The plateau in PC1 ~14.5-12.5 ka resembles the plateau in atmospheric CO_2 during this same time interval and not insolation or ice volume (Figure 3.7). Indeed, PC1 is notably similar to CO_2 over its entire length (r^2=0.97 with Dome C; r^2=0.88 with Siple Dome; r^2=0.88 with Dome F; $p<0.0001$ for all 3 comparisons) (Ahn et al., 2004; Kawamura et al., 2007; Monnin et al., 2001). Note that these CO_2 records were not used in this analysis and thus did not contribute to PC1.

EOF2 explains 11% of the variance in the database with a more complex factor loading pattern than EOF1 (Figure 3.6c). Generally negative loadings in the Southern Hemisphere and positive loadings in the Northern Hemisphere suggest EOF2 records a bipolar seesaw response, similar to the results of Clark et al. (2002). Tropical and subtropical loading signs are quite variable in both hemispheres. PC2 decreases from ~19 to 16 ka, with an abrupt increase ~14.7 ka, followed by a second decrease ~12.9 ka and increase ~11.6 ka (Figure 3.8). Comparison with a Pa/Th proxy record of AMOC strength (McManus et al., 2004) (not included in the analysis) shows significant commonality (Figure 3. 8) (r^2=0.55, $p<0.0001$).

Higher order EOFs account for little variance (<7%) in the database and do not show spatially coherent patterns. We therefore consider them insignificant and do not discuss them further.

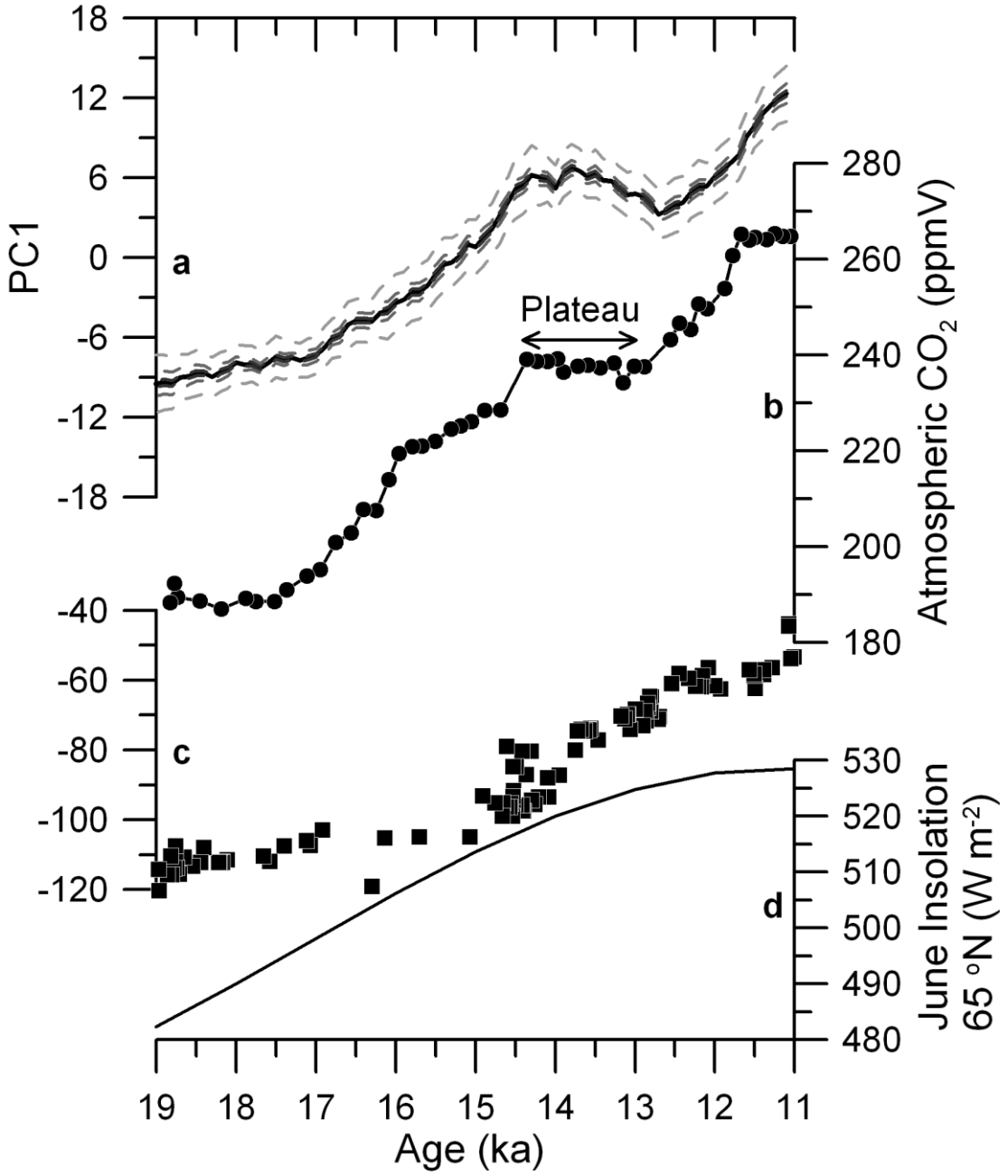

Figure 3.7: (**a**) 19-11 ka PC1 and deglacial time series. (**b**) Deglacial atmospheric CO_2 on EDC2 timescale (Monnin et al., 2001). (**c**) Boreal summer insolation (Berger and Loutre, 1991). (**d**) Deglacial relative sea level rise (Clark and Mix, 2002). The plateau in atmospheric CO_2 is denoted. The dashed gray line confidence intervals around the PC give the standard deviation of 100 EOF calculations performed after randomly removing 10, 50 and 90% (in progressively lighter shades of gray) of the records during the jackknifing procedure described in Section 3.3.

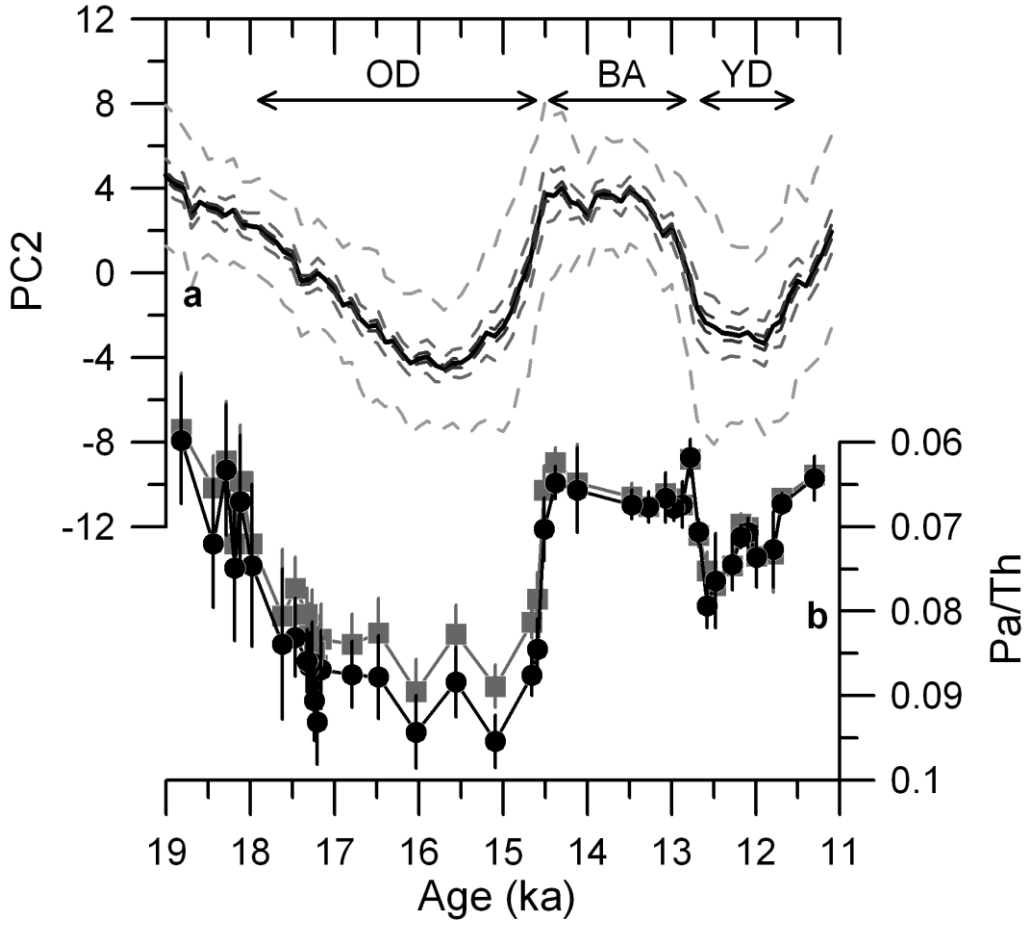

Figure 3.8: (**a**) 19-11 ka PC2 and (**b**) North Atlantic Pa/Th, a proxy for AMOC strength (McManus et al., 2004). The timing of the Younger Dryas (YD), Bølling/Allerød (B/A) and Oldest Dryas (OD) are denoted. Gray confidence intervals show the results of the jackknifing procedure described in Section 2 and are the same as in Figure 3.7.

3.5 Bølling/Allerød–Younger Dryas Climate Variability

3.5.1. EOF Analysis of Climate during the Bølling/Allerød–Younger Dryas

Most of the climate variability from 19 to 11 ka is associated with the overall deglacial trend with relatively little variance at millennial time scales. Therefore, we focus the EOF analysis to 15-11 ka using 90 records to better characterize climate variability during the Bølling/Allerød–Younger Dryas oscillations (Appendix B). Over half of the variance in this database can be explained by two modes of variability of nearly equal significance; EOF1 explains 32% and EOF2 explains 26% of the variance (Figure 3.9). The jackknifing results indicate these modes are robust (Figure 3.10). EOFs 3 and 4 account for only 12 and 5% of the variance with no pattern in their loadings and are thus considered insignificant.

The first two EOFs display what are to a first order opposite spatial patterns (Figure 3.9). EOF1 has large positive loadings in the extratropical Southern Hemisphere, which become progressively smaller and of mixed sign in the tropics and Northern Hemisphere (Figure 3.9b). EOF2 displays large positive loadings in the Northern Hemisphere and increasingly smaller and mixed signed loadings in the tropics and Southern Hemisphere (Figure 3.9c). Thus, EOF1 and EOF2 can be described as representing "southern" and "northern" modes of variability, similar to the results of an EOF analysis of Marine Isotope Stage 3 records (Clark et al., 2007). Interestingly, some low latitude records have intermediate to large loadings for EOF1 and/or EOF2 suggesting that tropical climate cannot be adequately explained without both EOFs. PC1 increases gradually from ~14.9 to 13.8 ka, is relatively constant from ~13.8 to 13.0 ka and increases again more strongly after ~13.0 ka (Figure 3.10a). PC2 shows three major transitions, with increases at ~14.6 and 11.7 ka separated by a decrease at ~13.0 ka (Figure 3.10b).

Dividing the records by region and recalculating the 15-11 ka EOFs helps to quantify the influence of these northern and southern modes around the world. EOFs were computed separately for records from the extratropical Northern Hemisphere (>30°N, n=25), tropics (30°N-30°S, n=47), and extratropical Southern Hemisphere

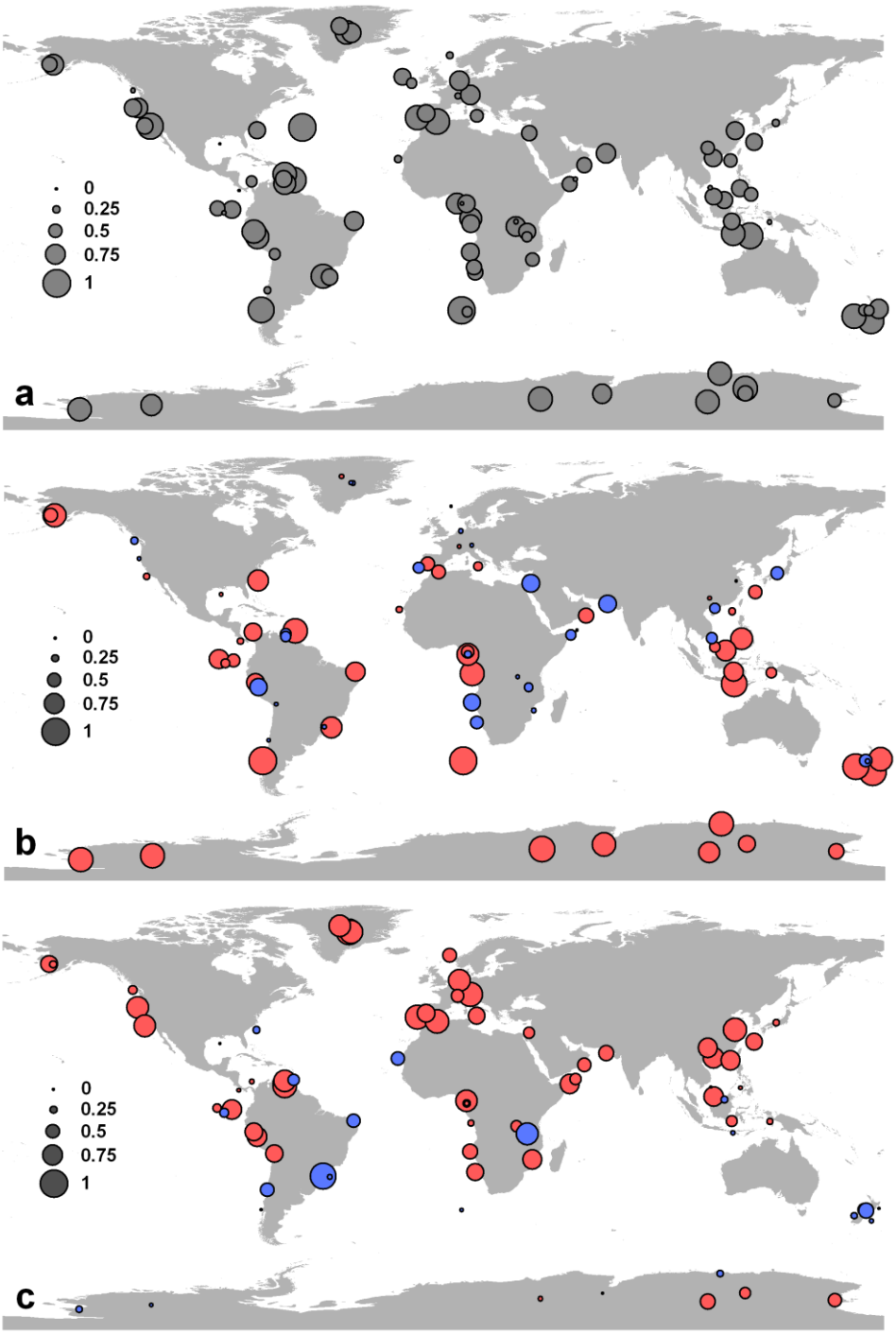

Figure 3.9: (**a**) Communality, (**b**) EOF1, and (**c**) EOF2 maps for the 15-11 ka analysis. EOF1 and EOF2 explain 32% and 26% of the Bølling/Allerød–Younger Dryas variability, respectively. Magnitude of each record's loading indicated by legend. Positive loadings are shown in red, negative loadings in blue.

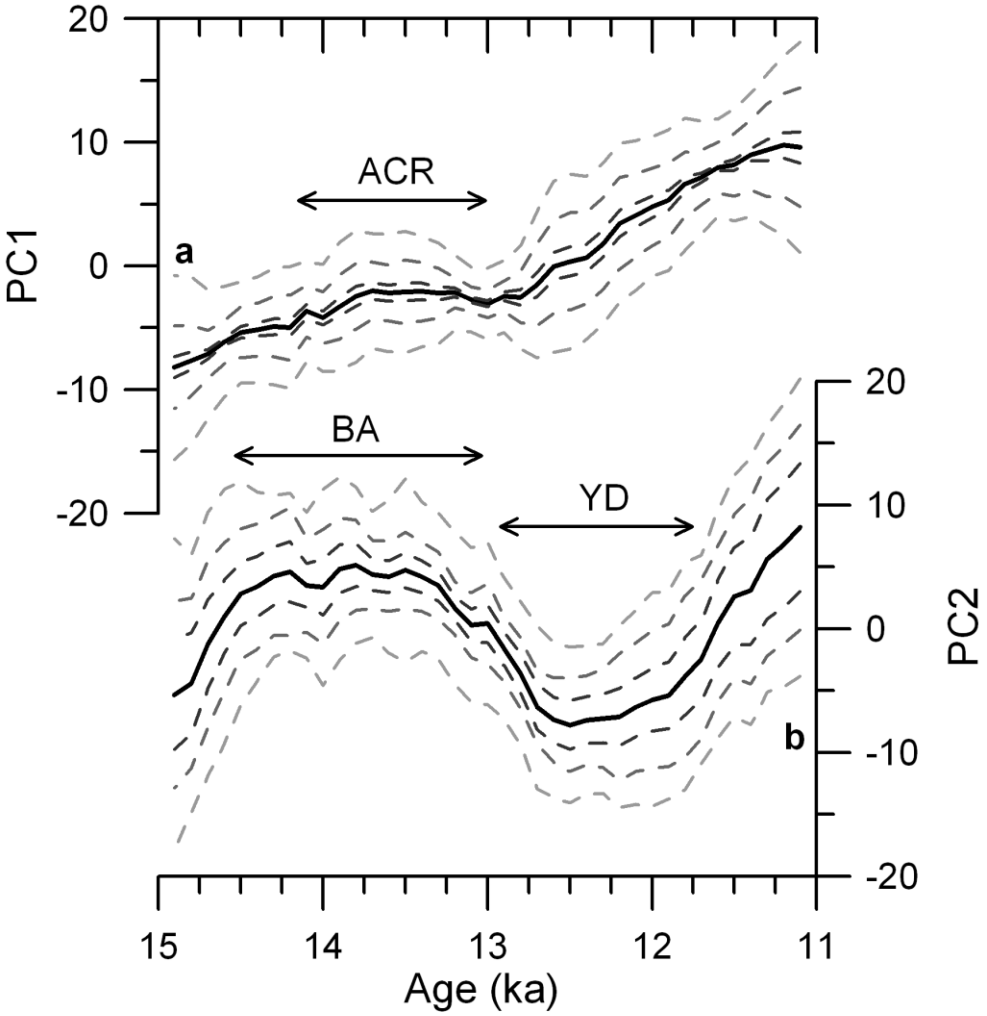

Figure 3.10: Bølling/Allerød–Younger Dryas PCs from 15-11 ka; (**a**) PC1 and (**b**) PC2. The Younger Dryas (YD), Bølling/Allerød (B/A) and Antarctic Cold Reversal (ACR) are denoted. Gray confidence intervals show the results of the jackknifing procedure described in Section 3.3 and are the same as in Figure 3.7.

(>30°S, n=18). EOF1 accounts for substantially more variance than EOF2 in both the northern (41 and 19%) and southern (60 and 14%) extratropics, but EOF1 and EOF2 are nearly equal in the tropics (29 and 25%). PC1 and PC2 for the tropics are quite similar to the first PCs for the southern (r^2=0.88, p<0.0001) and northern (r^2=0.88, p<0.0001) extratropics, respectively. Thus, there appear to be signals associated with the higher latitudes of each hemisphere that exerted similar sized influences on the lower latitudes. Northern extratropic PC1 shares similarities with the Pa/Th record of AMOC strength (r^2=0.46, p=0.004) (McManus et al., 2004) while southern extratropic PC1 resembles atmospheric CO_2 (r^2=0.85, p<0.0001) (Monnin et al., 2001). The northern mode, therefore, likely reflects the direct effects of AMOC variations, while the southern mode reflects greenhouse gas forcing and the processes affecting it such as changes in Southern Ocean circulation, sea ice extent and upwelling, which may have been forced in turn by AMOC variability (Monnin et al., 2001; Ahn and Brook, 2008; Barker et al., 2009).

Further separating the tropical records into those that are proxies for temperature (n=33) and precipitation/windiness (n=14) and again calculating 15-11 ka EOFs reveals differences in how the high latitudes of the two hemispheres affected low latitude climate. The tropical temperature PC1 and PC2 account for 34 and 18% of the variance, and are again similar to PC1 for the southern (r^2=0.93, p<0.0001) and northern (r^2=0.86, p<0.0001) extratropics, respectively. The tropical precipitation/windiness PC1 and PC2 explain 47% and 16% of the variance, and are similar to PC1 for the northern (r^2=0.79, p<0.0001) and southern extratropics (r^2=0.68, p<0.0001), respectively. These results indicate that the northern mode of AMOC-driven climate variability had a larger impact on tropical atmospheric circulation and hydrology, likely caused by meridional displacements of the Intertropical Convergence Zone (ITCZ) (Chiang and Bitz, 2005; Yancheva et al., 2007). In contrast, tropical temperature appears to be have been driven more strongly by the southern mode involving Southern Ocean processes and greenhouse gas forcing.

3.5.2 Relative Magnitude of the Younger Dryas

The magnitude of the Younger Dryas around the planet has been used as a fingerprinting technique to identify the forcing locus (Broecker, 1994; 2003; Peteet, 1995). The differing nature of proxy records (e.g., $\delta^{18}O$ value versus Mg/Ca ratio versus sediment color), however, makes it difficult to relate the magnitude of the Younger Dryas in one record to another. The shift from a glacial to interglacial state provides a common backdrop against which to compare shorter events like the Younger Dryas. That is, the magnitude of the Younger Dryas can be determined as a fraction of the glacial-interglacial range in each record. While the glacial-interglacial range certainly varied around the globe (Figure 3.5), particularly between the low and high latitudes, this method provides a first-order approach to mapping the size of the Younger Dryas. Here, we define the Younger Dryas interval in 72 records (Appendix B) in one of two ways: 1) in records where the Younger Dryas is distinct (e.g., Greenland ice cores, Cariaco Basin sediment, Hulu Cave speleothems) it is defined visually; 2) in records where the Younger Dryas is unclear or absent, the Greenland ice core Younger Dryas chronozone (12,850-11,650 years before 1950 AD) (Rasmussen et al., 2006) is used to define it. We compute a mean Younger Dryas value for the period 200 yr after the onset and 200 yr prior to the termination of the Younger Dryas interval. This 200 yr buffer is applied to ensure that only values from clearly within the Younger Dryas interval are used. The mean Younger Dryas value is then subtracted from the mean value for the interval 200-1000 yr preceding the Younger Dryas (approximately the Allerød). The difference between the Younger Dryas and Allerød is divided by the difference between the 1 kyr interval of highest (Altithermal) and lowest (LGM) values over the last 30 kyr. Therefore, Younger Dryas magnitudes range from -1 to +1, with larger absolute values reflecting larger Younger Dryas-age climate excursions. Positive numbers indicate a continuation of the overall deglacial trend during the Younger Dryas relative to the Allerød and negative numbers indicate a climate reversal.

Despite considerable spatial heterogeneity in the magnitude of the Younger Dryas, several patterns emerge from the map (Figure 3.11). The spatial pattern is similar to 19-11 ka EOF2, with mainly negative values in the Northern Hemisphere and positive values in the Southern Hemisphere (Figure 3.11a). As has long been known, the Younger Dryas was a return toward glacial conditions in many areas of the Northern Hemisphere, such as the mid to high latitudes and regions of the low latitudes affected by the ITCZ and monsoons. There is a slight latitudinal trend in the magnitude of the Younger Dryas, with a tendency for more negative values at higher Northern Hemisphere latitudes and more positive values at higher Southern Hemisphere latitudes (Figure 3.11b). Low latitude Younger Dryas anomalies tend to be larger in precipitation-related proxies (0.33 ± 0.14, n=10) than temperature records (0.13 ± 0.16, n=31), suggesting that the Younger Dryas may have had a greater impact on the tropical hydrological cycle than on tropical sea surface temperatures.

3.5.3 Younger Dryas Temperature Anomalies

While normalizing the magnitude of the Younger Dryas by the glacial-interglacial range facilitates comparison of different types of proxy records, a more direct comparison can be made by focusing on calibrated temperature proxy records (55 records are included here; Appendix B). Note that these records do not provide a 1:1 comparison due to differences in proxies and calibrations (e.g., Mg/Ca, $U^{k'}_{37}$) (Lea, 2003; Mix, 2006), as well as foraminifera depth habitats and seasonal biases. We compute mean Younger Dryas and Allerød temperatures using the same approach as described above for the magnitude of the Younger Dryas, and subtract to yield the Younger Dryas temperature anomaly relative to the preceding Allerød period.

The most striking feature of the temperature anomaly map and plot is the meridional gradient, particularly in the Northern Hemisphere (Figure 3.12). Average cooling in the Northern Hemisphere high and mid latitudes is ~5 °C (n=3) and 2 °C (n=13), respectively. Tropical temperature anomalies are between 1 and -1 °C, with

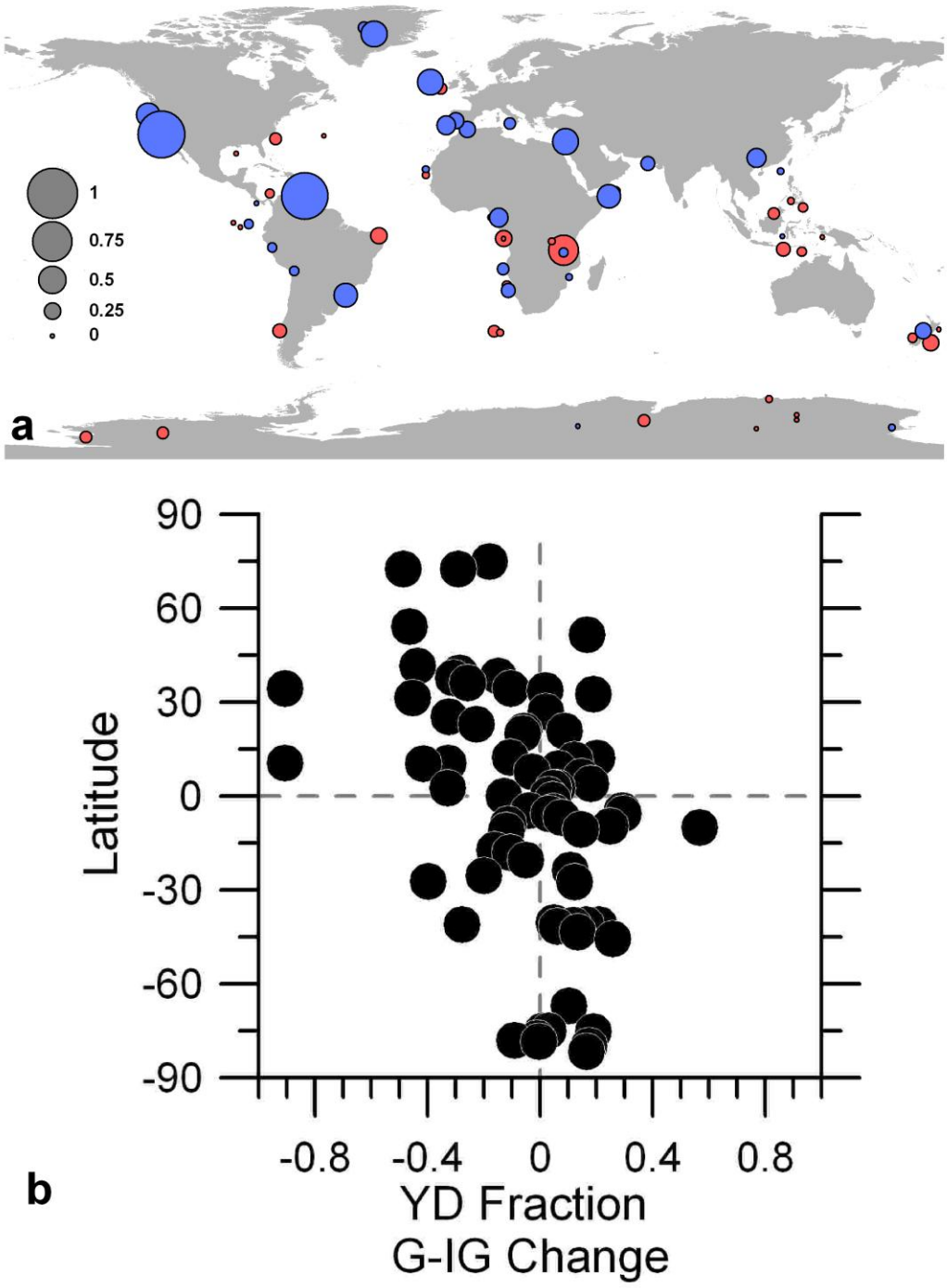

Figure 3.11: Magnitude of Younger Dryas climate change. (**a**) Map of the Younger Dryas fraction of the glacial-interglacial (G-IG) change. Red denotes Younger Dryas was continuation of deglacial trend while blue denotes it was a climate reversal. (**b**) Plot of the Younger Dryas (YD) fraction of the G-IG change relative to latitude.

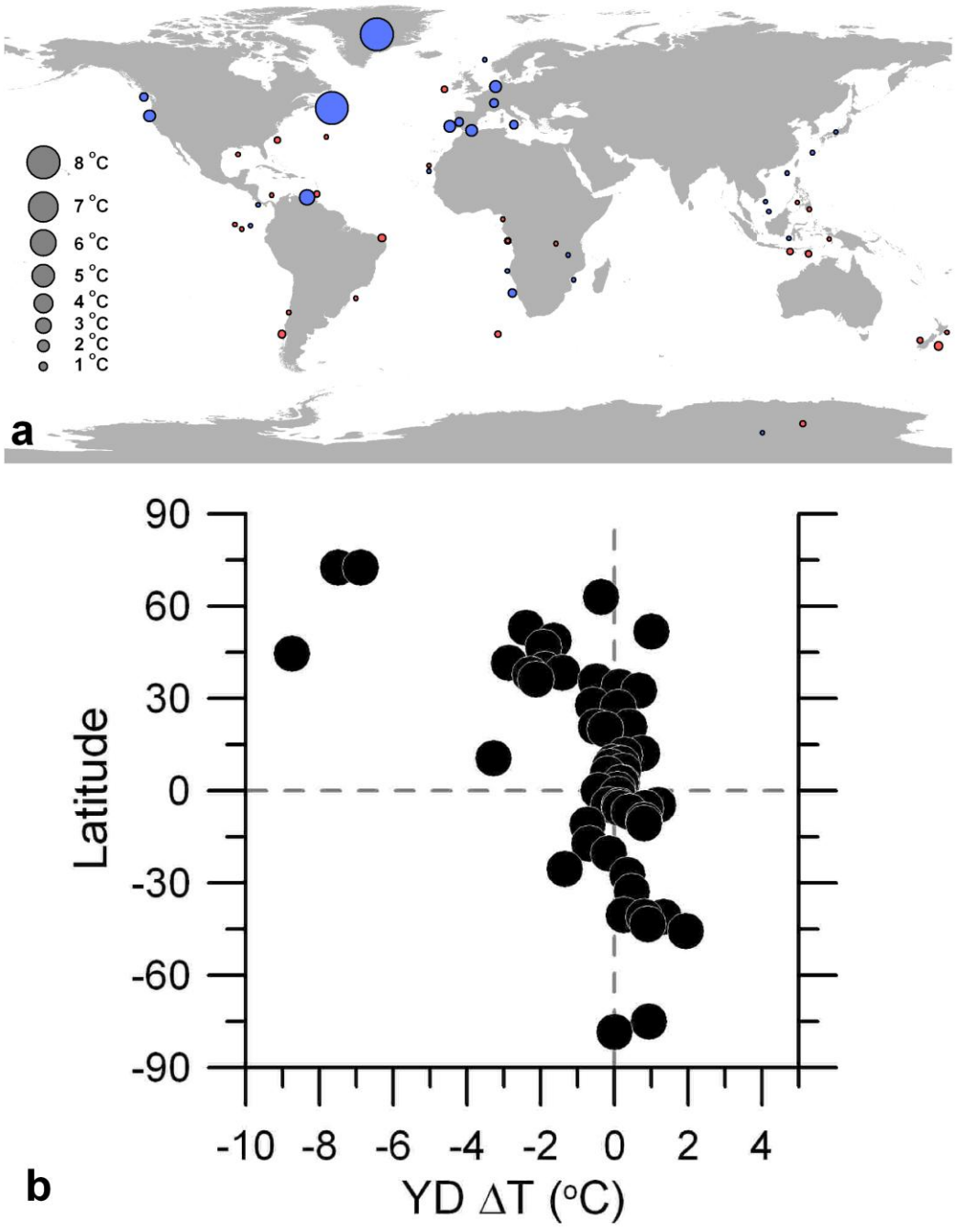

Figure 3.12: Magnitude of the Younger Dryas temperature change. (**a**) Map of the Younger Dryas temperature anomaly. Circle denotes the size of the temperature change. Blue is cooling, red warming. (**b**) Plot of the Younger Dryas (YD) temperature anomaly relative to latitude.

the exception of Cariaco Basin (-3.3 °C) (Lea et al., 2003), and average to nearly 0 °C in both hemispheres (n=31). The Southern Hemisphere mid to high latitude records show warming of 0-2 °C (n=8) with an average of ~1 °C. Anomalies greater than 2 °C are concentrated around the North Atlantic region, near deepwater formation sites and their associated sea ice feedback.

To extrapolate the Younger Dryas temperature data globally, we use a similar technique as that employed with the glacial-interglacial change in temperature (Section 3.2.). We fit a 3rd order polynomial to the Younger Dryas temperature anomalies as a function of latitude (r^2=0.50, $p<0.0001$) and weight by latitudinal area. The result is a global mean cooling of ~0.6 °C during the Younger Dryas.

3.5.4 Relative Magnitude of the Bølling/Allerød

We conduct an analysis similar to that presented above for the Younger Dryas (Section 4.2) on the Bølling/Allerød to quantify its magnitude in relation to the glacial-interglacial range in each record (71 records; Appendix B). The mean value for the interval 16.0-15.0 ka is subtracted from the mean 14.5-13.5 ka value (~the Bølling/Allerød) and divided by the difference between the highest (Altithermal) and lowest (LGM) values in the 1 kyr running mean of the time series. The results of this analysis are less clear than those for the Younger Dryas because the Bølling/Allerød was generally not a climate reversal and is therefore not as readily apparent against the overall deglaciation. Indeed, 82% of the records show positive anomalies for the magnitude of the Bølling/Allerød indicating a continuation of the deglacial trend (Figure 3.13a). One notable result is a significant anticorrelation between the magnitudes of the Bølling/Allerød and Younger Dryas (r^2=0.45, $p<0.0001$) (Figure 3.13b). Records with large positive (negative) anomalies during the Bølling/Allerød tend to have large negative (positive) anomalies during the Younger Dryas. This relationship provides support for the notion that these events represent opposite responses of the climate system to the same fundamental forcing mechanism.

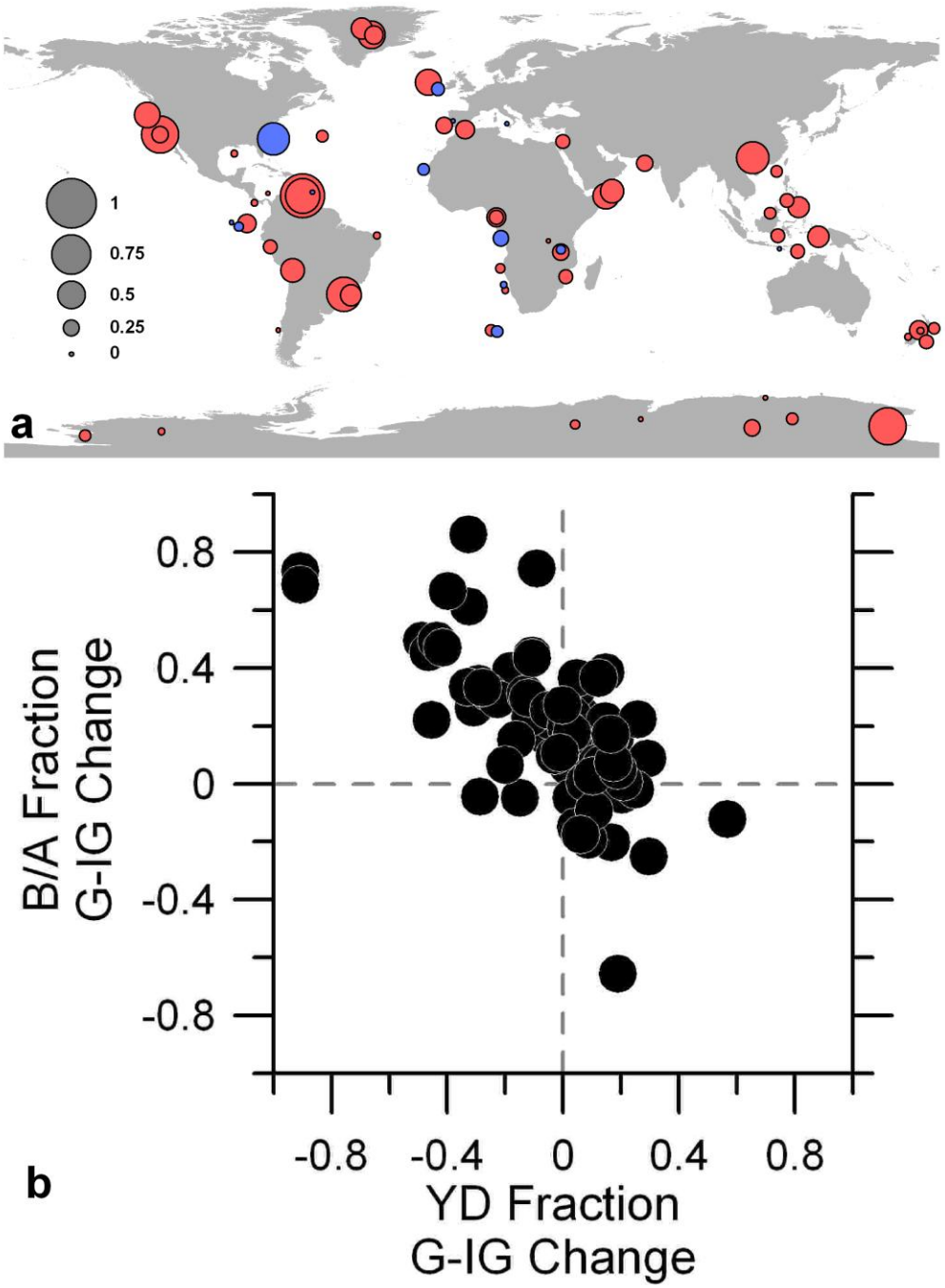

Figure 3.13: Magnitude of Bølling/Allerød climate change. (**a**) Map of the Bølling/Allerød fraction of the glacial-interglacial (G-IG) change. Red denotes Bølling/Allerød was continuation of deglacial trend while blue denotes it was a climate reversal. (**b**) Magnitude of the Younger Dryas (YD) anomaly versus the Bølling/Allerød (B/A) anomaly.

3.6 Discussion

The global average climate-defined LGM age of 22.2 ± 4.0 ka inferred from the 56 records analyzed here is broadly similar to both classical (CLIMAP, 1976 – 18 ^{14}C ka or ~21 ka) and more recent (Mix et al., 2001 – see below; Clark et al., 2009 – 26.5-19 ka) definitions of the LGM based on maximum global ice volume from foraminiferal δ^{18}O and/or sea level records. The LGM in 54% of the records fall within LGM Chronozone Level 2 (18-24 ka) and 39% are within LGM Chronozone Level 1 (19-23 ka) of Mix et al. (2001), suggesting that while these may be useful chronostratigraphic definitions of the LGM for the reasons presented by Mix et al. (2001), they do not appear to capture the length or variability of the LGM. It should be cautioned, however, that we identify the LGM in each record as a single point in time, which gives no indication of its duration or stability in any particular record; these would be worthwhile issues to investigate in the future. This similarity in timing between the climate and ice sheet-defined LGM intervals suggests a strong connection between maximum ice volume and glacial climate. Insofar as the onset of deglaciation immediately followed the minimum in a climate record (i.e., our LGM definition), our database indicates the deglaciation in most records began before the rise of CO_2 at ~17-18 ka (Monnin et al., 2001) and thus requires another forcing to have triggered deglaciation, even though CO_2 appears to have been a powerful feedback (see Section 3.4.3). Boreal summer insolation is the most likely candidate to explain the shift towards an interglacial ~22 ka, which implicates it as the ultimate forcing behind the termination of the LGM in the Northern Hemisphere (Barker et al., 2009; Clark et al., 2009). How, or if, this change in Northern Hemisphere energy impacted Southern Hemisphere climate is difficult to assess from our existing database (e.g., Clark et al., 2004, 2009; Huybers and Denton, 2008).

The similar timing of the LGM and Altithermal between the Northern and Southern Hemispheres (Figure 3.4) suggests that the hemispheres were synchronized at orbital timescales. Atmospheric greenhouse gases are the most likely synchronizer given their global nature and strong forcing (Alley and Clark, 1999; Alley et al., 2002;

Barrows et al., 2007a), which the 19-11 ka PC1 supports by showing global deglaciation tracked the rise in atmospheric CO_2. However, as noted above, many of the climate records from both hemispheres begin their deglacial progression prior to the initial rise in CO_2. Imbrie et al. (1993) and Gildor and Tziperman (2001) suggested that the effects of upwelled North Atlantic Deepwater on Southern Ocean temperatures may have also synchronized the hemispheres, but Alley and Clark (1999) argued that empirical evidence favors an out of phase response between the hemispheres due to changes in deepwater formation (Crowley, 1992). Alternatively, or additionally, both hemispheres may have responded to local insolation forcing, with a minimum in boreal summer *intensity* in the north and a minimum in austral summer *length* in the south leading to similar timing of the maximum glacial climate (Huybers and Denton, 2008). Our compilation of LGM records points to the difficulty in determining leads and lags between the hemispheres in the timing of LGM termination. Given the large spread in the timing of the LGM in both hemispheres, caution should be taken when selecting only one or several records for the basis of arguments on the forcing and phasing of orbital scale climate change.

The timing of the Northern Hemisphere Altithermal at 8.0 ± 3.2 ka (Figure 3.4) is consistent with forcing from boreal summer insolation in combination with greenhouse gases. The ~4 kyr lag behind peak insolation may, in part, reflect the effects of the waning Northern Hemisphere ice sheets, which did not completely disappear until ~6.5 ka (Antevs, 1953; Carlson et al., 2007b; 2008a; Kaplan and Wolfe, 2006; Kaufman et al., 2004). While the Southern Hemisphere also has a modest peak in the early Holocene (Figure 3.4b), there is a more even distribution of Altithermal ages throughout the Holocene than the Northern Hemisphere, suggesting that the concept of a peak interglacial climate state may not be as meaningful in the Southern Hemisphere.

The different magnitudes of glacial-interglacial temperature changes between the hemispheres (Figure 3.5) are consistent with multiple forcing/feedback mechanisms of glacial cooling for each hemisphere. In the Northern Hemisphere, the

expansion of large ice sheets and North Atlantic sea ice, lower greenhouse gases, and changes in vegetation and aerosols likely combined to produce the LGM climate (Braconnot et al., 2007; Broccoli, 2000; Manabe and Broccoli, 1985; Otto-Bliesner et al., 2006; Schneider von Deimling et al., 2006). In the Southern Hemisphere, the continental shelf edge limited the expansion of the only major ice sheet (Antarctic) suggesting that Southern Ocean sea ice expansion, lowered greenhouse gases, and increased aerosols were the major drivers of Southern Hemisphere LGM climate (Braconnot et al., 2007; Gildor and Tziperman, 2001; Imbrie et al., 1993; Lambert et al., 2008; Otto-Bliesner et al., 2006). Thus, the large ice sheet forcing may account for much of the greater cooling and steeper meridional temperature gradient in the Northern Hemisphere relative to the Southern Hemisphere (Figure 3.5).

The EOF results identify major drivers of climate change over the deglaciation. The agreement between 19-11 ka PC1 and atmospheric CO_2 implicates the carbon cycle as an important feedback of global deglacial climate change (Figure 3.6b & 7) (Chamberlin, 1897; Lea et al., 2006; Mix et al., 1986a; Otto-Bliesner et al., 2006; Visser et al., 2003). The correlation between 19-11 ka PC2 and AMOC strength supports arguments that variations in AMOC are another important deglacial climate forcing with a bipolar seesaw climate response (Blunier and Brook, 2001; Broecker, 1998; Clark et al., 2002; Liu et al., 2009) (Figure 3.6c & 8). Indeed, the climate effects of the initial decrease in AMOC strength at ~19 ka to a minimum during the Oldest Dryas are well-represented in PC2 (Figure 3.8). The attendant bipolar seesaw climate response (Northern Hemisphere cooling/drying, Southern Hemisphere warming/wetting) to this AMOC reduction may help explain the often noted “lead” in Southern Hemisphere climate (e.g., Koutavas et al., 2002; Lea et al., 2006; Shackleton, 2000; Stott et al., 2007; Visser et al., 2003) over Northern Hemisphere climate and ice sheets (Alley et al., 2002; Carlson et al., 2008b; Clark et al., 2004; 2009).

AMOC variability was expressed as relatively coherent northern and southern climate modes in the higher latitudes of each hemisphere, whereas the climate

response was spatially more variable in the low latitudes (see Sections 3.4.3 and 3.5.1). This difference may reflect the larger number of climate variables recorded by proxies as well as the variety of transmission mechanisms operating in different subtropical and tropical regions. For example, a reduction in AMOC during the Younger Dryas would cause a southward shift in the ITCZ, changing latitudinal precipitation and wind patterns as well as upwelling regimes (Benway et al., 2006; Chiang et al., 2003; Chiang and Bitz, 2005; Haug et al., 2001; Lea et al., 2003; Mix et al., 1986b; Zhang and Delworth, 2005). Reduced northward heat transport associated with weakened AMOC may store heat in the subtropics and tropics of the western Atlantic (Carlson et al., 2008c; Crowley, 1992; Grimm et al., 2006; Rühlemann et al., 1999; Schmidt et al., 2004; Weldeab et al., 2006), causing warming during an overall North Atlantic cooling event. Another polar connection to the tropics is via the oceanic tunnel of thermocline subduction and the atmospheric bridge of the Hadley Circulation (Liu and Yang, 2003). Warming of Southern Ocean thermocline water (at the end of the Antarctic Cold Reversal) from a reduction in AMOC strength (Schmittner et al., 2003) may crop out in the tropical surface ocean within decades causing tropical warming during the Younger Dryas. Therefore, the bipolar seesaw behavior at the high latitudes of the two hemispheres (Bølling/Allerød warming-Antarctic Cold Reversal followed by Younger Dryas cooling-termination of Antarctic Cold Reversal) (Blunier and Brook, 2001; Broecker, 1998; Clark et al., 2002; Weaver et al., 2003) may have affected different tropical-subtropical regions possibly at different times.

Bipolar seesaw temperature responses during the Younger Dryas are likewise best expressed in the mid to high latitudes of each hemisphere, but less clear in the low latitudes. North Hemisphere cooling of 2-8 °C is evident above ~35 °N whereas Southern Hemisphere warming of 1-2 °C is apparent below ~45 °S (Figure 3.12). The tropical and subtropical temperature changes, in contrast, are between -1 and +1 °C (with the exception of Cariaco Basin, -3.3 °C; Lea et al., 2003), or ~0 °C when considering the error in calculating temperature from proxies (e.g., Mg/Ca, $U^{k'}_{37}$; Lea,

2003). We suggest that the seesaw model does not adequately represent tropical temperature variability, which instead seems to be predominantly controlled by greenhouse gases. Lower latitude precipitation does appear to exhibit a seesaw pattern, however.

All of the patterns discussed above suggest a northern high latitude origin for the Younger Dryas cold event, because 1) the largest negative climate anomalies occur in the extratropical Northern Hemisphere focused around the North Atlantic, 2) there is a variable expression of the Younger Dryas in both sign and magnitude in the tropics and subtropics, and 3) modest positive climate anomalies occur in the extratropical Southern Hemisphere (Figure 3.11 & 12). This is consistent with the Younger Dryas being a redistribution of heat, as would accompany a reduction in AMOC strength (Figure 3.8), rather than a global-scale cooling event, which requires a change in the planetary energy balance. Younger Dryas cooling in the north does appear to slightly outweigh warming in the south, however, with a global mean cooling of ~0.6 °C (Figure 3.12b). As greenhouse gases, insolation, and global ice volume were nearly unchanged from the Allerød to the Younger Dryas (Figure 3.7), a *net* global cooling could most plausibly be explained by increased Northern Hemisphere albedo due to greater snow and sea ice cover and aerosol loading (Alley, 2000; Denton et al., 2005). This small global mean temperature decrease during the Younger Dryas relative to the global cooling of ~4.9 °C at the LGM would suggest that the Younger Dryas was hardly a return to ice age climate. It is instead on par with the global cooling of ~0.8 °C during the Little Ice Age relative to the present (Mann et al., 2008).

Several other differences stand out between the Younger Dryas and the LGM. Meridional temperature gradients were generally smaller for the Younger Dryas. One hemisphere warmed while the other cooled during the Younger Dryas whereas both were colder during the LGM. Tropical temperatures were largely unaffected by the Younger Dryas with an average temperature change of 0.0 ± 0.8 °C (n=31), but the tropics cooled by 2.5 ± 0.9 °C (n=28) during the LGM. Moreover, temperature

anomalies during the LGM were generally several times larger than those during the Younger Dryas (Figure 3.5 & 11). One similarity, however, is that greater climate change occurred in the Northern Hemisphere than in the Southern Hemisphere and the meridional temperature gradient steepened considerably in the northern extratropics, suggesting the northern higher latitudes may be more sensitive to climate change.

Arguments for Southern Hemisphere cooling, and thus global cooling, during the Younger Dryas are predominately based on valley glacier records constrained by limiting radiocarbon dates (Broecker, 1994, 2003; Ariztegui et al., 1997; Denton et al., 1999b; Denton and Hendy, 1994; Lowell et al., 1995). The most often cited record is the Waiho Loop Moraine of New Zealand (Denton and Hendy, 1994). The majority of Waiho radiocarbon dates, however, precede the onset of the Younger Dryas (Broecker, 2003), a result recently confirmed by Turney et al. (2007). Moreover, this moraine may not represent a climatic event, but rather an anomalous landslide-triggered glacier advance through the insulating effect of the debris (Tovar et al., 2008). Much work has recently applied cosmogenic dating to late-glacial Southern Hemisphere moraines to address the extent of the Younger Dryas (Ackert et al., 2008; Barrows et al., 2007b; Douglass et al., 2005, 2006; Kaplan et al., 2008; Kilian et al., 2007; McCulloch et al., 2005; Moreno et al., 2009; Strelin and Malagnino, 2000; Sugden, 2005; Sugden et al., 2005). Given current debates on the limitations in dating glacial events (Applegate et al., 2008; Barrows et al., 2008; Lowell and Kelly, 2008; Putnam et al., 2010), however, these glacial records do not at present provide strong evidence for or against Southern Hemisphere cooling during the Younger Dryas. We suggest that the modes of deglacial climate variability identified in our analyses of high-resolution, well-dated climate records predict Southern Hemisphere moraines of Younger Dryas age are, in general, unlikely to be found.

The main mechanism proposed for atmospheric, and not AMOC, forcing of the Younger Dryas calls on El Nino-Southern Oscillation (ENSO)-like processes originating in the tropics (Broecker, 2003; Cane and Clement, 1999; Clement and Cane, 1999; Clement et al., 2001; Clement and Peterson, 2008). Such a scenario

would likely result in three observable patterns. Presumably, ENSO-like forcing would produce 1) interhemispheric symmetry in the response of the climate system (Hoerling and Kumar, 2000; Seager et al., 2005), 2) a marked change in the global energy balance via changes in planetary albedo and greenhouse trapping (Cane and Clement, 1999; Thompson et al., 2008), and 3) the largest climate signals in the tropics (Mantua and Hare, 2002; Ropelewski and Halpert, 1987) as occurs with modern ENSO variability. The analyses presented above contradict these predictions, and rather demonstrate the existence of two different hemispheric modes of climate variability that are most pronounced at higher latitudes and interact in a complex manner in the tropics. They also suggest a relatively diminutive perturbation to the planetary energy budget during the Younger Dryas, which in any case was driven largely by the northern high latitudes and not the tropics.

3.7 Conclusions

There are five main conclusions drawn from these analyses of deglacial climate records.

1) The timing of the LGM and Altithermal varied considerably around the globe but were statistically synchronous between the hemispheres. The LGM and Altithermal occurred at 22.1 ± 4.3 ka and 8.0 ± 3.2 ka in the Northern Hemisphere and 22.3 ± 3.6 ka and 7.4 ± 3.7 ka in the Southern Hemisphere, respectively. Global mean cooling during the LGM was likely at least ~4.9 °C relative to the Altithermal.
2) The first mode of deglacial climate variability is common to most climate records and is likely related to rising CO_2, implicating it as a major deglacial forcing/feedback.
3) The second mode of deglacial climate variability shows a bipolar seesaw pattern between the hemispheres most likely driven by fluctuations in AMOC strength. This bipolar climate pattern may partly explain the apparent “lead” of Southern Hemisphere climate over Northern Hemisphere climate and ice sheets.

4) The Bølling/Allerød–Younger Dryas climate oscillations were an expression of this bipolar seesaw with the Antarctic Cold Reversal representing the opposite sign response of the Southern Hemisphere. However, these climate events are most clear at mid to high latitudes with a complex climate response in the tropics and subtropics of both hemispheres.

5) While the Younger Dryas may have been a near-global scale climate change, in the sense that climatic anomalies occurred in many regions during this time, it was not a major global cooling event (approximately -0.6 °C change), with many records showing warming or a shift toward interglacial conditions through the Younger Dryas. This is particularly evident in the low latitudes of the Northern Hemisphere and in many areas of the Southern Hemisphere. Globally, the Younger Dryas was by no means a return to ice age climate.

3.8 Acknowledgments

The authors would like to thank P. Clark, J. Kutzbach, S. Marcott, A. Mix, N. Pisias, and J. Shaman for helpful discussions, and T. Bauska, P. Clark, S. Marcott for reading an earlier version of this manuscript. Four anonymous reviewers improved the clarity of the original manuscript. J. Shakun is funded by the National Science Foundation Paleoclimate Program. A. Carlson is funded by the National Science Foundation Paleoclimate Program and University of Wisconsin-Madison start-up funds. Datasets were graciously provided by J. Andrews, S. Burns, T. Barrows, P. Clark, O.M. Heiri, J. Hellstrom, I. Hendy, F.S. Hu, L. Labeyrie, V. Peck, C. Pelejero, J. Sachs, E. Schefub, J. Tierney, and P. Williams. The authors would also like to acknowledge the extensive databases provided by NOAA NGDC and PANGAEA.

3.9 References

Ackert, R. P., Jr., Becker, R. A., Singer, B. S., Kurz, M. D., Caffee, M. W., and Mickelson, D. M. 2008. Patagonian glacier response during the late glacial-Holocene transition. Science, 321**,** 392-395.

Ahn, J., Wahlen, M., Deck, B., L., Brook, E. J., Mayewski, P. A., Taylor, K. C., and White, J. W. C. 2004. A record of atmospheric CO_2 during the last 40,000 years from the Siple Dome, Antarctica ice core. Journal of Geophysical Research, 109**,** doi:10.1029/2003JD004415.

Ahn, J., and Brook, E. J. 2008. Atmospheric CO_2 and climate on millennial time scales during the last glacial period. Science, 322, 83-85.

Alley, R. B. 2000. The Younger Dryas cold interval as viewed from central Greenland. Quaternary Science Reviews, 19**,** 213-226.

Alley, R. B., Brook, E. J., and Anandakrishnan, S. 2002. A northern lead in the orbital band: north-south phasing of Ice-Age events. Quaternary Science Reviews, 21**,** 431-441.

Alley, R. B., and Clark, P. U. 1999. The deglaciation of the northern hemisphere: A global perspective. Annual Reviews of Earth and Planetary Sciences, 27**,** 149-182.

Antevs, E. 1953. Geochronology of the deglacial and neothermal ages. The Journal of Geology, 61**,** 195-230.

Applegate, P. J., Lowell, T. V., and Alley, R. B. 2008. Comment on "Absence of cooling in New Zealand and the adjacent Ocean during the Younger Dryas chronozone". Science, 320**,** 746d.

Ariztegui, D., Bianchi, M. M., Masaferro, J., Lafargue, E., and Niessen, F. 1997. Interhemispheric synchrony of Late-glacial climatic instability as recorded in proglacial Lake Mascardi, Argentina. Journal of Quaternary Science, 12**,** 333-338.

Barker, S., Diz, P., Vautravers, M. J., Pike, J., Knorr, G., Hall, I. R., and Broecker, W. S. 2009. Interhemispheric Atlantic seesaw response during the last deglaciation. Nature, 457, 1097-1102.

Barrows, T. T., Juggins, S., De Deckker, P., Calvo, E., and Pelejero, C. 2007a. Long-term sea surface temperature and climate change in the Australian-New Zealand region. Paleoceanography, 22**,** doi:10.1029/2006PA001328.

Barrows, T. T., Lehman, S. J., Fifield, L. K., and De Deckker, P. 2007b. Absence of cooling in New Zealand and the adjacent Ocean during the Younger Dryas chronozone. Science, 318**,** 86-89.

Barrows, T. T., Lehman, S. J., Fifield, L. K., and De Deckker, P. 2008. Response to comment on "Absence of cooling in New Zealand and the adjacent Ocean during the Younger Dryas chronozone." Science, 320**,** 746e.

Benway, H. M., Mix, A. C., Haley, B. A., and Klinkhammer, G. P. 2006. Eastern Pacific warm pool paleosalinity and climate variability: 0-30 kyr. Paleoceanography, 21**,** doi:10.1029/2005PA001208.

Berger, A., and Loutre, M.-F. 1991. Insolation values for the climate of the last 10 million years. Quaternary Science Reviews, 10**,** 297-317.

Blunier, T., and Brook, E. J. 2001. Timing of millennial-scale climate change in Antarctica and Greenland during the last glacial period. Science, 291**,** 109-112.

Boyle, E. A., and Keigwin, L. 1987. North Atlantic thermohaline circulation during the past 20,000 years linked to high-latitude surface temperature. Nature, 330**,** 35-40.

Braconnot, P., Otto-Bliesner, B., Harrison, S., Joussaume, S., Peterchmitt, J.-Y., Abe-Ouchi, A., Crucifix, M., Driesschaert, E., Fichefet, T., Hewitt, C. D., Kageyama, M., Kitoh, A., Loutre, M.-F., Marti, O., Merkel, U., Ramstein, G., Valdes, P., Weber, L., Yu, Y., and Zhao, Y. 2007. Results of PMIP2 coupled simulations of the mid-Holocene and Last Glacial Maximum – Part 2: feedbacks with emphasis on the location of the ITCZ and mid- and high latitudes heat budget. Climate of the Past, 3**,** 279-296.

Broccoli, A. J. 2000. Tropical cooling at the Last Glacial Maximum: An atmosphere-mixed layer ocean model simulation. Journal of Climate, 13, 951-976.

Broecker, W. S. 1994. Massive iceberg discharges as triggers for global climate change. Nature, 372**,** 421-424.

Broecker, W. S. 1998. Paleocean circulation during the last deglaciation: A bipolar seesaw? Paleoceanography, 13**,** 119-121.

Broecker, W. S. 2003. Does the trigger for abrupt climate change reside in the ocean or in the atmosphere? Science, 300**,** 1519-1522.

Cane, M., and Clement, A. C. 1999. A role for the tropical Pacific coupled ocean-atmosphere system on Milankovitch and millennial timescales. Part II: Global impacts. In: Clark, P.U., Webb, R.S., Keigwin, L.D. (Eds.), Mechanisms of Global Climate Change at Millennial Time Scales. American Geophysical Union, Washington, D.C, pp. 373-383.

Carlson, A. E., Clark, P. U., Haley, B. A., Klinkhammer, G. P., Simmons, K. R., Brook, E., and Meissner, K. J. 2007a. Geochemical proxies of North American freshwater routing during the Younger Dryas. Proceedings of the National Academy of Sciences, 104**,** 6556-6561.

Carlson, A. E., Clark, P. U., Raisbeck, G. M., and Brook, E. J. 2007b. Rapid Holocene deglaciation of the Labrador sector of the Laurentide Ice Sheet. Journal of Climate, 20**,** 5126-5133.

Carlson, A. E., LeGrande, A. N., Oppo, D. W., Came, R. E., Schmidt, G. A., Anslow, F. S., Licciardi, J. M., and Obbink, E. A. 2008a. Rapid early Holocene deglaciation of the Laurentide ice sheet. Nature Geoscience, 1**,** 620-624.

Carlson, A. E., Stoner, J. S., Donnelly, J. P., and Hillaire-Marcel, C. 2008b. Response of the southern Greenland Ice Sheet during the last two deglaciations. Geology, 36**,** 359-362.

Carlson, A. E., Oppo, D., Came, R. E., LeGrande, A. N., Keigwin, L., and Curry, W. B. 2008c. Subtropical salinity variability and Atlantic meridional circulation during deglaciation. Geology, 12, 991-994.

Chamberlin, T. C. 1897. A group of hypotheses bearing on climatic changes. Journal of Geology, 5**,** 653-683.

Chiang, J. C. H., Biasutti, M., and Battisti, D. S. 2003. Sensitivity of the Atlantic ITCZ to Last Glacial Maximum boundary conditions. Paleoceanography, 18**,** doi:10.1029/2003PA000916.

Chiang, J. C. H., and Bitz, C. M. 2005. The influence of high latitude ice on the position of the marine Intertropical Convergence Zone. Climate Dynamics, doi:10.1007/s00382-005-0040-5.

Clark, P. U., and Mix, A. C. 2002. Ice sheets and sea level of the Last Glacial Maximum. Quaternary Science Reviews, 21**,** 1-7.

Clark, P. U., Pisias, N. G., Stocker, T. F., and Weaver, A. J. 2002. The role of the thermohaline circulation in abrupt climate change. Nature, 415**,** 863-869.

Clark, P. U., McCabe, A. M., Mix, A. C., and Weaver, A. J. 2004. Rapid rise of sea level 19,000 years ago and its global implications. Science, 304**,** 1141-1144.

Clark, P. U., Hostetler, S., Pisias, N., Schmittner, A., and Meissner, K. J. 2007. Mechanisms for a ~7-kyr climate and sea-level oscillation during marine isotope stage 3. In: Schmittner, A., Chiang, J.C.H., Hemming, S. (Eds.), Ocean

Circulation: Mechanisms and Impacts. American Geophysical Union, Washington, D.C., pp. 315-334.

Clark, P. U., Dyke, A. S., Shakun, J. D., Carlson , A. E., Clark, J., Wohlfarth, B., Hostetler, S. W., and McCabe, A. M. 2009. The Last Glacial Maximum. Science, 325, 710-714.

Clement, A. C., and Cane, M. 1999. A role for the tropical Pacific coupled ocean-atmosphere system on Milankovitch and millennial timescales. Part II: A modeling study of tropical Pacific variability. In: Clark, P.U., Webb, R.S., Keigwin, L.D. (Eds.), Mechanisms of Global Climate Change at Millennial Time Scales. American Geophysical Union, Washington, D.C, pp. 363-371.

Clement, A. C., Cane, M. A., and Seager, R. 2001. An orbitally driven tropical source for abrupt climate change. Journal of Climate, 14**,** 2369-2375.

Clement, A. C., and Peterson, L. C. 2008. Mechanisms of abrupt climate change of the last glacial period. Reviews of Geophysics, 46**,** doi:10.1029/2006RG000204.

CLIMAP Project Members. 1976. The surface of the ice-age earth. Science, 191, 1131-1137.

Crowley, T. J. 1992. North Atlantic deep water cools the Southern Hemisphere. Paleoceanography, 7, 489-497.

Cuffey, K., and Clow, G. D. 1997. Temperature, accumulation, and ice sheet elevation in central Greenland through the last deglacial transition. Journal of Geophysical Research, 102**,** 26383-26396.

Denton, G. H., and Hendy, C. H. 1994. Younger Dryas age advance of Franz Josef glacier in the Southern Alps of New Zealand. Science, 264**,** 1434-1437.

Denton, G. H., Heusser, C. J., Lowell, T. V., Moreno, P. I., Andersen, B. G., Huesser, L. E., Schlüchter, C., and Marchant, D. R. 1999a. Interhemispheric linkage of paleoclimate during the last glaciation. Geografiska Annaler, 81A**,** 107-153.

Denton, G. H., Andersen, B. G., Heusser, L. E., Moreno, P. I., Marchant, D. R., Lowell, T. V., Heusser, C. J., and Schluchter, C. 1999b. Geomorphology, stratigraphy, and radiocarbon chronology of Llanquihue drift in the area of the southern Lake District, Seno Reloncavi, and Isla Grande de Chiloe, Chile. Geographiska Annaler Series A: Physical Geography, 81**,** 167-229.

Denton, G. H., Alley, R. B., Comer, G. C., and Broecker, W. S. 2005. The role of seasonality in abrupt climate change. Quaternary Science Reviews, 24**,** 1159-1182.

Douglass, D. C., Singer, B. S., Kaplan, M. R., Ackert, R. P., Mickelson, D. M., and Caffee, M. W. 2005. Evidence of early Holocene glacial advances in southern South America from cosmogenic surface-exposure dating. Geology, 33**,** 237-240.

Douglass, D. C., Singer, B. S., Kaplan, M. R., Mickelson, D. M., and Caffee, M. W. 2006. Cosmogenic nuclide surface exposure dating of boulders on last-glacial and late-glacial moraines, Lago Buenos Aires, Argentina: Interpretive strategies and paleoclimate implications. Quaternary Geochronology, 1**,** 43-58.

Gildor, H., and Tziperman, E. 2001. Physical mechanisms behind biogeochemical glacial-interglacial CO_2 variations. Geophysical Research Letters, 28**,** 2421-2424.

Grimm, E. C., Watts, W. A., Jacobson, J. G. L., Hansen, B. C. S., Almquist, H. R., and Dieffenbacher-Krall, A. C. 2006. Evidence for warm wet Heinrich events in Florida. Quaternary Science Reviews, 25**,** 2197-2211.

Haug, G. H., Hughen, K. A., Sigman, D. M., Peterson, L. C., and Rohl, U. 2001. Southward migration of the Intertropical Convergence Zone through the Holocene. Science, 293**,** 1304-1308.

Hoerling, T. C., and Kumar, A., 2000. Understanding and Predicting Extratropical Teleconnections Related to ENSO. In: Diaz, H, Markgraf, V. (Eds.), El Niño and the Southern Oscillation: Multi-scale Variability, and Global and Regional Impacts, Cambridge University Press, pp. 57-88.

Huesser, C. J., and Rabassa, J. 1987. Cold climatic episode of Younger Dryas age in Tierra del Fuego. Nature, 328**,** 609-611.

Huybers, P., and Denton, G. 2008. Antarctic temperature at orbital timescales controlled by local summer duration. Nature Geoscience, 1, 787-792.

Imbrie, J., Berger, A., Boyle, E. A., Clemens, S. C., Duffy, A., Howard, W. R., Kukla, G., Kutzbach, J., Martinson, D. G., McIntyre, A., Mix, A. C., Molfino, B., Morley, J. J., Peterson, L. C., Pisias, N. G., Prell, W. L., Raymo, M. E., Shackleton, N. J., and Toggweiler, J. R. 1993. On the structure and origin of major glaciation cycles. 2. The 100,000-year cycle. Paleoceanography, 8**,** 699-735.

Ivy-Ochs, S., Schlüchter, C., Kubik, P. W., and Denton, G. H. 1999. Moraine exposure dates imply synchronous Younger Dryas glacier advances in the European Alps and in the Southern Alps of New Zealand. Geografiska Annaler, 81**,** 313-323.

Jouzel, J., Vaikmae, R., Petit, J. R., Martin, M., Duclos, Y., Stievenard, M., Lorius, C., Toots, M., Melieres, M. A., Burckle, L. H., Barkov, N. I., and Kotlyakov, V. M. 1995. The two-step shape and timing of the last deglaciation in Antarctica. Climate Dynamics, 11, 151-161.

Kaplan, M. R., and Wolfe, A. P. 2006. Spatial and temporal variability of Holocene temperature in the North Atlantic region. Quaternary Research, 65**,** 223-231.

Kaplan, M. R., Fogwill, C. J., Sugden, D. E., Hulton, N. R. J., Kubik, P. W., and Freeman, S. P. H. T. 2008. Southern Patagonian glacial chronology for the Last Glacial period and implications for Southern Ocean climate. Quaternary Science Reviews, 27**,** 284-294.

Kaufman, D. S., Ager, T. A., Anderson, N. J., Anderson, P. M., Andrews, J. T., Bartlein, P. J., Brubaker, L. B., Coats, L. L., Cwynar, L. C., Duvall, M. L., Dyke, A. S., Edwards, M. E., Eisner, W. R., Gajewski, K., Geirsdóttir, A., Hu, F. S., Jennings, A. E., Kaplan, M. R., Kerwin, M. W., Lozhkin, A. V., MacDonald, G. M., Miller, G. H., Mock, C. J., Oswald, W. W., Otto-Bliesner, B. L., Porinchu, D. F., Rühland, K., Smol, J. P., Steig, E. J., and Wolfe, B. B. 2004. Holocene thermal maximum in the western Arctic (0-180°W). Quaternary Science Reviews, 23**,** 529-560.

Kawamura, K., Parrenin, F., Lisiecki, L., Uemura, R., Vimeux, F., Severinghaus, J. P., Hutterli, M. A., Nakazawa, T., Aoki, S., Jouzel, J., Raymo, M. E., Matsumoto, K., Nakata, H., Motoyama, H., Fujita, S., Goto-Azuma, K., Fujii, Y., and Watanabe, O. 2007. Northern Hemisphere forcing of climatic cycles in Antarctica over the past 360,000 years. Nature, 448**,** 912-916.

Kilian, R., Schneider, C., Koch, J., Fesq-Martin, M., Biester, H., Casassa, G., Arevalo, M., Wendt, G., Baeza, O., and Behrmann, J. 2007. Palaeoecological constraints on late Glacial and Holocene ice retreat in the Southern Andes (53°S). Global and Planetary Change, 59, 49-66.

Koutavas, A., Lynch-Stieglitz, J., Marchitto, T. M., Jr., and Sachs, J. M. 2002. El Niño-like pattern in Ice Age tropical Pacific sea surface temperature. Science, 297**,** 226-230.

Lambert, F., Delmonte, B., Petit, J. R., Bigler, M., Kaufman, P. R., Hutterli, M. A., Stocker, T. F., Ruth, U., Steffensen, J. P., and Maggi, V. 2008. Dust-climate

couplings over the past 800,000 years from the EPICA Dome C ice core. Nature, 452, 616-619.

Lea, D. W. 2003. Elemental and isotopic proxies of marine temperatures. In: Elderfield, H. (Ed.), The Oceans and Geochemistry, Elsevier-Pergamon, Oxford, pp. 365-390.

Lea, D. W., Pak, D. K., Peterson, L. C., and Hughen, K. A. 2003. Synchroneity of tropical and high-latitude Atlantic temperatures over the last glacial termination. Science, 301**,** 1361-1364.

Lea, D. W., Pak, D. K., Belanger, C. L., Spero, H. J., Hall, M. A., and Shackleton, N. J. 2006. Paleoclimate history of Galápagos surface waters over the last 135,000 yr. Quaternary Science Reviews, 25**,** 1152-1167.

Liu, Z., and Yang, H. 2003. Extratropical control on tropical climate: atmospheric bridge and oceanic tunnel. Geophysical Research Letters, 30**,** doi:10.1029/2002GL016492.

Liu, Z., Otto-Bliesner, B., He, F., Brady, E., Thomas, R., Clark, P.U., Carlson, A.E., Lynch-Stieglitz, J., Curry, W., Brook, E., Erickson, D., Jacob, R., Kutzbach, J., and Chen, J., 2009. Transient Climate Simulation of Last Deglaciation with a New Mechanism for Bølling-Allerød Warming. Science, 325, 310-314.

Lowell, T. V., Heusser, C. J., Andersen, B. G., Moreno, P. I., Hauser, A., Heusser, L. E., Schluchter, C., Marchant, D. R., and Denton, G. H. 1995. Interhemispheric correlation of Late Pleistocene glacial events. Science, 269**,** 1541-1549.

Lowell, T. V., and Kelly, M. A. 2008. Was the Younger Dryas global? Science, 321**,** 348-349.

Manabe, S., and Broccoli, A. J. 1985. The influence of continental ice sheets on the climate of an ice age. Journal of Geophsyical Research, 90, 2167-2190.

Mann, M. E., Zhangk, Z., Hughes, M. K., Bradley, R. S., Miller, S. K., Rutherford, S., and Ni, F. 2009. Proxy-based reconstructions of hemispheric and global surface temperature variations over the past two millennia. Proceedings of the National Academy of Sciences, 105, 13252-12257.

Mantua, N. J., and Hare, S. R. 2002. The Pacific Decadal Oscillation. Journal of Oceanography, 58**,** 35-44.

McCulloch, R. D., Fogwill, C. J., Sugden, D. E., Bentley, M. J., and Kubik, P. W. 2005. Chronology of the last glaciation in central Strait of Magellan and Bahia Inutil, southernmost South America. Geografiska Annaler, 87**,** 289-312.

McManus, J. F., Francois, R., Gherardi, J. M., Keigwin, L. D., and Brown-Leger, S. 2004. Collapse and rapid resumption of Atlantic meridional circulation linked to deglacial climate changes. Nature, 428**,** 834-837.

Mix, A. C. 2006. Running hot and cold in the eastern equatorial Pacific. Quaternary Science Reviews, 25**,** 1147-1149.

Mix, A. C., Ruddiman, W. F., and McIntyre, A. 1986a. Late Quaternary paleoceanography of the tropical Atlantic, 1: spatial variability of annual mean sea-surface temperatures, 0-20,000 years B.P. Paleoceanography, 1**,** 43-66.

Mix, A. C., Ruddiman, W. F., and McIntyre, A. 1986b. Late Quaternary paleoceanography of the tropical Atlantic, 2: the seasonal cycle of sea surface temperatures, 0-20,000 years B.P. Paleoceanography, 1**,** 339-353.

Mix, A. C., Bard, E., and Schneider, R. 2001. Environmental Processes of the Ice age: Land, Ocean, Glaciers (EPILOG). Quaternary Science Reviews, 20**,** 627-657.

Monnin, E., Indermühle, A., Dällenbach, A., Flückiger, J., Stauffer, B., Stocker, T. F., Raynaud, D., and Barnola, J.-M. 2001. Atmospheric CO_2 concentrations over the last glacial termination. Science, 291**,** 112-114.

Moreno, P. I., Jacobson, G. L. J., Lowell, T. V., and Denton, G. H. 2001. Interhemispheric climate links revealed by a late-glacial cooling episode in southern Chile. Nature, 409**,** 804-808.

Moreno, P.I., Kaplan, M.R., François, J.P., Villa-Martínez, R., Moy, C.M., Stern, C.R., and Kubik, P.W. 2009. Renewed glacial activity during the Antarctic cold reversal and persistence of cold conditions until 11.5 ka in southwestern Patagonia. Geology, 37, 375-378.

Otto-Bliesner, B. L., Brady, E. C., Clauzet, G., Tomas, R., Levis, S., and Kothavala, Z. 2006. Last Glacial Maximum and Holocene climate in CCSM3. Journal of Climate, 19, 2526-2544.

Peteet, D. 1995. Global Younger Dryas? Quaternary International, 28**,** 93-104.

Pinot, S., Ramstein, G., Harrison, S. P., Prentice, I. C., Guiot, J., Stute, M., and Joussaume, S. 1999. Tropical paleoclimates at the Last Glacial Maximum:

comparison of Paleoclimate Modeling Intercomparison Project (PMIP) simulations and paleodata. Climate Dynamics, 15, 857-874.

Putnam, A. E., Schaefer, J. M., Barrell, D. J. A., Vandergoes, M., Denton, G. H., Kaplan, M. R., Finkel, R. C., Schwartz, R., Goehring, B. M., Kelley, S. E. 2010. In situ cosmogenic ^{10}Be production-rate calibration from the Southern Alps, New Zealand. Quaternary Geochronology, doi:10.1016/j.quageo.2009.12.001.

Rasmussen, S. O., Andersen, K. K., Svensson, A. M., Steffensen, J. P., Vinther, B. M., Clausen, H. B., Siggaard-Andersen, M.-L., Johnsen, S. J., Larsen, L. B., Dahl-Jensen, D., Bigler, M., Rothlisberger, R., Fischer, H., Goto-Azuma, K., Hansson, M., and Ruth, U. 2006. A new Greenland ice core chronology of the last glacial termination. Journal of Geophysical Research, 111**,** doi:10.1029/2005JD006079.

Robinson, L. F., Adkins, J. F., Keigwin, L. D., Southon, J., Fernandez, D. P., Wang, S. L., and Scheirer, D. S. 2005. Radiocarbon variability in the western North Atlantic during the last deglaciation. Science, 310**,** 1469-1473.

Ropelewski, C. F., and Halpert, M. S. 1987. Global and regional scale precipitation patterns associated with the El Nino/Southern Oscillation (ENSO). Monthly Weather Review, 115**,** 1606-1626.

Rühlemann, C., Mulitza, S., Muller, P. J., Wefer, G., and Zahn, R. 1999. Warming of the tropical Atlantic Ocean and slowdown of thermohaline circulation during the last deglaciation. Nature, 402**,** 511-514.

Schmidt, M. W., Spero, H. J., and Lea, D. W. 2004. Links between salinity variation in the Caribbean and North Atlantic thermohaline circulation. Nature, 428**,** 160-163.

Schmittner, A., Saenko, O., and Weaver, A. J. 2003. Coupling of the hemispheres in observations and simulations of glacial climate change. Quaternary Science Reviews, 22**,** 659-672.

Schneider von Deimling, T., Ganopolski, A., Held, H., and Rahmstorf, S. 2006. How cold was the Last Glacial Maximum? Geophysical Research Letters, 33, doi:10.1029/2006GL026484.

Seager, R., Harnik, N., Robinson, W. A., Kushnir, Y., Ting, M. F., Huang, H. P., and Velez, J. 2005. Mechanisms of ENSO-forcing of hemispherically symmetric precipitation variability. Quarterly Journal of the Royal Meteorological Society, 131**,** 1501-1527.

Shackleton, N. J. 2000. The 100,000 year Ice-Age cycle identified and found to lag temperature, carbon dioxide and orbital eccentricity. Science, 289**,** 1897-1902.

Stott, L., Timmermann, A., and Thunell, R. 2007. Southern hemisphere and deep-sea warming led deglacial atmospheric CO_2 rise and tropical warming. Science, 318**,** 435-438.

Stouffer, R. J., Yin, J., Gregory, J. M., Dixon, K. W., Spelman, M. J., Hurlin, W., Weaver, A. J., Eby, M., Flato, G. M., Hasumi, H., Hu, A., Jungclaus, J. H., Kamenkovich, I. V., Levermann, A., Montoya, M., Murakami, S., Nawrath, S., Oka, A., Peltier, W. R., Robitaille, D. Y., Sokolov, A., Vettoretti, G., and Weber, S. L. 2006. Investigating the causes of the response of the thermohaline circulation to past and future climate changes. Journal of Climate, 19**,** 1365-1387.

Strelin, J. A., and Malagnino, E. C. 2000. Late-glacial history of Lago Argentino, Argentina, and age of the Puerto Bandera moraines. Quaternary Research, 54**,** 339-347.

Sugden, D. 2005. Late-glacial glacier events in southernmost South America and their global significance. Geografiska Annaler, 87**,** 271-271.

Sugden, D., Bentley, M. J., Fogwill, C. J., Hulton, N. R. J., McCulloch, R. D., and Purves, R. S. 2005. Late-Glacial glacier events southernmost South America: a blend of "northern" and "southern" hemispheric climatic signals? Geografiska Annaler, 87A**,** 273-288.

Thompson, D. W. J., Kennedy, J. J., Wallace, J. M., and Jones, P. D. 2008. A large discontinuity in the mid-twentieth century in observed global-mean surface temperature. Nature, 453**,** 646-649.

Tovar, D. S., Shulmeister, J., and Davies, T. R. 2008. Evidence for a landslide origin of New Zealand's Waiho Loop moraine. Nature Geoscience, 1, 524-526.

Turney, C. S. M., Roberts, R. G., de Jonge, N., Prior, C., Wilmshurst, J. M., McGlone, M. S., and Cooper, J. 2007. Redating the advance of the New Zealand Franz Josef Glacier during the last termination: evidence for asynchronous climate change. Quaternary Science Reviews, 26**,** 3037-3042.

Visser, K., Thunell, R., and Stott, L. 2003. Magnitude and timing of temperature change in the Indo-Pacific warm pool during deglaciation. Nature, 421**,** 152-155.

Weaver, A. J., Saenko, O., Clark, P. U., and Mitrovica, J. X. 2003. Meltwater pulse 1A from Antarctica as a trigger of the Bølling-Allerød warm interval. Science, 299**,** 1709-1713.

Weldeab, S., Schneider, R. R., and Kölling, M. 2006. Deglacial sea surface temperature and salinity increase in the western tropical Atlantic in synchrony with high latitude climate instabilities. Earth and Planetary Science Letters, 241**,** 699-706.

Yancheva, G., Nowaczyk, N. R., Mingram, J., Dulski, P., Schettler, G., Negendank, J. F. W., Liu, J., Sigman, D. M., Peterson, L. C., and Haug, G. H. 2007. Influence of the intertropical convergence zone on the East Asian monsoon. Nature, 445**,** 74-77.

Zhang, R., and Delworth, T. L. 2005. Simulated tropical response to a substantial weakening of the Atlantic thermohaline circulation. Journal of Climate, 18, 1853-1860.

Chapter 4

The Role of CO_2 During the Last Deglaciation

Jeremy D. Shakun[1] and Peter U. Clark[1]

[1]Department of Geosciences, Oregon State University
Corvallis, OR 97331

In preparation for submission to Science

4.1 Abstract

The role of greenhouse gases in Quaternary climate change remains unclear (Huybers, 2009; Dorale et al., 2010). While CO_2 is often considered the globalizer of glacial cycles and thus a major forcing, the lag of CO_2 behind Antarctic temperature in the ice-core record (Monnin et al., 2001) may imply CO_2 is a feedback of more modest importance (e.g., Toggweiler and Lea, 2010). As the relationship between local temperature and a global forcing such as CO_2 may not be straightforward due to heat redistributions within the climate system, however, we analyze a global network of proxy records to determine how global mean temperature varied during the last deglaciation. We find that global temperature was strongly correlated and varied near-synchronously with CO_2, suggesting a primary role for greenhouse gases in driving warming and the global deglaciation. Differences in the temperature evolution of the Northern and Southern Hemispheres are largely attributable to the seesawing of heat between them in response to variations in the strength of the Atlantic Meridional Overturning Circulation (AMOC). Deglacial warming began synchronously throughout the Southern Hemisphere and tropics at ~19 ka and was coeval with northern extratropical cooling. These temperature patterns may reflect the response to a collapse of the AMOC due to boreal insolation-driven melting of northern ice sheets, which points to a classic Milankovitch trigger for the last deglaciation.

4.2 Introduction

Quaternary ice ages were ultimately tied to periodic variations in earth's orbital parameters (Hays et al., 1976). Nonetheless, a "fly in the ointment" for Milankovitch theory has long been the synchroneity of ice age terminations between the hemispheres despite opposing insolation forcing (Mercer, 1984). Greenhouse gases have often been invoked to explain this synchronization, implying a leading role for them in driving global climate (Broecker, 1982; Genthon et al., 1987; Shackleton, 2000; Schaefer et al., 2006). On the other hand, the lag of CO_2 behind Antarctic temperature in the ice core record (Monnin et al., 2001; Caillon et al., 2003) has been

taken to imply a lesser role for greenhouse gases as a feedback on global warming rather than its primary driver. This CO_2 lag has also been widely discussed in popular literature and media as refuting the link between greenhouse gases and climate change. Lastly, the conventional wisdom that terminations were globally synchronous has recently been challenged by the hypothesis that they were instead characterized by massive redistributions of heat between the hemispheres, which would even further downplay the role of CO_2 in driving global warming (Toggweiler and Lea, 2010). Critically, none of these conflicting viewpoints on the role of CO_2 in global climate change have been demonstrated empirically. Here, we use a global dataset of 77 high-resolution proxy temperature records to show that CO_2 was the major driver of global warming and synchronized the hemispheres during the last deglaciation. Our results also bear on the processes triggering deglaciation.

4.3 Methods

The records used in this study are based on various calibrated temperature proxies including alkenones, Mg/Ca, TEX_{86}, pollen, bioassemblages and provide reasonable coverage of the globe (Figure 4.1). All 77 records span 19-11 ka and 70 extend to 6.5 ka. They are combined as unweighted averages to yield mean temperature time series for the globe and various regions of interest. All ^{14}C dates were recalibrated with CALIB 6.0.1 using the INTCAL09 and MARINE09 calibrations (Reimer et al., 2009). ^{14}C reservoir corrections were taken from the original publications. Proxy values were converted into temperature units with the calibrations used by the original authors, except alkenone records, which were exclusively calibrated with the global core-top calibration of Müller et al. (1998). We used a Monte Carlo approach to fully account for chronological and temperature uncertainty in the records. Specifically, calibrated ^{14}C dates were allowed to vary within their error bars and age model "jitter" between ^{14}C dates was modeled following Huybers and Wunsch (2004) using a jitter value of 100. Ice core and records tuned to ice cores were assumed to have 2% chronological uncertainty (1σ).

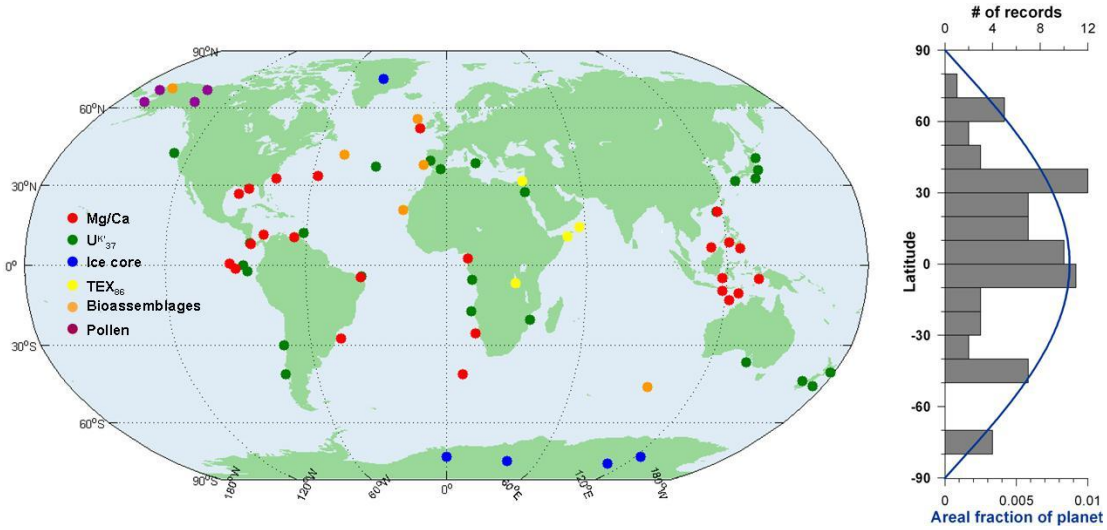

Figure 4.1: The locations of the proxy records utilized in this study. Symbol color denotes the proxy type. The histogram on the right shows the latitudinal distribution of the records (gray), and the blue line shows the areal fraction of the planet by latitude.

Temperature uncertainties (1σ) were taken to be 1.7°C for TEX_{86} (Kim et al., 2008), 1.5°C for pollen and bioassemblages, 10% for ice cores (Jouzel et al., 2003), and are based on quoted calibration errors for Mg/Ca (Anand et al., 2003) and alkenones (Müller et al., 1998). We assumed temperature errors are random through time and among records, which is a maximally conservative approach as errors are likely autocorrelated.

4.4 Global Temperature and CO_2

Information on the phasing of temperature and CO_2 at a given locale, such as from Antarctic ice cores, is important for understanding the mechanisms governing internal climate dynamics. Nonetheless, the temperature of the earth as a whole must be considered when addressing the importance of a global radiative forcing such as CO_2 since heat redistributions within the climate system may confound the greenhouse forced signal in any particular location (Lindzen, 1993; Hoffert and Covey, 1993). Accordingly, we calculate the mean of the 77 globally distributed proxy records over the last deglaciation. This global mean temperature time series shows a two-step rise, with warming concentrated during the Oldest and Younger Dryas intervals and relatively flat temperatures during the Last Glacial Maximum (LGM), Bølling/Allerød, and early Holocene (Figure 4.2d). Atmospheric CO_2 exhibits a similar two-step structure during the last deglaciation and is strongly correlated with global temperature (r^2=0.95) (Figure 4.2c). We use lag correlations to address the phasing of CO_2 and global temperature and find CO_2 exhibited a small but insignificant lead of 45 ± 130 years from 19-11 ka, increasing to 835 ± 240 years when considering the entire time interval of ice sheet melting from 19-6.5 ka (Figure 4.3). We note that a modest, but perhaps significant, 0.25°C warming precedes the initial rise in CO_2 at ~17.5 ka, suggesting that CO_2 was not the initial trigger of deglaciation. Nonetheless, these two points – the close correlation and phasing of global temperature and CO_2 – implicate CO_2 as a major driver of global deglaciation and highlight its importance in controlling global temperature.

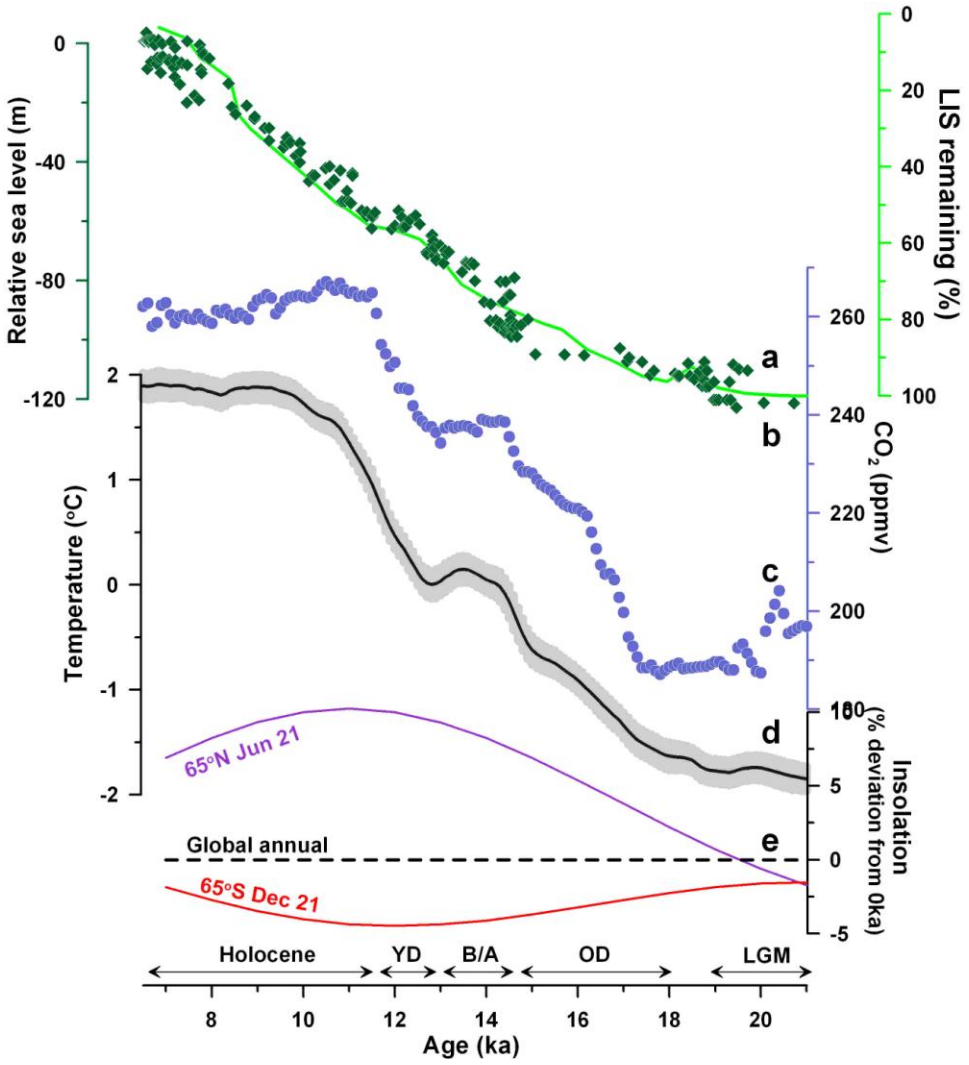

Figure 4.2: Global mean temperature and climate forcings over the last deglaciation. (**a**) Laurentide Ice Sheet area (Dyke, 2004). (**b**) Relative sea level (Clark and Mix, 2002). (**c**) Atmospheric CO_2 from the Dome C ice core (Monnin et al., 2001) on the Lemieux-Dudon et al. (2010) age model, which is the most recent and likely most accurate chronology. (**d**) Global mean temperature anomalies with 1σ errors due to chronological and proxy calibration uncertainties estimated from 1000 Monte Carlo simulations. (**e**) Insolation forcing for 65°N (purple) and 65°S (red) on the local summer solstice and global mean annual insolation (dashed black) (Laskar et al., 2004). The Holocene, Younger Dryas (YD), Bølling/Allerød (B/A), Oldest Dryas (OD), and Last Glacial Maximum (LGM) intervals are denoted.

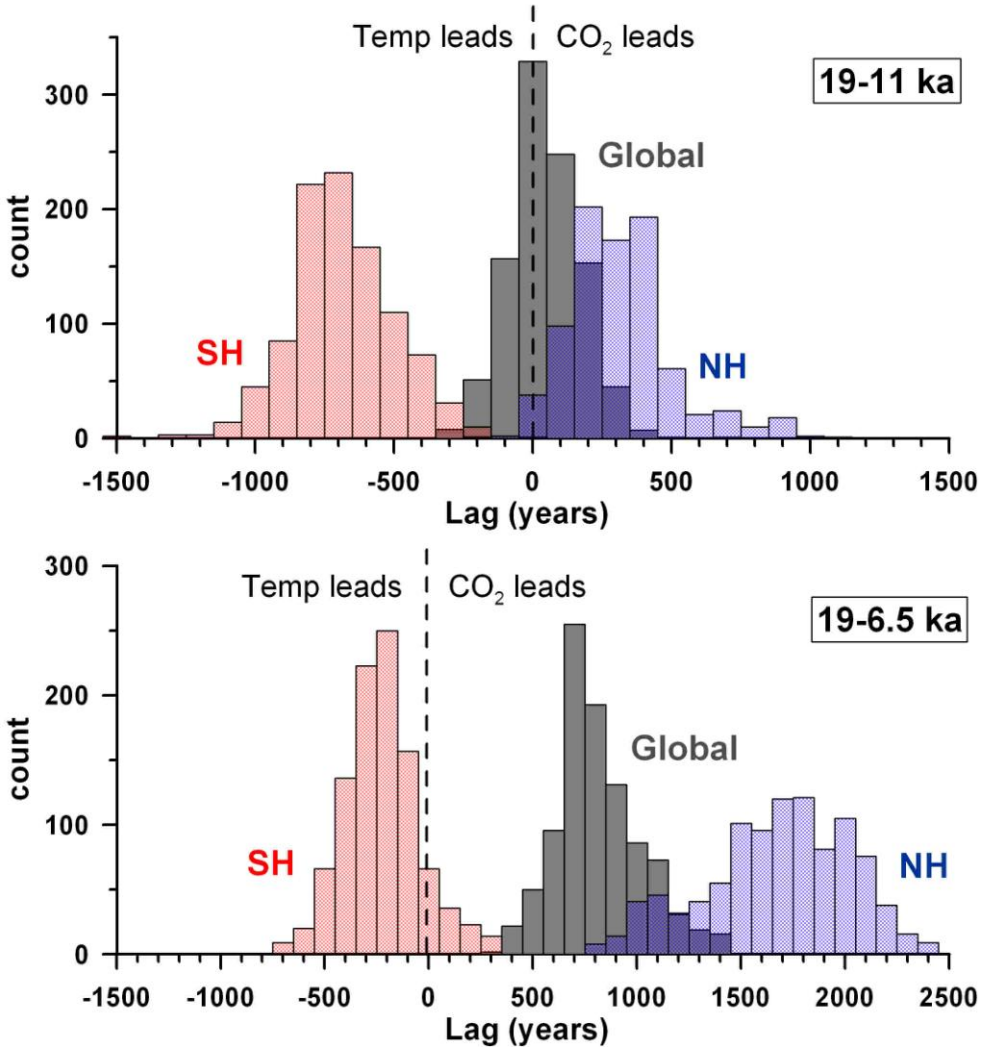

Figure 4.3: The phasing of CO_2 and temperature for the globe (gray) and Northern (blue) and Southern (red) Hemispheres based on lag correlations over 19-11 ka (top) and 19-6.5 ka (bottom). 1000 temperature time series were used for each geographic area derived from Monte Carlo simulations perturbing the proxy records with chronological and proxy temperature error. Note the different scales in the two plots.

The close link between global temperature and CO_2 may seem surprising given that ice sheets exerted an equal, if not larger, radiative forcing than greenhouse gases during the deglaciation (Jansen et al., 2007; Köhler et al., 2010). It is clear, however, that ice sheet melting exhibited markedly different temporal variability than the global temperature time series and thus apparently did not greatly influence it. Global ice volume was relatively stable during intervals of maximum warming such as the Oldest and Younger Dryas, while the greatest melting occurred during temperature plateaus around 19 ka, the Bølling/Allerød, and the early Holocene (Figure 4.2b). While ice sheet area, rather than volume, is the relevant term for forcing temperature change through its effect on planetary albedo, the similarity of the Laurentide Ice Sheet areal extent and relative sea level records indicates that sea level provides a reasonable proxy for ice sheet area (Figure 4.2a). Climate models provide the physical basis for understanding the dominance of the greenhouse-gas signal identified here. While the forcing from well-mixed greenhouse gases was globally uniform at the LGM, ice-sheet albedo forcing was confined to the ice-covered areas in the Northern Hemisphere (Broccoli, 2000). The thermal response to these forcings reflected these disparate spatial patterns. In contrast to the global-scale cooling from greenhouse gases, the thermal response to ice-sheet forcing remained confined to the Northern Hemisphere, with strong cooling over the ice sheets and only modest to no cooling in the northern tropics and subtropics (Manabe and Broccoli, 1985; Broccoli and Manabe, 1987; Broccoli, 2000). The proxy network utilized in this study thus remains removed from the largest effects of the ice sheets. Further confirmation of the modest ice-sheet imprint on the global mean time series is its ~4°C warming over the deglaciation, which is considerably less than the 5.8 ± 1.4°C estimated for LGM cooling from data-constrained modeling (Schneider von Deimling et al., 2006). As proxy records cannot sample regions previously covered by ice, unlike climate models, the smaller proxy-based warming estimate may reflect the attenuated ice-sheet signal it records. Despite this limitation in fully constraining global temperature changes, we suggest that including ice-covered areas in our global mean temperature

time series (were it possible) would cause it to lag CO_2 by an even greater amount given the relatively late timing of ice sheet melting.

Orbital forcing likewise cannot explain much of the rise in global mean temperature over the deglaciation. Insolation varies as a smooth sinusoid and does not exhibit the prominent steps and plateaus seen in global temperature. It is also antiphased between the hemispheres and essentially invariant in the global annual mean (~0.005% variation since the LGM) (Figure 4.2e). Climate models confirm the regional importance but small global effect of insolation variations (Weaver et al., 1998; Broccoli, 2000).

4.5 Hemispheric Temperatures and AMOC

The in-phase relationship between global temperature and CO_2 differs from the previously identified lag of CO_2 relative to Antarctic temperature (Monnin et al., 2001), which suggests spatial variability in the pattern of deglacial warming. We therefore calculate Northern and Southern Hemisphere mean temperature time series to explore this variability. Both hemispheres show a two-step warming pattern like the global mean and atmospheric CO_2 (Figure 4.4a,b), though lag correlations suggest the south led CO_2 whereas the north lagged it (Figure 4.3). The major difference between the hemispheric time series is that the north exhibits modest coolings coincident with the onset of southern warmings, and the warming steps are concave-up in the north but concave-down in the south. The mirrored nature of these structures suggests that they might result from heat redistributions between the hemispheres rather than climate changes isolated to one hemisphere. Differencing the Northern and Southern Hemisphere mean temperature time provides a means of investigating such heat redistributions. The resulting delta-T time series reveals two large millennial-scale oscillations that are one-quarter to one-half of the glacial-interglacial range in global temperature (Figure 4.4c).

Variations in the strength of the Atlantic Meridional Overturning Circulation (AMOC) provide a potential mechanism to explain variability in delta-T as the AMOC

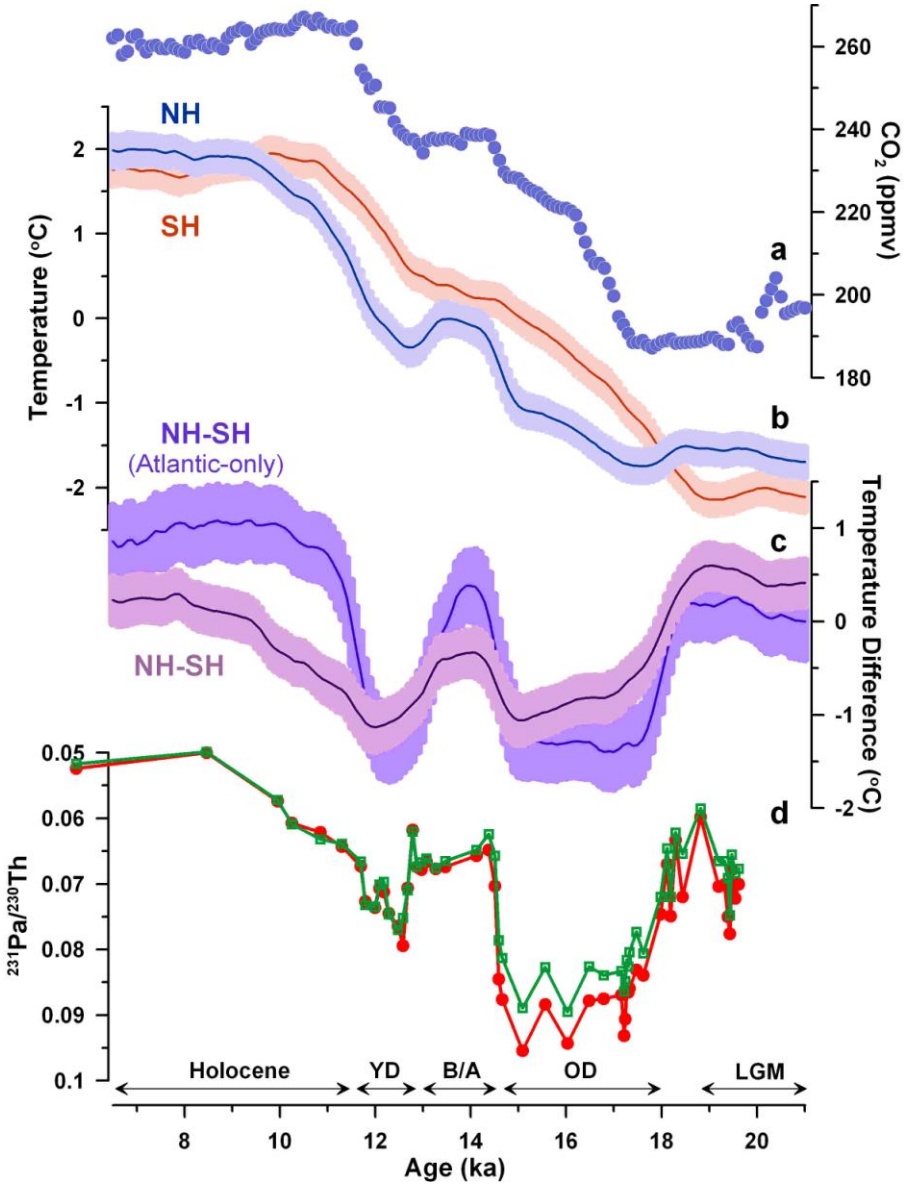

Figure 4.4: Hemispheric temperatures during the last deglaciation. (**a**) Atmospheric CO_2 as in Figure 4.2. (**b**) Northern (blue) and Southern (red) Hemisphere mean temperature anomalies with 1σ errors. (**c**) Difference between Northern and Southern Hemispheric mean temperatures with 1σ errors (light purple). Difference between North and South Atlantic mean temperatures with 1σ errors (blue-purple). (**d**) North Atlantic sediment core OCE326-GGC5 $^{231}Pa/^{230}Th$, a proxy for the strength of the AMOC (McManus et al., 2004). Time interval designations are shown at the bottom as in Figure 4.2.

is a major agent of cross-equatorial heat transport and currently warms the Northern Hemisphere at the expense of the Southern Hemisphere (Crowley, 1992; Broecker, 1998; Toggweiler and Lea, 2010). Comparison of delta-T with a North Atlantic Pa/Th record, which is interpreted as a kinematic proxy for the strength of the AMOC (McManus et al., 2004), reveals a notable correlation (Figure 4.4d). Delta-T decreases during the Oldest and Younger Dryas intervals when the AMOC is weak and heat exchange between the hemispheres is reduced, and delta-T increases during the LGM, Bolling/Allerod, and Holocene when the AMOC is strong and exporting southern heat to the north. Recalculating delta-T for Atlantic-only records yields the same structures, but they are larger and more rapid as would be expected given the importance of the AMOC in this ocean basin (Figure 4.4c). These hemispheric time series thus provide strong support for an anti-phased seesaw response to AMOC variations during the last deglaciation superimposed upon globally in-phase warming due to CO_2 (Shakun and Carlson, 2010). The similar magnitude of deglacial warming in both time series (~4°C) also reinforces the spatially restricted influence of northern ice sheets on temperature, as models suggest that the Northern Hemisphere warmed significantly more than the Southern Hemisphere due to the added ice-sheet forcing in the north (Broccoli, 2000; Schnedier von Deimling et al., 2006).

4.6 Temperatures by Latitude and the Deglacial Trigger

The hemispheric time series above, as well as earlier work (Imbrie et al., 1992; Charles et al., 1996; Bard et al., 1997; Petit et al., 1999; Stott et al., 2007), indicate that the Southern Hemisphere began warming before the Northern Hemisphere during the last deglaciation. Nonetheless, it has long been known that glacial cycles varied in phase with boreal summer insolation (Hays et al., 1976; Roe, 2006), which would seem to imply a northern lead during deglaciation. At least three hypotheses exist to explain this apparent paradox. First, boreal summer insolation could trigger southern warming and rising CO_2 via an oceanic or atmospheric teleconnection (Imbrie et al., 1992; Clark et al., 2004, 2009; Barker et al., 2009; Anderson et al., 2009). Second,

austral summer length covaries with boreal summer intensity, and it has been suggested that these local insolation forcings could drive approximately synchronous deglaciations in each hemisphere (Huybers and Denton, 2008). Third, austral spring insolation could have induced Southern Ocean sea ice retreat, warming, and CO_2 outgassing, leading to global deglaciation (Stott et al., 2007).

These three mechanisms would be expected to produce different spatiotemporal patterns of temperature variability at the onset of deglaciation, suggesting a means of evaluating them. We therefore calculate mean temperature time series for 30° latitude bins. The two northernmost bins (60-90°N and 30-60°N) are dominated by the millennial-scale oscillations of the Oldest Dryas-Bølling/Allerød-Younger Dryas sequence, followed by strong warming into the early Holocene as the northern ice sheets retreated (Figure 4.5c,d). These patterns likely reflect the importance of AMOC and ice sheet variations in the northern extratropics (Figure 4.5a,b). The northern tropical and Southern Hemisphere bins, on the other hand, show a more gradual warming pattern with an increasingly two-step structure moving southward (Figure 4.5e-h). These four bins also reach interglacial warmth by the onset of the Holocene. Temperature variability in these regions thus closely resembles atmospheric CO_2 (Figure 4.5i), consistent with a greater relative role for greenhouse forcing in these areas.

A striking feature of Figure 4.5 is the near-synchroneity of warming from 30°N to 90°S and cooling from 30°N to 90°N commencing at ~19 ka. The close temporal association of these events suggests that they are related. Northern Hemisphere ice sheet melting began at ~19 ka in response to boreal summer insolation, producing the 19-kyr melt water pulse (mwp) (Figure 4.5a) (Clark et al., 2004, 2009). The resulting freshwater flux to the North Atlantic may have caused a collapse of the AMOC at this time, which is recorded in the Pa/Th proxy (Figure 4.5b) (McManus et al., 2004) and would have induced the observed northern cooling and tropical-southern warming. Earlier and more rapid warming is evident in the tropics and southern mid-latitudes than over Antarctica, which may be related to the large

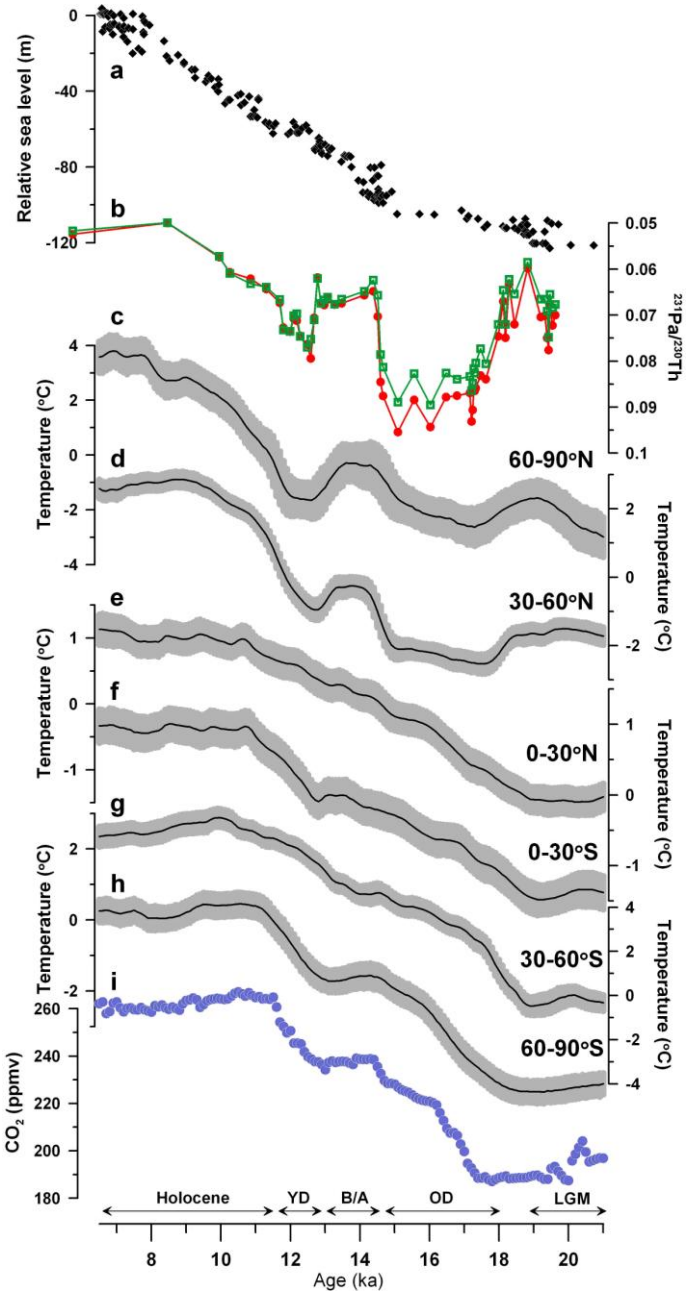

Figure 4.5: Deglacial temperature variations by latitude and climate forcings. (**a**) Relative sea level (Clark and Mix, 2002). (**b**) North Atlantic core OCE326-GGC5 $^{231}Pa/^{230Th}$ (McManus et al., 2004). Mean temperature and 1σ range for (**c**) 60-90°N, (**d**) 30-60°N, (**e**) 0-30°N, (**f**) 0-30°S, (**g**) 30-60°S, and (**h**) 60-90°S. Note the different temperature scales. (**i**) Atmospheric CO_2 as in Figure 4.2. Time interval designations are shown at the bottom as in Figure 4.2.

thermal inertia of the Southern Ocean surrounding it. Southern Ocean warming and the resulting decrease in sea-ice cover and stratification are then thought to have caused CO_2 outgassing (Monnin et al., 2001; Anderson et al., 2009; Skinner et al., 2010).

These latitudinal temperature variations thus support the first deglacial trigger hypothesis outlined above, with northern summer insolation causing southern warming via an oceanic seesaw and the resulting rise in CO_2 yielding global warming in turn. The latter two hypotheses focus on southern high latitude insolation to trigger southern warming at ~19 ka, but these localized forcings cannot readily account for the simultaneous tropical warming and northern cooling or the associated 19-kyr mwp and AMOC collapse.

4.7 Conclusions

Southern Hemisphere warming during the last deglaciation is partially attributable to a bipolar-seesaw response to AMOC variations, which can explain the lead of Antarctic temperature over CO_2 recorded in ice cores. This southern seesaw warming is part of an interhemispheric heat redistribution, however, that is counterbalanced by northern cooling and largely cancels out in the global mean (Weaver et al., 1998). As a result, global average temperature generally varied in phase with atmospheric CO_2. Our results underscore the importance of insolation, ice sheets, and ocean circulation in affecting temperature on a regional scale and triggering deglaciation, and point to the critical role played by CO_2 in driving global warming during this time.

4.8 Acknowledgments

Discussions with numerous people contributed to this research, including E. J. Brook, A. E. Carlson, S. A. Marcott, A. C. Mix, N. G. Pisias, and J. Shaman. Datasets were provided by S. Barker, T. Barrows, E. Calvo, G. Danabasoglu, M. Eby, N. R. Edwards, A. Ganopolski, H. Goosse, P. B. Holden, A. Jonko, J. Kaiser, A. Koutavas,

M.-F. Loutre, V. Peck, C. Pelejero, J.-R. Petit, J. Sachs, E. Schefub, A. Sokolov, J. Tierney, and G. Wei. The NOAA NGDC and PANGAEA databases were also essential to this work. J.D.S. and P.U.C. are supported by the National Science Foundation Paleoclimate Program.

4.9 References

Anand, P., Elderfield, H. and Conte, M. H. 2003. Calibration of Mg/Ca thermometry in planktonic foraminifera from a sediment trap time series. Paleoceanography, 18, 1050, doi:10.1029/2002PA000846.

Anderson, R. F., Ali, S., Bradtmiller, L. I., Nielsen, S. H. H., Fleisher, M. Q., Anderson, B. E., and Burckle, L. H. 2009. Wind-driven upwelling in the Southern Ocean and the deglacial rise in atmospheric CO_2. Science, 323, 1443-1448.

Bard, E., Rostek, F., and Sonzogni, C. 1997. Interhemispheric synchrony of the last deglaciation inferred from alkenone palaeothermometry. Nature, 385, 707-710.

Barker, S., Diz, P., Vautravers, M. J., Pike, J., Knorr, G., Hall, I. R., and Broecker, W. S. 2009. Interhemispheric Atlantic seesaw response during the last deglaciation. Nature, 457, 1097-1102.

Broccoli, A. J. and Manabe, S. 1987. The influence of continental ice, atmospheric CO_2, and land albedo on the climate of the last glacial maximum. Climate Dynamics, 1, 87-99.

Broecker, W. S. 1982. Glacial to interglacial changes in ocean chemistry. Progress in Oceanography, 11, 151-197.

Broecker, W. S. 1998. Paleocean circulation during the last deglaciation: A bipolar seesaw? Paleoceanography 13, 119-121.

Caillon, N., Severinghaus, J. P., Jouzel, J., Barnola. J.-M., Kang, J., and Lipenkov, V. Y. 2003. Timing of atmospheric CO_2 and Antarctic temperature changes across Termination III. Science, 299, 1728-1731.

Charles, C., Lynch-Stieglitz, J., Ninnemann, U. S., and Fairbanks, R. 1996. Climate connections between the hemisphere revealed by deep sea sediment core/ice core correlations. Earth and Planetary Science Letters, 142, 19-27.

Clark, P. U., and Mix, A. C. 2002. Ice sheets and sea level of the Last Glacial Maximum. Quaternary Science Reviews, 21**,** 1-7.

Clark, P. U., McCabe, A. M., Mix, A. C., and Weaver, A. J. 2004. Rapid rise of sea level 19,000 years ago and its global implications. Science, 304**,** 1141-1144.

Clark, P. U., Dyke, A. S., Shakun, J. D., Carlson , A. E., Clark, J., Wohlfarth, B., Hostetler, S. W., and McCabe, A. M. 2009. The Last Glacial Maximum. Science, 325, 710-714.

Crowley, T. J. 1992. North Atlantic Deep Water cools the Southern Hemisphere. Paleoceanography, 7, 489-497.

Dorale, J. A., Onac, B. P., Fornós, J. J., Ginés, J., Ginés, A., Tuccimei, P., and Peate, D. W. 2010. Sea-level highstand 81,000 years ago in Mallorca. Science, 327, 860-863.

Dyke, A. S. 2004. An outline of North American deglaciation with emphasis on central and northern Canada. Quaternary glaciations – extent and chronology, part II. North America (eds. Ehlers, J. and Gibbard, P. L.) (Elsevier Science and Technology Books).

Genthon, G., Barnola, J. M., Raynaud, D., Lorius, C., Jouzel, J., Barkov, N. I., Korotkevich, Y. S., and Kotlyakov, V. M. 1987. Vostok ice core: climatic response to CO2 and orbital forcing changes over the last climatic cycle. Nature, 329, 414-418.

Hays, J. D., Imbrie, J., and Shackleton, N. J. 1976. Variations in the Earth's orbit; Pacemaker of the ice ages. Science, 194, 1121-1132.

Hoffert, M. I., and Covey, C. 1993. Palaeoclimate sensitivity: response. Nature, 363, 26.

Huybers, P., and Wunsch, C. 2004. A depth-derived Pleistocene age model: Uncertainty estimates, sedimentation variability, and nonlinear climate change. Paleoceanography, 19, PA1028, doi:10.1029/2002PA000857.

Huybers, P. 2009. Antarctica's orbital beat. Science, 325, 1085-1086.

Huybers, P., and Denton, G. 2008. Antarctic temperature at orbital timescales controlled by local summer duration. Nature Geoscience, 1, 787-792.

Imbrie, J., Boyle, E. A., Clemens, S. C., Duffy, A., Howard, W. R., Kukla, G., Kutzbach, J., Martinson, D.G., McIntyre, A., Mix, A.C., Molfino, B., Morley,

J. J., Peterson, L. C., Pisias, N. G., Prell, W. L., Raymo, M. E., Shackleton, N. J., and Toggweiler, J. R. 1992. On the structure and origin of major glaciation cycles 1. Linear responses to Milankovitch forcing. Paleoceanography, 7, 701-738.

Jansen, E. et al. 2007. Palaeoclimate. Climate Change 2007: The Scientific Basis. Contribution of Working Group I to the Fourth Assessment Report of the Intergovernmental Panel on Climate Change (eds. Solomon, S. et al.) (Cambridge Univ. Press, Cambridge, UK).

Jouzel, J., Vimeux, F. Caillon, N., Delaygue, G., Hoffmann, G., Masson-Delmotte, V., and Parrenin, F. 2003. Magnitude of isotope/temperature scaling for interpretation of central Antarctic ice cores. Journal of Geophysical Research, 108, doi:10.1029/2002JD002677.

Kim, J.-H., Schouten, S., Hopmans, E. C., Donner, B., Sinninghe Damste, J. S. 2008. Global sediment core-top calibration of the TEX_{86} paleothermometer in the ocean. Geochemica et Cosmochica Acta, 72, 1154-1173.

Köhler, P., Bintanja, R., Fischer, H., Joos, F., Knutti, R., Lohmann, G., and Masson-Delmotte, V. 2010. What caused Earth's temperature variations during the last 800,000 years? Data-based evidence on radiative forcing and constraints on climate sensitivity. Quaternary Science Reviews, 29, 129-145.

Laskar, J., Robutel, P., Joutel, F., Gastineau, M., Correia, A. C. M. and Levrard, B. A. 2004. Long-term numerical solution for the insolation quantities of the Earth. Astronomy and Astrophysics, 428, 261-285.

Lemieux-Dudon, B., Blayo, E., Petit, J.-R., Waelbroeck, C., Svensson, A., Ritz, C., Barnola, J.-M., Narcisi, B., and Parrenin, F. 2010. Consistent dating for Antarctic and Greenland ice cores. Quaternary Science Reviews, 29, 8-20.

Lindzen, R. S. 1993. Palaeoclimate sensitivity. Nature, 363, 25-26.

Manabe, S. and Broccoli, A. J. 1985. The influence of continental ice sheets on the climate of an ice age. Journal of Geophysical Research, 90, 2167-2190.

McManus, J. F., Francois, R., Gherardi, J.-M., Keigwin, L. D., and Brown-Leger, S. 2004. Collapse and rapid resumption of Atlantic meridional circulation linked to deglacial climate changes. Nature, 428, 834-837.

Mercer, J. 1984. In: Ewing, M. (Ed.), Climate Processes and Climate Sensitivity. American Geophysical Union, Washington D.C., pp. 307-313.

Monnin, E., Indermühle, A., Dällenbach, A., Flückiger, J., Stauffer, B., Stocker, T. F., Raynaud, D., and Barnola, J.-M. 2001. Atmospheric CO_2 concentrations over the last glacial termination. Science, 291**,** 112-114.

Müller, P. J., Kirst, G., Ruhland, G., von Storch, I., Rosell-Melé, A. 1998. Calibration of the alkenone paleotemperature index $U^{K'}_{37}$ based on core-tops from the eastern South Atlantic and the global ocean (60°N-60°S). Geochimica et Cosmochimica Acta, 62, 1757-1772.

Petit, J. R., Jouzel, J., Raynaud, D., Barkov, N. I., Barnola, J.-M., Basile, I., Bender, M., Chappellaz, J., Davis, M., Delaygue, G., Delmotte, M., Kolyakov, V. M., Legrand, M., Lipenkov, V. Y., Lorius, C., Pépin, L., Ritz, C., Saltzman, E., and Stievenard, M. 1999. Climate and atmospheric history of the past 420,000 year from the Vostok ice core, Antarctica. Nature, 399, 429-436.

Reimer, P. J., Baillie, M. G. L., Bard, E., Bayliss, A., Beck, J. W., Blackwell, P. G., Bronk Ramsey, C., Buck, C. E., Burr, G. S., Edwards, R. L., Friedrich, M., Grootes, P. M., Guilderson, T. P., Hajdas, I., Heaton, T. J., Hogg, A. G., Hughen, K. A., Kaiser, K. F., Kromer, B., McCormac, F. G., Manning, S. W., Reimer, R. W., Richards, D. A., Southon, J. R., Talamo, S., Turney, C. S. M., van der Plicht, J., and Weyhenmeyer, C.E. 2009. INTCAL 09 and MARINE09 radiocarbon age calibration curves, 0-50,000 years Cal BP. Radiocarbon, 51, 1111-1150.

Roe, G. 2006. In defense of Milankovitch. Geophysical Research Letters, 33, L24703, doi:10.1029/2006GL027817.

Schaefer, J. M., Denton, G. H., Barrell, D. J. A., Ivy-Ochs, S., Kubik, P. W., Andersen, B. J., Phillips, F. M., Lowell, T. V., and Schluchter, C. 2006. Near-synchronous interhemispheric termination of the Last Glacial Maximum in mid-latitudes. Science, 312, 1510-1513.

Schneider von Deimling, T., Ganopolski, A., Held, H., and Rahmstorf, S. 2006. How cold was the Last Glacial Maximum? Geophysical Research Letters, 33, doi:10.1029/2006GL026484.

Shackleton, N. J. 2000. The 100,000 year Ice-Age cycle identified and found to lag temperature, carbon dioxide and orbital eccentricity. Science, 289**,** 1897-1902.

Shakun, J. D., and Carlson, A. E. 2010. A global perspective on Last Glacial Maximum to Holocene climate change. Quaternary Science Reviews, 29, 1801-1816.

Skinner, L. C., Fallon, S., Waelbroeck, C., Michel, E., and Barker, S. 2010. Ventilation of the deep Southern Ocean and deglacial CO_2 rise. Science, 328, 1147-1151.

Stott, L., Timmermann, A., and Thunell, R. 2007. Southern hemisphere and deep-sea warming led deglacial atmospheric CO_2 rise and tropical warming. Science, 318**,** 435-438.

Toggweiler, J. R., and Lea, D. W. 2010. Temperature differences between the hemispheres and ice age climate variability. Paleoceanography, 25, PA2212, doi:10.1029/2009PA001758.

Weaver, A. J., Eby, M., Fanning, A. F. and Wiebe, E. C. 1998. Simulated influence of carbon dioxide, orbital forcing and ice sheets on the climate of the Last Glacial Maximum. Nature, 394, 847-853.

Chapter 5

Conclusions

This dissertation has used statistical analyses of large climate datasets to identify spatiotemporal patterns of climate variability in the Pacific Ocean during the 20th century and globally during the last deglaciation. Comparison of these patterns to potential climate forcings, in part with the aid of statistical models, is used to identify the most likely driving mechanisms of the observed variability. The results inform our understanding of natural climate variability on decadal to multi-millennial time scales.

Chapter 2 uses statistical approaches to explore the nature and origin of Pacific decadal variability over the 20th century. EOF analysis is used to identify the leading mode of SST variability in the South Pacific Ocean over the 20th century. This mode explains 23% of South Pacific SST variability, just as its North Pacific counterpart (i.e., the PDO index) does in its domain. These North and South Pacific leading modes are found to contain considerable redundant information suggesting that the two may be physically linked. Both modes also exhibit pronounced seasonality in autocorrelation with maximum autocorrelation during local winter and minimum autocorrelation during local summer. Thus, winter SST anomalies appear to often persist from year to year in both subbasins despite their disappearance during the intervening summer, which may be attributable to reemergence. These two findings – interhemispheric symmetry of Pacific SST variability and wintertime persistence of SST anomalies – suggest that Pacific decadal variability may be a basin-wide phenomenon driven by reddening of interannual variability initiated in the tropical Pacific. This hypothesis is tested with an AR-1 model forced solely by observed ENSO anomalies and parameterized using observed coefficients for reddening. This *very* simple model explains 40% of the observed temporal variability in North Pacific

SST and 50% in South Pacific SST, consistent with a tropical origin for Pacific decadal variability.

Chapter 3 synthesizes and analyzes 104 paleoclimate records spanning parts or all of the interval from the LGM to the Holocene. The timing of peak glacial and interglacial conditions exhibited considerable variability with each spread over >10 ky. Nonetheless, both extreme climate states wee statistically synchronous between the polar hemispheres, suggesting the hemispheres were synchronized by greenhouse gases, ocean circulation, and/or local insolation. EOF analysis of 71 records spanning 19-11 ka indicates that >70% of deglacial climate variability can be explained by two modes. The first mode explains 61% of the variance, exhibits a globally near-uniform spatial pattern, and is well-correlated with atmospheric CO_2 concentrations over this time interval. The second mode explains 11% of the variance, exhibits a general hemispheric seesaw pattern, and parallels variations in AMOC strength. The EOF analysis thus suggests that greenhouse forcing was a major forcing or feedback during the last deglaciation, while ocean circulation was a smaller, though still important, driver of deglacial climate variability. The magnitude of the Younger Dryas climate anomaly shows a general hemispheric antiphasing, and the largest negative anomalies are centered around the North Atlantic. These patterns are consistent with the bipolar seesaw model for the Younger Dryas in which a reduction in deepwater formation in the North Atlantic led to greatest cooling there with attendant warming in the Southern Hemisphere due to reduced oceanic cross-equatorial heat transport. Global cooling during the LGM was likely ≥4.9°C, whereas it was only ~0.6°C during the Younger Dryas 'cold interval'. These contrasting global mean temperature anomalies reflect the differing forcings of each climate event. The LGM was characterized by major perturbations to the global energy balance, primarily from lower greenhouse gas concentrations and expanded ice sheets. The Younger Dryas, on the other hand, was caused by variations in ocean circulation, which primarly redistributed heat around the planet rather than altered the global energy budget.

Chapter 4 focuses on the patterns and drivers of temperature variability during the last deglaciation based on 77 globally-distributed, calibrated, proxy temperature records. Global mean temperature is strongly correlated and varies near-synchronously with atmospheric CO_2 during the deglaciation, suggesting greenhouse gases exerted a major control on global temperature variability and were important for synchronizing the hemispheres. While ice sheets are undoubtedly important in driving temperature variability, their influence appears to be largely confined to regions proximal to the ice. Prominent millennial-scale differences in Northern and Southern Hemisphere temperature variability likely reflect the seesawing of heat between the hemispheres driven by changes in the strength of the AMOC. The onset of deglaciation involves near-synchronous warming of the Southern Hemisphere and tropics and cooling of the northern extratropics at ~19 ka, which may represent the response to an AMOC collapse driven by boreal insolation-forced melting of northern ice sheets. Classic Milankovitch forcing may thus have provided the trigger for the last deglaciation.

APPENDICES

Appendix A. Sensitivity of Southern Hemisphere PDO index to dataset

It could be argued that the reduced space optimal interpolation technique (RSOI) used to create the HadISST1 dataset may have caused the SST reconstruction in the relatively data-sparse South Pacific to have been unduly influenced by Northern Hemisphere modes of climate variability where more data exists. Such a scenario would suggest our finding of similar Northern and Southern Hemisphere PDV is spurious. Two points suggest this is not likely the case, however. First, the HadISST1 RSOI was performed separately for the area south of 20°S from the rest of the globe (Rayner et al., 2003) helping to minimize the input of Northern Hemisphere climate information to the reconstructed Southern Hemisphere SSTs upon which our analysis is based. Second, we evaluated the robustness of South Pacific PC1 using the HadSST2 reconstruction, which is neither interpolated nor variance adjusted (Rayner et al., 2006). This dataset is too sparse to permit meaningful EOF analysis of the South Pacific. Nonetheless, PCs can often be approximated by differences of SST averages near EOF maxima and minima. We first verified the validity of this approach using HadISST1 and found the areal average analogue yielded a correlation of r=0.88 with South Pacific PC1. We then applied this technique to HadSST2 and obtained monthly correlations of r=~0.6 and annual correlations of r=~0.7 between South Pacific PC1 and two areal average analogues. Thus, the leading mode of South Pacific SST variability identified here appears to be robust.

A.A References

Rayner, N. A., Parker, D. E., Horton, E. B., Folland, C. K., Alexander, L. V., Rowell, D. P., Kent, E. C., and Kaplan, A. 2003. Global analyses of sea surface temperature, sea ice, and night marine air temperature since the late nineteenth century. Journal of Geophysical Research, 108, 4407, doi:10.1029/2002JD002670.

Rayner, N. A., Brohan, P., Parker, D. E., Folland, C. K., Kennedy, J. J., Vanicek, M., Ansell, T. J., and Tett, S. F. B. 2006. Improved analyses of changes and uncertainties in sea surface temperature measured in situ since the mid-nineteenth century: the HadSST2 dataset. Journal of Climate, 19, 446-469.

Appendix B. Last Glacial Maximum to Holocene database used in Chapter 3

Table A.B.1

#	Reference	Location	Core	Proxy	Signal	Lat	Long	Elev (m)
1	Svensson et al., 2008	NGRIP, Greenland	-	ice core $\delta^{18}O$	t	75.1	-42.3	2917
2	Severinghaus et al., 1998; Severinghaus and Brook, 1999	GISP2, Greenland	-	ice core $\delta^{15}N$, $\delta^{40}Ar$	t	72.6	-38.5	3207
3	Alley, 2000	GISP2, Greenland	-	ice core $\delta^{18}O$ and borehole temp	t	72.6	-38.5	3207
4	Brook et al., 1996; Severinghaus and Brook, 1999	GISP2, Greenland	-	ice core CH_4	ghg	72.6	-38.5	3207
5	Rasmussen et al., 2006; Dansgaard et al., 1993	GRIP, Greenland	-	ice core δ18O	t	72.5	-37.6	3200
6	Andrews et al., 2009	Iceland margin	15 core composite	ice rafted debris (qtz)	t	66.6	-19.0	-
7	Dolven et al., 2002	Nordic Sea	HM79-4, MD95-2011	radiolarian assemblages	t	63.1	2.6	-983, -1048
8	Fisher et al., 2008	Mt. Logan, Yukon	-	ice core δ18O	s	60.6	-140.4	5959
9	Hu et al., 2006	Arolik Lake, Alaska	-	biogenic silica	t	59.5	-161.1	145
10	Hu et al., 2006	Ongo Lake, Alaska	-	biogenic silica	t	59.3	-159.4	200
11	Bond et al., 2001	North Atlantic	MC52, VM29-191	ice rafted debris (HSG)	t	54.3	-16.6	-2370
12	Bond et al., 1999	North Atlantic	VM23-81	N. pachy (s) %	t	54.3	-16.8	-2393
13	Heiri et al., 2007	Hijkermeer, Netherlands	-	chironomids	t	52.9	6.5	14
14	McDermott et al., 2001	Crag Cave, Ireland	-	speleothem δ18O	t	52.2	-9.5	30
15	Peck et al., 2008	Northeast Atlantic	MD01-2461	foram Mg/Ca	t	51.8	-12.9	-1153
16	Kienast and McKay, 2001	Northeast Pacific	JT96-09	UK'37	t	48.9	-126.9	-920
17	von Grafenstein et al., 1999	Ammersee, Germany	-	marl δ18O	t	47.1	11.0	533
18	Heiri and Millet, 2005	Lac Lautrey, France	-	chironomids	t	46.6	5.9	788
19	deVernal et al., 1996	Gulf of St. Lawrence	HU90031-44	dinoflaggelate cysts	t	44.7	-55.6	-1381

20	Barron et al., 2003	Northeast Pacific	ODP 1019	UK'37	t	41.7	-124.9	-980
21	Mix et al., 1999	Northeast Pacific	ODP 1019	N. pachy (s) %	t	41.7	-124.9	-980
22	Cacho et al., 2001	Western Mediterranean	M39-008	$U^{K'}_{37}$	t	39.4	-7.1	-576
23	Cacho et al., 2001	Western Mediterranean	BS79-38	$U^{K'}_{37}$	t	38.4	13.6	-1489
24	Bard et al., 2002	Iberian margin	MD95-2042, SU8118	$U^{K'}_{37}$	t	37.8	-10.7	-3140
25	Cacho et al., 1999	Western Mediterranean	MD95-2043	$U^{K'}_{37}$	t	36.1	-2.6	-1841
26	Nakagawa et al., 2003	Lake Suigetsu, Japan	-	pollen	t	35.6	135.9	0
27	Hendy et al., 2002	Santa Barbara Basin	ODP 893A	foram $\delta^{18}O$	t	34.3	-120.0	-577
28	Behl and Kennett, 1996	Santa Barbara Basin	ODP 893A	bioturbation index	v	34.3	-120.0	-577
29	Carlson et al., 2008	Bermuda Rise	OCE326-GGC5	foram Mg/Ca	t	33.7	-57.6	-4550
30	Carlson et al., 2008	Blake outer ridge	KNR140-51GGC	foram Mg/Ca	t	32.6	-76.3	-1790
31	Wang et al., 2001	Hulu Cave, China	-	speleothem $\delta^{18}O$	p	32.5	119.2	100
32	Bar-Matthews et al., 2003	Soreq Cave, Israel	-	speleothem $\delta^{18}O$	p	31.5	35.0	400
33	Sun et al., 2005	East China Sea	A7	foram Mg/Ca	t	27.8	127.0	-1264
34	Flower et al., 2004	Gulf of Mexico	EN32-PC6	foram Mg/Ca	t	27.0	-91.3	-2280
35	Dykoski et al., 2005	Dongge Cave, China	-	speleothem $\delta^{18}O$	p	25.3	108.1	680
36	Schulz et al., 1998	Arabian Sea TOC	SO90-136KL	TOC	w	23.1	66.5	-568
37	Yancheva et al., 2007	Huguang Maar, China	-	titanium	w	21.2	110.3	23
38	deMenocal et al., 2000	West African margin	ODP 658C	foram assemblages	t	20.8	-18.6	-2263
39	Zhao et al., 1995	West African margin	ODP 658C	$U^{K'}_{37}$	t	20.8	-18.6	-2263
40	Pelejero et al., 1999	South China Sea	17940	$U^{K'}_{37}$	t	20.1	117.4	-1968
41	Altabet et al., 2002	Arabian Sea	RC27-14	$\delta^{15}N$	w	18.3	57.7	-596
42	Gupta et al., 2003	Arabian Sea	ODP 723A	G. bulloides %	w	18.1	57.6	-808
43	Fleitmann et al., 2003	Qunf Cave, Oman	-	speleothem $\delta^{18}O$	p	17.2	54.3	650
44	Shakun et al., 2007	Socotra Island, Yemen	-	speleothem $\delta^{18}O$	p	12.5	54.0	400
45	Rühlemann et al., 1999	Western tropical Atlantic	M35003-4	$U^{K'}_{37}$	t	12.1	-61.3	-1299
46	Schmidt et al., 2004	Western Caribbean Sea	VM28-122	foram Mg/Ca	t	11.6	-78.4	-3623

47	Haug et al., 2001	Cariaco Basin, Venezuala	ODP 1002	titanium	p	10.7	-65.2	-893
48	Hughen et al., 1996	Cariaco Basin, Venezuala	PL07-56PC	grayscale	w	10.7	-65.0	-810
49	Peterson et al., 2000	Cariaco Basin, Venezuala	ODP 1002	550 nm reflectance	p	10.7	-65.2	-893
50	Lea et al., 2003	Cariaco Basin, Venezuala	PL07-39PC	foram Mg/Ca	t	10.7	-65.0	-790
51	Ivanochko et al., 2005	Arabian Sea	ODP 905	$\delta^{15}N$	w	10.5	51.6	-1567
52	Kienast et al., 2001	South China Sea	18252-3	$U^{K'}_{37}$	t	9.1	109.2	-1273
53	Rosenthal et al., 2003	Sulu Sea	MD97-2141	foram Mg/Ca	t	8.8	121.3	-3633
54	Benway et al., 2006	Eastern equatorial Pacific	ME0005A-43JC	foram Mg/Ca	t	7.9	-83.6	-1368
55	Stott et al., 2007	West Pacific warm pool	MD98-2181	foram Mg/Ca	t	6.3	125.8	-2114
56	Kienast et al., 2001	South China Sea	18287-3	$U^{K'}_{37}$	t	5.4	110.4	-598
57	Partin et al., 2007	Borneo	-	speleothem $\delta^{18}O$	p	4.0	114.8	150
58	Weldeab et al., 2007	Gulf of Guinea	MD03-2707	foram Ba/Ca	p	2.5	9.4	-1295
59	Weldeab et al,. 2005	Eastern equatorial Atlantic	GeoB 4905	foram Mg/Ca	t	2.5	9.4	-1328
60	Weldeab et al., 2007	Gulf of Guinea	MD03-2707	foram Mg/Ca	t	2.5	9.4	-1295
61	Lea et al., 2006	Eastern equatorial Pacific	TR163-22	foram Mg/Ca	t	0.5	-92.4	-2830
62	Kienast et al., 2006	Eastern equatorial Pacific	ME0005A-24JC	$U^{K'}_{37}$	t	0.0	-86.5	-2941
63	Koutavas et al., 2002	West Pacific warm pool	V21-30	foram Mg/Ca	t	-1.2	-89.7	-617
64	Thompson et al., 2002	Kilimanjaro, Tanzania	-	ice core $d^{18}O$	t	-3.1	37.4	5895
65	Weldeab et al, 2006	Western tropical Atlantic	GeoB 3129	foram Mg/Ca	t	-4.6	-36.6	-830
66	Visser et al., 2003	West Pacific warm pool	MD9821-62	foram Mg/Ca	t	-4.7	117.9	-1855
67	Stott et al., 2007	West Pacific warm pool	MD98-2176	foram Mg/Ca	t	-5.0	133.4	-2382
68	Schefuß et al., 2005	Gulf of Guinea	GeoB 6518-1	$U^{K'}_{37}$	t	-5.6	11.2	-962
69	Weijers et al., 2007	Gulf of Guinea	GeoB 6518-1	MBT, CBT	t	-5.6	11.2	-962
70	Tierney and Russel, 2007	Lake Tanganyika	NP04-KH3	biogenic silica	w	-6.7	29.8	773
71	Tierney et al., 2008	Lake Tanganyika	NP04-KH3, KH4	TEX_{86}	t	-6.7	29.6	773
72	Thompson et al., 1995	Huascaran, Peru	-	ice core $\delta^{18}O$	t	-9.0	-77.5	6050
73	Waelbroek et al., 2006; Levi et al., 2007	West Pacific warm pool	MD98-2165	foram Mg/Ca	t	-9.7	118.4	-2100

74	Johnson et al., 2002	Lake Malawi	M98-2P	biogenic silica	w	-10.0	34.2	500
75	Stott et al., 2007	West Pacific warm pool	MD98-2170	foram Mg/Ca	t	-10.6	125.4	-832
76	Seltzer et al., 2000	Lake Junin, Peru	-	marl δ18O	p	-11.0	-76.1	4082
77	Powers et al., 2005	Lake Malawi	MD98-1P, 2P	TEX_{86}	t	-11.0	34.2	500
78	Kim et al., 2002	Southeast Atlantic	GeoB 1023-5	$U^{K'}_{37}$	t	-17.2	11.0	-1978
79	Thompson et al., 1998	Sajama, Bolivia	-	ice core $\delta^{18}O$	t	-18.0	-69.0	6540
80	Bard et al., 1997	Indian Ocean	MD79257	$U^{K'}_{37}$	t	-20.4	36.3	-1260
81	Little et al., 1997	South Atlantic	GeoB 1711	N. pachy (s) %	t	-23.6	12.4	-1967
82	Holmgren et al., 2003	Cold Air Cave, South Africa	-	speleothem $\delta^{18}O$	t	-24.0	29.2	-
83	Farmer et al., 2005	Southeast Atlantic	ODP 1084B	foram Mg/Ca	t	-25.5	13.0	-1992
84	Cruz et al., 2005	Caverna Botuvera, Brazil	-	speleothem $\delta^{18}O$	p	-27.2	-49.2	250
85	Wang et al., 2007	Caverna Botuvera, Brazil	-	speleothem $\delta^{18}O$	p	-27.2	-49.2	250
86	Carlson et al., 2008	Brazilian margin	KNR159-5-36GGC	foram Mg/Ca	t	-27.5	-46.5	-1268
87	Kim et al,. 2002	Southeast Pacific	GIK17748-2	$U^{K'}_{37}$	t	-32.8	-72.0	-2545
88	Pahnke and Sachs, 2006	New Zealand	MD97-2121	$U^{K'}_{37}$	t	-40.4	178.0	-3014
89	Williams et al., 2005	New Zealand	-	speleothem $\delta^{18}O$	t	-41.0	172.0	170
90	Kaiser et al., 2005; Lamy et al., 2007	Chilean margin	ODP 1233	$U^{K'}_{37}$	t	-41.0	-74.5	-838
91	Sachs et al., 2001	Southeast Atlantic	TN057-21-PC2	$U^{K'}_{37}$	t	-41.1	7.5	-4981
92	Hellstrom et al., 1998; Drysdale et al., 2005; Genty et al., 2006; Hellstrom, 2006	New Zealand	-	speleothem $\delta^{18}O$	t	-41.2	172.7	590
93	Charles et al., 1996	South Atlantic	RC11-83	foram $\delta^{18}O$	t	-41.6	9.8	-4718
94	Barrows et al., 2007	New Zealand	SO136-GC11	$U^{K'}_{37}$	t	-43.5	167.9	-1556
95	Pahnke and Sachs, 2006	New Zealand	MD97-2120	$U^{K'}_{37}$	t	-45.5	174.9	-1210
96	Morgan et al., 2002	Law Dome, Antarctica	-	ice core $\delta^{18}O$	t	-67.0	113.0	1390
97	Monnin et al., 2001	Dome C, Antarctica	-	ice core CO_2	ghg	-75.1	123.4	3240
98	Stenni et al., 2001	Dome C, Antarctica	-	ice core $\delta^{18}O$	t	-75.1	123.4	3240

99	EPICA Members, 2006	EDML, Antarctica	-	ice core $\delta^{18}O$	t	-75.2	65.0	2900
100	Kawamura et al., 2007	Dome Fuji, Antarctica	-	ice core $\delta^{18}O$, δD	t	-77.3	39.7	3810
101	Steig et al., 2000	Taylor Dome, Antarctica	-	ice core $\delta^{18}O$	t	-78.0	160.0	2365
102	Petit et al., 1999	Vostok, Antarctica	-	ice core δD	t	-78.5	108.0	3500
103	Hammer et al., 1997; Blunier and Brook, 2001	Byrd, Antarctica	-	ice core $\delta^{18}O$	t	-79.9	-119.4	1530
104	Brook et al., 2005; Steig and White, 2003	Siple Dome, Antarctica	-	ice core $\delta^{18}O$	t	-81.6	-148.8	621

#	Alti	LGM	19-11 ka comm	19-11 ka EOF1	19-11 ka EOF2	15-11 ka comm	15-11 ka EOF1	15-11 ka EOF2	YD Mag	B/A Mag	YD ΔT	G-IG ΔT
1	7600	29900	0.67	0.70	0.43	0.63	0.21	0.76	-0.18	0.39	-	-
2	-	-	-	-	-	-	-	-	-	-	-7.50	-
3	-	-	-	-	-	-	-	-	-	-	-6.89	-17.03
4	-	-	0.87	0.90	0.25	0.83	0.05	0.91	-0.49	0.50	-	-
5	9350	23940	0.56	0.39	0.64	0.68	-0.04	0.82	-0.29	0.35	-	-
6	9870	-	-	-	-	-	-	-	-	-	-	-
7	8880	-	-	-	-	0.24	0.07	0.49	-	-	-0.37	-
8	8610	-	-	-	-	-	-	-	-	-	-	-
9	-	-	-	-	-	0.51	0.52	0.50	-	-	-	-
10	-	-	-	-	-	0.75	0.85	0.14	-	-	-	-
11	2090	-	-	-	-	-	-	-	-	-	-	-
12	6890	26120	0.89	0.91	0.24	0.57	0.22	0.72	-0.47	0.46	-	-
13	-	-	-	-	-	0.66	-0.05	0.81	-	-	-2.40	-
14	6340	-	-	-	-	-	-	-	-	-	-	-
15	-	21630	0.41	0.40	-0.50	0.35	0.59	-0.05	0.17	-0.20	1.00	-3.45
16	10110	-	-	-	-	0.13	-0.20	0.29	-	-	-1.66	-
17	3860	-	-	-	-	0.70	0.04	0.84	-	-	-	-
18	-	-	-	-	-	0.16	0.13	0.38	-	-	-1.93	-
19	-	-	-	-	-	-	-	-	-	-	-8.76	-
20	9840	-	-	-	-	0.65	0.03	0.80	-	-	-2.87	-
21	10710	24190	0.74	0.79	0.33	0.66	-0.01	0.81	-0.44	0.49	-	-
22	10870	-	0.62	0.79	-0.01	0.65	0.57	0.57	-0.29	-0.04	-1.89	-4.08
23	8370	23300	0.52	0.72	-0.03	0.41	0.35	0.54	-0.15	-0.05	-1.42	-6.54
24	9410	29190	0.65	0.63	0.50	0.90	-0.29	0.90	-0.31	0.26	-2.28	-4.98
25	9490	17170	0.79	0.82	0.34	0.91	0.56	0.78	-0.26	0.32	-2.14	-6.73
26	-	-	-	-	-	0.22	-0.42	0.23	-	-	-0.50	-
27	7230	17260	0.87	0.92	0.15	0.60	0.25	0.73	-0.10	0.28	-	-
28	14560	-	0.42	0.48	0.43	0.93	-0.82	0.51	-0.91	0.74	-	-

29	10540	-	0.32	0.56	0.08	0.98	0.91	0.38	0.02	0.16	0.14	-3.42
30	-	21910	0.66	-0.60	-0.54	0.59	0.70	-0.32	0.19	-0.65	0.67	-1.76
31	-	16030	0.81	0.66	0.61	0.61	0.07	0.77	-	-	-	-
32	7530	19140	0.50	0.71	-0.03	0.50	-0.54	0.45	-0.45	0.22	-	-
33	9910	-	-	-	-	0.55	0.55	0.50	-	-	-0.59	-
34	-	-	0.78	0.86	-0.23	0.01	0.07	-0.06	0.02	0.06	0.10	-4.16
35	7570	-	-	-	-	0.46	0.16	0.66	-0.33	0.61	-	-
36	-	29710	0.80	-0.36	0.82	0.69	-0.57	0.60	-0.23	0.29	-	-
37	13790	-	-	-	-	0.63	-0.24	0.76	-	-	-	-
38	4020	-	-	-	-	-	-	-	-0.06	-	-0.51	-3.54
39	6590	20420	0.73	-0.86	-0.01	0.25	0.15	-0.48	0.09	-0.19	0.39	-1.53
40	920	22130	0.93	0.95	0.18	0.49	0.32	0.62	-0.06	0.17	-0.25	-2.66
41	-	26060	0.74	0.80	0.33	0.51	0.57	0.43	-	-	-	-
42	9860	-	-	-	-	-	-	-	-	-	-	-
43	7650	-	-	-	-	-	-	-	-	-	-	-
44	-	23600	0.66	0.72	0.37	0.11	0.05	0.33	-0.11	0.44	-	-
45	1290	18860	0.89	0.77	-0.55	0.93	0.83	-0.49	0.20	-0.04	0.74	-2.28
46	-	21340	0.86	0.91	-0.19	0.39	0.62	0.06	0.12	0.04	0.26	-1.31
47	8700	-	-	-	-	-	-	-	-	-	-	-
48	930	-	-	-	-	0.82	-0.29	0.85	-	-	-	-
49	10250	15700	0.72	0.66	0.53	0.57	0.20	0.73	-0.33	0.86	-	-
50	8180	22700	0.51	0.45	0.55	0.79	-0.25	0.86	-0.91	0.69	-3.28	-2.82
51	8890	29510	0.80	0.75	0.48	0.54	-0.23	0.70	-0.42	0.47	-	-
52	-	-	-	-	-	0.15	-0.39	0.06	-	-	-0.05	-
53	-	22130	0.79	0.88	-0.08	0.58	0.76	-0.03	0.06	0.21	0.19	-2.37
54	3480	19010	0.74	0.82	-0.26	0.04	0.19	0.04	-0.03	0.10	-0.12	-2.01
55	10300	-	0.85	0.92	-0.06	0.47	0.69	-0.01	0.15	0.39	0.23	-3.47
56	-	-	-	-	-	0.55	0.41	0.61	-	-	-0.19	-
57	4650	16300	0.56	0.73	0.16	0.57	0.70	-0.28	0.18	0.16	-	-
58	9960	20420	0.72	0.83	0.19	0.75	0.49	0.71	-0.33	0.34	-	-

59	7000	-	0.69	0.83	0.03	0.08	-0.21	0.19	0.06	0.24	0.19	-2.14
60	8820	19140	0.89	0.94	0.01	0.61	0.77	0.12	0.05	0.33	0.16	-2.92
61	11380	22330	0.72	0.78	-0.34	0.54	0.71	0.20	0.03	-0.05	0.08	-1.84
62	-	15920	0.61	0.30	0.72	0.63	0.48	0.63	-0.13	0.31	-0.43	-1.00
63	3950	27600	0.13	0.09	-0.35	0.15	0.21	-0.32	0.04	-0.15	0.07	-0.37
64	10390	-	-	-	-	-	-	-	-	-	-	-
65	12190	-	0.81	0.81	-0.40	0.69	0.61	-0.56	0.29	0.09	1.18	-3.23
66	6050	21840	0.89	0.95	-0.03	0.55	0.68	0.28	-0.04	0.22	-0.16	-3.27
67	8250	-	0.88	0.94	0.05	0.13	0.35	0.10	0.05	0.37	0.12	-2.90
68	750	-	0.40	0.39	-0.50	0.78	0.88	0.07	0.29	-0.25	0.83	-1.88
69	2120	16890	0.80	0.87	0.23	0.64	0.80	-0.05	0.03	0.24	0.14	-3.22
70	-	-	-	-	-	0.14	-0.03	0.38	-	-	-	-
71	5400	27190	0.50	0.65	-0.29	0.70	0.81	0.20	0.07	0.01	0.40	-4.17
72	9300	-	0.80	0.87	0.20	0.82	0.71	0.56	-0.11	0.23	-	-
73	10780	20580	0.90	0.84	-0.44	0.84	0.89	-0.24	0.25	-0.02	0.80	-2.54
74	3880	23700	0.32	0.41	-0.39	0.60	0.00	-0.78	0.57	-0.12	-	-
75	9900	-	0.91	0.95	-0.05	0.93	0.96	0.02	0.14	0.22	0.80	-3.095
76	12180	-	-	-	-	0.84	-0.56	0.72	-	-	-	-
77	5200	-	0.83	0.91	-0.01	0.32	-0.21	0.52	-0.12	0.30	-0.73	-3.15
78	6240	-	0.71	0.83	-0.13	0.64	-0.50	0.63	-0.16	0.15	-0.68	-3.38
79	4770	18500	0.58	0.72	0.24	0.39	0.01	0.62	-0.11	0.44	-	-
80	6620	19630	0.85	0.90	0.17	0.49	-0.03	0.70	-0.05	0.25	-0.15	-1.64
81	7630	28330	0.88	0.79	-0.50	0.53	0.73	-0.03	0.11	-0.09	-	-
82	9510	21630	-	-	-	-	-	-	-	-	-	-
83	11630	-	0.25	0.50	-0.05	0.54	-0.36	0.64	-0.20	0.07	-1.36	-2.69
84	8210	15440	-	-	-	-	-	-	-	-	-	-
85	9230	16670	0.95	-0.84	-0.49	0.86	-0.22	-0.90	-0.40	0.67	-	-
86	-	-	0.33	0.55	0.18	0.56	0.71	-0.24	0.12	0.37	0.35	-1.35
87	6600	-	-	-	-	0.24	-0.12	-0.48	-	-	0.47	-
88	-	23650	0.79	0.89	-0.01	0.69	0.83	-0.09	0.05	0.16	0.25	-4.23

89	3470	23050	0.33	0.56	0.12	0.38	-0.36	0.50	-0.28	0.33	-	-
90	10430	22600	0.86	0.81	-0.45	0.93	0.96	-0.12	0.21	0.01	1.33	-5.05
91	-	19150	0.98	0.96	-0.22	0.97	0.97	-0.20	0.16	0.16	0.79	-3.56
92	2580	19920	0.58	0.76	0.01	0.31	-0.21	-0.51	0.12	0.07	-	-
93	-	-	0.74	0.70	-0.50	0.33	0.52	0.24	0.06	-0.17	-	-
94	11630	21420	0.82	0.85	-0.33	0.88	0.89	-0.28	0.13	0.07	0.90	-5.20
95	11270	24050	0.83	0.90	-0.15	0.92	0.93	-0.23	0.26	0.22	1.93	-4.52
96	-	-	0.96	0.92	-0.33	0.83	0.87	-0.25	0.10	0.03	-	-
97	-	-	-	-	-	0.90	0.92	0.21	0.01	0.20	-	-
98	11100	26700	0.91	0.94	-0.19	0.51	0.64	0.32	0.03	0.18	0.93	-8.87
99	10830	24560	0.89	0.85	-0.41	0.68	0.82	-0.13	0.19	0.05	-	-
100	10950	25410	0.98	0.96	-0.26	0.89	0.94	0.04	-0.01	0.11	-	-8.26
101	11020	17760	0.87	0.90	0.23	0.48	0.57	0.40	-0.09	0.74	-	-
102	10900	27470	0.97	0.98	-0.04	0.85	0.80	0.46	0.00	0.27	-0.01	-7.78
103	2170	22500	0.88	0.88	-0.32	0.74	0.85	-0.15	0.17	0.07	-	-
104	530	22780	0.91	0.94	-0.16	0.82	0.87	-0.25	0.16	0.17	-	-

Table A.B.1: List of the time series used in this study. Left column indicates the corresponding number in Figure 3.2. Signal column indicates if record is a proxy of temperature (t), greenhouse gases (ghg), precipitation (p), wind (w), source (s), or ventilation (v). The following columns give numerical results from the analyses: Altithermal timing (Alti), LGM timing (LGM), 19-11 ka communalities (19-11 ka comm), 19-11 ka factor 1 loadings (19-11 ka EOF1), 19-11 ka factor 2 loadings (19-11 ka EOF2), 15-11 ka communalities (15-11 ka comm), 15-11 ka factor 1 loadings (15-11 ka EOF1), 15-11 ka factor 2 loadings (15-11 ka EOF2), magnitude of the Younger Dryas (YD Mag) and Bølling/Allerød (B/A Mag), Younger Dryas temperature anomalies (YD ΔT), glacial-interglacial temperature changes (G-IG ΔT).

A.B References

Alley, R. B., 2000. The Younger Dryas cold interval as viewed from central Greenland. Quaternary Science Reviews 19**,** 213-226.

Altabet, M. A., Higginson, M. J., and Murray, D. W., 2002. The effect of millennial-scale changes in Arabian Sea denitrification on atmospheric CO_2. Nature 415, 159-162.

Andrews, J. T., Darby, D. A., Eberl, D. D., Jennings, A. E., Moros, M., and Ogilvie, A., 2009. A robust multi-site Holocene history of drift ice off northern Iceland: Implications for North Atlantic climate. The Holocene 19, 71-77.

Bard, E., Rostek, F., and Sonzogni, C., 1997. Interhemispheric synchrony of the last deglaciation inferred from alkenone palaeothermometry. Nature 385**,** 707-710.

Bard, E., 2002. Climate shock: Abrupt changes over millennial time scales. Physics Today 55**,** 32-38.

Bar-Matthews, M., Ayalon, A., Gilmour, M., Matthews, A., and Hawkesworth, C. J., 2003. Sea-land oxygen isotopic relationships from planktonic foraminifera and speleothems in the Eastern Mediterranean region and their implication for paleorainfall during interglacial intervals. Geochimica et Cosmochimica Acta 67**,** 3181-3199.

Barron, J. A., Heusser, L., Herbert, T. D., and Lyle, M., 2003. High-resolution climatic evolution of coastal northern California during the past 16,000 years. Paleoceanography 18**,** doi:10.1029/2002PA000768.

Barrows, T. T., Lehman, S. J., Fifield, L. K., and De Deckker, P., 2007. Absence of cooling in New Zealand and the adjacent Ocean during the Younger Dryas chronozone. Science 318**,** 86-89.

Behl, R. J., and Kennett, J. P., 1996. Brief interstadial events in the Santa Barbara basin, NE Pacific, during the past 60 kyr. Nature 379**,** 243-246.

Benway, H. M., Mix, A. C., Haley, B. A., and Klinkhammer, G. P., 2006. Eastern Pacific warm pool paleosalinity and climate variability: 0-30 kyr. Paleoceanography 21**,** doi:10.1029/2005PA001208.

Blunier, T., and Brook, E. J., 2001. Timing of millennial-scale climate change in Antarctica and Greenland during the last glacial period. Science 291**,** 109-112.

Bond, G. C., Showers, W., Elliot, M., Evans, M., Lotti, R., Hajdas, I., Bonani, G., and Johnson, S., 1999. The North Atlantic's 1-2 kyr climate rhythm: relation to Heinrich Events, Dansgaard/Oeschger cycles and the Little Ice Age. In: Clark, P.U., Webb, R.S., Keigwin, L.D. (Eds.), Mechanisms of Global Climate Change at Millennial Time Scales. American Geophysical Union, Washington, D.C, pp. 35-58.

Bond, G., Kromer, B., Beer, J., Muscheler, R., Evans, M. N., Showers, W., Hoffmann, S., Lotti-Bond, R., Hajdas, I., and Bonani, G., 2001. Persistent solar influence on North Atlantic climate during the Holocene. Science 294**,** 2130-2136.

Brook, E. J., Sowers, T., and Orchardo, J., 1996. Rapid variations in atmospheric methane concentration during the past 110,000 years. Science 273**,** 1087-1091.

Brook, E. J., White, J. W. C., Schilla, A. S. M., Bender, M. L., Barnett, B., Severinghaus, J. P., Taylor, K. C., Alley, R. B., and Steig, E. J., 2005. Timing of millennial-scale climate change at Siple Dome, West Antarctica, during the last glacial period. Quaternary Science Reviews 24**,** 1333-1343.

Cacho, I., Grimalt, J. O., Pelejero, C., Canals, M., Sierro, F. J., Flores, J. A., and Shackelton, N. J., 1999. Dansgaard-Oeschger and Heinrich Event imprints in Alboran Sea paleotemperatures. Paleoceanography 14**,** 698-705.

Cacho, I., Grimalt, J. O., Canals, M., Sbaffi, L., and Shackelton, N. J., 2001. Variability of the western Mediterranean Sea surface temperature during the last 25,000 years and its connection with the Northern Hemisphere climatic changes. Paleoceanography 16**,** 40-52.

Carlson, A. E., Oppo, D., Came, R. E., LeGrande, A. N., Keigwin, L., and Curry, W. B., 2008. Subtropical salinity variability and Atlantic meridional circulation during deglaciation. Geology 12, 991-994.

Charles, C., Lynch-Stieglitz, J., Ninnemann, U. S., and Fairbanks, R., 1996. Climate connections between the hemisphere revealed by deep sea sediment core/ice core correlations. Earth and Planetary Science Letters 142**,** 19-27.

Cruz, F. W., Burns, S. J., Karmann, I., Sharp, W. D., Vuille, M., Cardoso, A. O., Ferrari, J. A., Silva Dias, P. L., and Viana, O., 2005. Insolation-driven changes in atmospheric circulation over the past 116,000 years in subtropical Brazil. Nature 434**,** 63-66.

Dansgaard, W., Johnsen, S. J., Clausen, H. B., Dahl-Jensen, D., Gundestrup, N. S., Hammer, C. U., Hvidberg, C. S., Steffensen, J. P., Sveinbjörnsdottir, A. E.,

Jouzel, J., and Bond, G., 1993. Evidence for general instability of past climate from a 250-kyr ice core record. Nature 364**,** 218-220.

deMenocal, P. B., Ortiz, J., Guilderson, T., and Sarnthein, M., 2000. Coherent high- and low-latitude climate variability during the Holocene warm period. Science 288**,** 2198-2202.

deVernal, A., Hillaire-Marcel, C., and Bilodeau, G., 1996. Reduced meltwater outflow from the Laurentide ice margin during the Younger Dryas. Nature 381**,** 774-777.

Dolven, J. K., Cortese, G., and Bjorklund, K. R., 2002. A high-resolution radiolarian-derived paleotemperature record for the Late Pleistocene-Holocene in the Norwegian Sea. Paleoceanography 17**,** doi:10.1029/2002PA000780.

Drysdale, R., Zanchetta, G., Hellstrom, J., Fallick, A. E., and Zhao, J. X., 2005. Stalagmite evidence for the onset of the last interglacial in southern Europe at 129 ± 1 ka. Geophysical Research Letters 32**,** doi:10.1029/2005GL024658.

Dykoski, C. A., Edwards, R. L., Cheng, H., Yuan, D., Cai, Y., Zhang, M., Lin, Y., Qing, J., An, Z., and Revenaugh, J., 2005. A high-resolution, absolute-dated Holocene and deglacial Asian monsoon record from Dongge Cave, China. Earth and Planetary Science Letters 233**,** 71-86.

EPICA Community Members, 2006. One-to-one coupling of glacial climate variability in Greenland and Antarctica. Nature 444**,** 195-198.

Farmer, E. C., DeMendocal, P. B., and Marchitto, T. M., 2005. Holocene and deglacial ocean temperature variability in the Benguela upwelling region: Implications for low-latitude atmospheric circulation. Paleoceanography 20**,** doi:10.1029/2004PA001049.

Fisher, D., Osterberg, E., Dyke, A., Dahl-Jensen, D., Demuth, M., Zdanowicz, C., Bourgeois, J., Koerner, R. M., Mayewski, P., Wake, C., Kreutz, K., Steig, E., Zheng, J., Yalcin, K., Goto-Azuma, K., Luckman, B., and Rupper, S., 2008. The Mt Logan Holocene--late Wisconsinan isotope record: tropical Pacific-Yukon connections. The Holocene 18**,** 667-677.

Fleitmann, D., Burns, S. J., Mudelsee, M., Neff, U., Kramers, J., Mangini, A., and Matter, A., 2003. Holocene forcing of the Indian monsoon recorded in a stalagmite from southern Oman. Science 300**,** 1737-1739.

Flower, B. P., Hastings, D. W., Hill, H. W., and Quinn, T. M., 2004. Phasing of deglacial warming and Laurentide Ice Sheet meltwater in the Gulf of Mexico. Geology 32**,** 597-600.

Genty, D., Blamart, D., Ghaleb, B., Plagnes, V., Causse, C., Bakalowicz, M., Zouari, K., Chkir, N., Hellstrom, J., Wainer, K., and Bourges, F., 2006. Timing and dynamics of the last deglaciation from European and North African $\delta^{13}C$ stalagmite profiles-comparison with Chinese and South Hemisphere stalagmites. Quaternary Science Reviews 25**,** 2118-2142.

Gupta, A. K., Anderson, D. M., and Overpeck, J. T., 2003. Abrupt changes in the Asian southwest monsoon during the Holocene and their links to the North Atlantic Ocean. Nature 421**,** 354-357.

Hammer, C., Clausen, H., and Langway, C. C., 1997. 50,000 Years of recorded global volcanism. Climatic Change 35**,** 1-15.

Haug, G. H., Hughen, K. A., Sigman, D. M., Peterson, L. C., and Rohl, U., 2001. Southward migration of the Intertropical Convergence Zone through the Holocene. Science 293**,** 1304-1308.

Heiri, O., and Millet, L., 2005. Reconstruction of Late Glacial summer temperatures from chironomid assemblages in Lac Lautrey (Jura, France). Journal of Quaternary Science 20**,** 33-44.

Heiri, O., Cremer, H., Engels, S., Hoek, W. Z., Peeters, W., and Lotter, A. F., 2007. Lateglacial summer temperatures in the Northwest European lowlands: a chironomid record from Hijkermeer, the Netherlands. Quaternary Science Reviews 26**,** 2420-2437.

Hellstrom, J., McCulloch, M., and Stone, J., 1998. A Detailed 31,000-Year Record of climate and vegetation change, from the isotope geochemistry of two New Zealand speleothems. Quaternary Research 50**,** 167-178.

Hellstrom, J., 2006. U-Th dating of speleothems with high initial ^{230}Th using stratigraphical constraint. Quaternary Geochronology 1**,** 289-295.

Hendy, I. L., Kennett, J. P., Roark, E. B., and Ingram, B. L., 2002. Apparent synchroneity of submillennial scale climate events between Greenland and Santa Barbara Basin, California from 30-10 ka. Quaternary Science Reviews 21**,** 1167-1184.

Holmgren, K., Lee-Thorp, J. A., Cooper, G. R. J., Lundblad, K., Partridge, T. C., Scott, L., Sithaldeen, R., Siep Talma, A., and Tyson, P. D., 2003. Persistent

millennial-scale climatic variability over the past 25,000 years in Southern Africa. Quaternary Science Reviews 22**,** 2311-2326.

Hu, F. S., Nelson, D. M., Clarke, G. H., Ruhland, K. M., Huang, Y., Kaufman, D., and Smol, J., 2006. Abrupt climatic events during the last glacial-interglacial transition in Alaska. Geophysical Research Letters 33**,** doi:10.1029/2006GL027261.

Hughen, K. A., Overpeck, J., Peterson, L. C., and Trumbore, S., 1996. Rapid climate changes in the tropical Atlantic region during the last deglaciation. Nature 380**,** 51-54.

Ivanochko, T. S., Ganeshram, R. S., Brummer, G.-J. A., Ganssen, G., Jung, S. J. A., Moreton, S. G., and Kroon, D., 2005. Variations in tropical convection as an amplifier of global climate change at the millennial scale. Earth and Planetary Science Letters 235**,** 302-314.

Johnson, T. C., Brown, E. T., McManus, J., Barry, S., Barker, P., and Gasse, F., 2002. A high-resolution paleoclimate record spanning the past 25,000 years in southern East Africa. Science 296**,** 113-132.

Kaiser, J., Lamy, F., and Hebbeln, D., 2005. A 70-kyr sea surface temperature record off southern Chile (Ocean Drilling Program Site 1233). Paleoceanography 20**,** doi:10.1029/2005PA001146.

Kawamura, K., Parrenin, F., Lisiecki, L., Uemura, R., Vimeux, F., Severinghaus, J. P., Hutterli, M. A., Nakazawa, T., Aoki, S., Jouzel, J., Raymo, M. E., Matsumoto, K., Nakata, H., Motoyama, H., Fujita, S., Goto-Azuma, K., Fujii, Y., and Watanabe, O., 2007. Northern Hemisphere forcing of climatic cycles in Antarctica over the past 360,000 years. Nature 448**,** 912-916.

Kienast, M., and McKay, J., 2001. Sea surface temperatures in the subarctic Northeast Pacific reflect millennial-scale climate oscillations during the last 16 kyrs. Geophysical Research Letters 28**,** 1563-1566.

Kienast, M., Steinke, S., Stattegger, K., and Calvert, S. E., 2001. Synchronous tropical South China Sea SST change and Greenland warming during deglaciation. Science 291**,** 2132-2134.

Kienast, M., Kienast, S. S., Calvert, S. E., Eglinton, T. I., Mollenhauer, G., Francois, R., and Mix, A. C., 2006. Eastern Pacific cooling and Atlantic overturning circulation during the last deglaciation. Nature 443**,** 846-849.

Kim, J.-H., Schneider, R. R., Muller, P. J., and Wefer, G., 2002. Interhemispheric comparison of deglacial sea-surface temperature patterns in Atlantic eastern boundary currents. Earth and Planetary Science Letters 194**,** 383-393.

Koutavas, A., Lynch-Stieglitz, J., Marchitto, T. M., Jr., and Sachs, J. M., 2002. El Niño-like pattern in Ice Age tropical Pacific sea surface temperature. Science 297**,** 226-230.

Lamy, F., Kaiser, J., Arz, H. W., Hebbeln, D., Ninnemann, U., Timm, O., Timmermann, A., and Toggweiler, J. R., 2007. Modulation of the bipolar seesaw in the Southeast Pacific during Termination 1. Earth and Planetary Science Letters 259**,** 400-413.

Lea, D. W., Pak, D. K., Peterson, L. C., and Hughen, K. A., 2003. Synchroneity of tropical and high-latitude Atlantic temperatures over the last glacial termination. Science 301**,** 1361-1364.

Lea, D. W., Pak, D. K., Belanger, C. L., Spero, H. J., Hall, M. A., and Shackleton, N. J., 2006. Paleoclimate history of Galápagos surface waters over the last 135,000 yr. Quaternary Science Reviews 25**,** 1152-1167.

Levi, C., Labeyrie, L., Bassinot, F. C., Guichard, F., Cortijo, E., Waelbroeck, C., Caillon, N., Duprat, J., Garidel-Thoron, T., and Elderfield, H., 2007. Low-latitude hydrological cycle and rapid climate changes during the last deglaciation. Geochemistry, Geophysics, Geosystems 8**,** doi:10.1029/2006GC001514.

Little, M. G., Schneider, R. R., Kroon, D., Price, B., Summerhayes, C. P., and Segl, M., 1997. Trade Wind forcing of upwelling, seasonality, and Heinrich events as a response to sub-Milankovitch climate variability. Paleoceanography 12, 568-576.

McDermott, F., Mattey, D. P., and Hawkesworth, C., 2001. Centennial-scale Holocene climate variability revealed by a high-resolution speleothem $\delta^{18}O$ record from SW Ireland. Science 294**,** 1328-1331.

Mix, A. C., Lund, D. C., Pisias, N. G., Boden, P., Bornmalm, L., Lyle, M., and Pike, J., 1999. Rapid climate oscillations in the northeast Pacific during the last deglaciation reflect Northern and Southern Hemisphere sources. In: Clark, P.U., Webb, R.S., Keigwin, L.D. (Eds.), Mechanisms of Global Climate Change at Millennial Time Scales. American Geophysical Union, Washington, D.C, pp. 127-148.

Monnin, E., Indermühle, A., Dällenbach, A., Flückiger, J., Stauffer, B., Stocker, T. F., Raynaud, D., and Barnola, J.-M., 2001. Atmospheric CO_2 concentrations over the last glacial termination. Science 291**,** 112-114.

Morgan, V., Delmotte, M., van Ommen, T., Jouzel, J., Chappellaz, J., Woon, S., Masson-Delmotte, V., and Raynaud, D., 2002. Relative timing of deglacial climate events in Antarctica and Greenland. Science 297**,** 1862-1864.

Nakagawa, T., Kitagawa, H., Yasuda, Y., Tarasov, P. E., Nishida, K., Gotanda, K., Sawai, Y., and Members, Y. R. C. P., 2003. Asynchronous climate changes in the North Atlantic and Japan during the last termination. Science 299**,** 688-691.

Pahnke, K., and Sachs, J. M., 2006. Sea surface temperatures of southern midlatitudes 0–160 kyr B.P. Paleoceanography 21**,** doi:10.1029/2005PA001191.

Partin, J. W., Cobb, K. M., Adkins, J. F., Clark, B., and Fernandez, D. P., 2007. Millennial-scale trends in west Pacific warm pool hydrology since the Last Glacial Maximum. Nature 449**,** 452-455.

Peck, V. L., Hall, I. R., Zahn, R., and Elderfield, H., 2008. Millennial-scale surface and subsurface paleothermometry from the northeast Atlantic, 55-8 ka BP. Paleoceanography 23, doi:10.1029/2008PA001631.

Pelejero, C., Grimalt, J. O., Heilig, S., Kienast, M., and Wang, L., 1999. High-resolution U^k_{37} temperature reconstructions in the South China Sea over th past 220 kyr. Paleoceanography 14**,** 224-231.

Peterson, L. C., Haug, G. H., Hughen, K. A., and Rohl, U., 2000. Rapid changes in the hydrologic cycle of the tropical Atlantic during the last glacial. Science 290**,** 1947-1951.

Petit, J. R., Jouzel, J., Raynaud, D., Barkov, N. I., Barnola, J.-M., Basile, I., Bender, M., Chappellaz, J., Davis, M., Delaygue, G., Delmotte, M., Kotlyakov, V. M., Legrand, M., Lipenkov, V. Y., Lorius, C., Pepin, L., Ritz, C., Saltzman, E., and Stievenard, M., 1999. Climate and atmospheric history of the past 420,000 years from the Vostok ice core, Antarctic. Nature 399**,** 429-436.

Powers, L., Johnson, T. C., Werne, J. P., Castaneda, I. S., Hopmans, E. C., Sinninghe Damste, J. S., and Schouten, S., 2005. Large termperature variability in the southern African tropics since the Last Glacial Maximum. Geophysical Research Letters 32**,** doi:10.1029/2004GL022014.

Rasmussen, S. O., Andersen, K. K., Svensson, A. M., Steffensen, J. P., Vinther, B. M., Clausen, H. B., Siggaard-Andersen, M.-L., Johnsen, S. J., Larsen, L. B., Dahl-Jensen, D., Bigler, M., Rothlisberger, R., Fischer, H., Goto-Azuma, K.,

Hansson, M., and Ruth, U., 2006. A new Greenland ice core chronology of the last glacial termination. Journal of Geophysical Research 111**,** doi:10.1029/2005JD006079.

Rosenthal, Y., Oppo, D., and Linsley, B. K., 2003. The amplitude and phasing of climate change during the last deglaciation in the Sulu Sea, western equatorial Pacific. Geophysical Research Letters 30**,** doi:10.1029/2002GL016612.

Rühlemann, C., Mulitza, S., Muller, P. J., Wefer, G., and Zahn, R., 1999. Warming of the tropical Atlantic Ocean and slowdown of thermohaline circulation during the last deglaciation. Nature 402**,** 511-514.

Sachs, J. P., Anderson, R. F., and Lehman, S. J., 2001. Glacial surface temperatures of the southeast Atlantic Ocean. Science 293**,** 2077-2079.

Schefuß, E., Schouten, S., and Schneider, R. R., 2005. Climatic controls on central African hydrology during the past 20,000 years. Nature 437**,** 1003-1006.

Schmidt, M. W., Spero, H. J., and Lea, D. W., 2004. Links between salinity variation in the Caribbean and North Atlantic thermohaline circulation. Nature 428**,** 160-163.

Schulz, H., von Rad, U., Erlenkeuser, H., and von Rad, U., 1998. Correlation between Arabian Sea and Greenland climate oscillations of the past 110,000 years. Nature 393**,** 54-57.

Seltzer, G., Rodbell, D., and Burns, S., 2000. Isotopic evidence for late Quaternary climatic change in tropical South America. Geology 28**,** 35-38.

Severinghaus, J. P., Sowers, T., Brook, E., Alley, R. B., and Bender, M., 1998. Timing of abrupt climate change at the end of the Younger Dryas interval from thermally fractionated gasses in polar ice. Nature 391**,** 141146.

Severinghaus, J. P., and Brook, E. J., 1999. Abrupt climate change at the end of the last glacial period inferred from trapped air in polar ice. Science 286**,** 930-934.

Shakun, J. D., Burns, S. J., Fleitmann, D., Kramers, J., Matter, A., and Al-Subary, A., 2007. A high-resolution, absolute-dated deglacial speleothem record of Indian Ocean climate from Socotra Island, Yemen. Earth and Planetary Science Letters 259**,** 442-456.

Steig, E. J., Morse, D. L., Waddington, E. D., Stuiver, M., Grootes, P. M., Mayewski, P. A., Twickler, M. S., and Whitlow, S. I., 2000. Wisconsinan and Holocene

climate history from an ice core at Taylor Dome, western Ross Embayment, Antarctica. Geografiska Annaler: Series A, Physical Geography 82**,** 213-235.

Steig, E., and White, J., 2003. Taylor Dome ice core data. Boulder, CO: National Snow and Ice Data Center. Digital Media.

Stenni, B., Masson-Delmotte, V., Johnsen, S., Jouzel, J., Longinelli, A., Monnin, E., Rothlisberger, R., and Selmo, E., 2001. An Oceanic cold reversal during the last deglaciation. Science 293**,** 2074-2077.

Stott, L., Timmermann, A., and Thunell, R., 2007. Southern hemisphere and deep-sea warming led deglacial atmospheric CO_2 rise and tropical warming. Science 318**,** 435-438.

Sun, Y., Oppo, D., Xiang, R., Liu, W., and Gao, S., 2005. Last deglaciation in the Okinawa Trough: Subtropical northwest Pacific link to Northern Hemisphere and tropical climate. Paleoceanography 20**,** doi:10.1029/2004PA001061.

Svensson, A., Andersen, K. K., Bigler, M., Clausen, H. B., Dahl-Jensen, D., Davies, S. M., Johnsen, S. J., Muscheler, R., Parrenin, F., Rasmussen, S. O., Röthlisberger, R., Seierstad, I., Steffensen, J. P., and Vinther, B. M., 2008. A 60 000 year Greenland stratigraphic ice core chronology. Climate of the Past 4**,** 47-57.

Thompson, L. G., Mosley-Thompson, E., Davis, M. E., Lin, P.-N., Henderson, K. A., Cole-Dai, J., Bolzan, J. F., and Liu, K.-b., 1995. Late Glacial Stage and Holocene Tropical Ice Core Records from Huascaran, Peru. Science 269**,** 46-50.

Thompson, L. G., Davis, M. E., Mosley-Thompson, E., Sowers, T. A., Henderson, K. A., Zagorodnov, V. S., Lin, P.-N., Mikhalenko, V. N., Campen, R. K., Bolzan, J. F., Cole-Dai, J., and Francou, B., 1998. A 25,000-year tropical climate history from Bolivian ice cores. Science 282**,** 1858-1864.

Thompson, L. G., Mosley-Thompson, E., Davis, M. E., Henderson, K. A., Brecher, H. H., Zagorodnov, V. S., Mashiotta, T. A., Lin, P.-N., Mikhalenko, V. N., Hardy, D. R., and Beer, J., 2002. Kilimanjaro ice core records: Evidence of Holocene climate change in tropical Africa. Science 298**,** 589-593.

Tierney, J. E., and Russell, J. M., 2007. Abrupt climate change in southeast tropical Africa influenced by Indian monsoon variability and ITCZ migration. Geophysical Research Letters 34**,** doi:10.1029/2007GL029508.

Tierney, J. E., Russell, J. M., Huang, Y., Damste, J. S. S., Hopmans, E. C., and Cohen, A. S., 2008. Northern Hemisphere controls on tropical southeast African climate during the past 60,000 years. Science 322**,** 252-255.

Visser, K., Thunell, R., and Stott, L., 2003. Magnitude and timing of temperature change in the Indo-Pacific warm pool during deglaciation. Nature 421**,** 152-155.

von Grafenstein, U., Erlenkeuser, H., Brauer, A., Jouzel, J., and Johnsen, S. J., 1999. A mid-European decadal isotope-climate record from 15,500 to 5000 years B.P. Science 284**,** 1654-1657.

Waelbroeck, C., Levi, C., Duplessy, J. C., Labeyrie, L., Michel, E., Cortijo, E., Bassinot, F., and Guichard, F., 2006. Distant origin of circulation changes in the Indian Ocean during the last deglaciation. Earth and Planetary Science Letters 243**,** 244-251.

Wang, Y. J., Cheng, H., Edwards, R. L., An, Z. S., Wu, J. Y., Shen, C.-C., and Dorale, J. A., 2001. A high-resolution absolute-dated late Pleistocene monsoon record from Hulu Cave, China. Science 294**,** 2345-2348.

Wang, X., Auler, A. S., Edwards, R. L., Cheng, H., Ito, E., Wang, Y., Kong, X., and Solheid, M., 2007. Millennial-scale precipitation changes in southern Brazil over the past 90,000 years. Geophysical Research Letters 34**,** doi:10.1029/2007GL031149.

Weijers, J. W. H., Schefuss, E., Schouten, S., and Damste, J. S. S., 2007. Coupled thermal and hydrological evolution of tropical Africa over the last deglaciation. Science 315**,** 1701-1704.

Weldeab, S., Schneider, R. R., Kölling, M., and Wefer, G., 2005. Holocene African droughts relate to eastern equatorial Atlantic cooling. Geology 33**,** 981-984.

Weldeab, S., Schneider, R. R., and Kölling, M., 2006. Deglacial sea surface temperature and salinity increase in the western tropical Atlantic in synchrony with high latitude climate instabilities. Earth and Planetary Science Letters 241**,** 699-706.

Weldeab, S., Lea, D. W., Schneider, R. R., and Andersen, N., 2007. 155,000 years of West African Monsoon and ocean thermal evolution. Science 316**,** 1303-1307.

Williams, P. W., King, D. N. T., Zhao, J. X., and Collerson, K. D., 2005. Late Pleistocene to Holocene composite speleothem ^{18}O and ^{13}C chronologies from

South Island, New Zealand-did a global Younger Dryas really exist? Earth and Planetary Science Letters 230**,** 301-317.

Yancheva, G., Nowaczyk, N. R., Mingram, J., Dulski, P., Schettler, G., Negendank, J. F. W., Liu, J., Sigman, D. M., Peterson, L. C., and Haug, G. H., 2007. Influence of the intertropical convergence zone on the East Asian monsoon. Nature 445**,** 74-77.

Zhao, M., Beveridge, N., Shackleton, N., Sarnthein, M., and Eglington, G., 1995. Molecular stratigraphy of cores off northwest Africa: Sea surface temperature history over the last 80ka. Paleoceanography 10**,** 661-675.

Appendix C. Deglacial temperature database used in Chapter 4

Table A.C.1

Location	Core	Proxy	Reference	Lat (°)	Lon (°)	Elev/ Depth (m)
GISP2, Greenland	-	ice core $d^{18}O$ and borehole	Alley, 2000	72.6	-38.5	3207
Burial Lake, Alaska	-	chironomids	Kurek et al., 2009	68.4	-159.2	460
Eastern Beringia (A)	-	pollen	Viau et al., 2008	67.5	-165	-
Eastern Beringia (B)	-	pollen	Viau et al., 2008	67.5	-137.5	-
Eastern Beringia (C)	-	pollen	Viau et al., 2008	62.5	-165	-
Eastern Beringia (D)	-	pollen	Viau et al., 2008	62.5	-137.5	-
Northeast Atlantic	NA 87-22	foram assemblages	Waelbroeck et al., 2001	55.5	-14.7	-2161
Northeast Atlantic	MD01-2461	Mg/Ca	Peck et al., 2008	51.8	-12.9	-1153
California margin	W8709A-8	$U^{K'}_{37}$	Prahl et al., 1995	42.5	-127.7	-3111
central North Atlantic	CH 69-09	foram assemblages	Waelbroeck et al., 2001	41.8	-47.4	-4100
Japan margin	PC-6	$U^{K'}_{37}$	Minoshima et al., 2007	40.4	143.5	-2215
Western Mediterranean	M39-008	$U^{K'}_{37}$	Cacho et al., 2001	39.4	-7.1	-576
Western Mediterranean	BS79-38	$U^{K'}_{37}$	Cacho et al., 2001	38.4	13.6	-1489
Iberian margin	MD95-2042	$U^{K'}_{37}$	Bard et al., 2002	37.8	-10.2	-3146
Iberian margin	SU81-18	foram assemblages	Waelbroeck et al., 2001	37.8	-10.2	-3135
North Atlantic	MD95-2037	$U^{K'}_{37}$	Calvo et al., 2001	37.1	-32.0	-2630
Alboran Sea	MD95-2043	$U^{K'}_{37}$	Cacho et al., 1999	36.1	-2.6	-1841
North Pacific	MD01-2421	$U^{K'}_{37}$	Yamamoto et al., 2010	36	141.8	-2224
Bermuda Rise	OCE326-GGC5	Mg/Ca	Carlson et al., 2008	33.7	-57.6	-4550
Japan margin	KT92-17 St. 14	$U^{K'}_{37}$	Sawada and Handa, 1998	32.6	138.6	-3252
Blake outer ridge	KNR140-51GGC	Mg/Ca	Carlson et al., 2008	32.6	-76.3	-1790

Nile Delta	GeoB 7702-3	TEX_{86}	Castañeda et al., 2010	31.7	34.1	-562
East China Sea	MD98-2195	$U^{K'}_{37}$	Ijiri et al., 2005	31.6	129	-746
Gulf of Mexico	MD02-2575	Mg/Ca	Ziegler et al., 2008	29.0	-87.1	-847
Red Sea	GeoB 5844-2	UK'37	Arz et al., 2008	27.7	34.7	-963
Gulf of Mexico	EN32-PC6	Mg/Ca	Flower et al., 2004	27.0	-91.3	-2280
Northwest African margin	ODP 658C	foram assemblages	deMenocal et al., 2000	20.8	-18.6	-2263
Northwest African margin	ODP 658C	$U^{K'}_{37}$	Zhao et al., 1995	20.8	-18.6	-2263
South China Sea	17940	$U^{K'}_{37}$	Pelejero et al., 1999	20.1	117.4	-1968
South China Sea	ODP 1144	Mg/Ca	Wei et al, 2007	20.1	117.6	-2037
Arabian Sea	74KL	$U^{K'}_{37}$	Huguet et al., 2006	14.3	57.3	-3212
Arabian Sea	74KL	TEX_{86}	Huguet et al., 2006	14.3	57.3	-3212
Western tropical North Atlantic	M35003-4	$U^{K'}_{37}$	Rühlemann et al., 1999	12.1	-61.3	-1299
Western Caribbean Sea	VM28-122	Mg/Ca	Schmidt et al., 2004	11.6	-78.4	-3623
Arabian Sea	NIOP-905	$U^{K'}_{37}$	Huguet et al., 2006	10.8	51.9	-1567
Arabian Sea	NIOP-905	TEX_{86}	Huguet et al., 2006	10.8	51.9	-1567
Cariaco Basin, Venezuala	PL07-39PC	Mg/Ca	Lea et al., 2003	10.7	-65.0	-790
Sulu Sea	MD97-2141	Mg/Ca	Rosenthal et al., 2003	8.8	121.3	-3633
Eastern equatorial Pacific	MD02-2529	$U^{K'}_{37}$	Leduc et al., 2007	8.2	-84.1	-1619
Eastern equatorial Pacific	ME0005A-43JC	Mg/Ca	Benway et al., 2006	7.9	-83.6	-1368
South China Sea	MD01-2390	$U^{K'}_{37}$	Steinke et al., 2008	6.6	113.4	-1545
South China Sea	MD01-2390	Mg/Ca	Steinke et al., 2008	6.6	113.4	-1545
West Pacific warm pool	MD98-2181	Mg/Ca	Stott et al., 2007	6.3	125.8	-2114
Gulf of Guinea	MD03-2707	Mg/Ca	Weldeab et al., 2007	2.5	9.4	-1295
Eastern equatorial Atlantic	GeoB 4905	Mg/Ca	Weldeab et al,. 2005	2.5	9.4	-1328
Eastern equatorial Pacific	TR163-22	Mg/Ca	Lea et al., 2006	0.5	-92.4	-2830
Eastern equatorial Pacific	ME0005A-24JC	$U^{K'}_{37}$	Kienast et al., 2006	0.0	-86.5	-2941

Eastern equatorial Pacific	V21-30	$U^{K'}_{37}$	Koutavas and Sachs, 2008	-1.2	-89.7	-617
Eastern equatorial Pacific	V21-30	Mg/Ca	Koutavas et al., 2002	-1.2	-89.7	-617
Eastern equatorial Pacific	V19-28	$U^{K'}_{37}$	Koutavas and Sachs, 2008	-2.4	-84.7	-2720
Brazilian margin	GeoB 3910	$U^{K'}_{37}$	Jaeschke et al., 2007	-4.2	-36.3	-2362
Western tropical Atlantic	GeoB 3129	Mg/Ca	Weldeab et al, 2006	-4.6	-36.6	-830
West Pacific warm pool	MD9821-62	Mg/Ca	Visser et al., 2003	-4.7	117.9	-1855
West Pacific warm pool	MD98-2176	Mg/Ca	Stott et al., 2007	-5.0	133.4	-2382
Gulf of Guinea	GeoB 6518-1	MBT, CBT	Weijers et al., 2007	-5.6	11.2	-962
Gulf of Guinea	GeoB 6518-1	$U^{K'}_{37}$	Schefuß et al., 2005	-5.6	11.2	-962
Lake Tanganyika	NP04-KH3, NP04-KH4	TEX_{86}	Tierney et al., 2008	-6.7	29.6	773
West Pacific warm pool	MD98-2165	Mg/Ca	Levi et al., 2007	-9.7	118.4	-2100
West Pacific warm pool	MD98-2170	Mg/Ca	Stott et al., 2007	-10.6	125.4	-832
Timor Sea, Indian Ocean	MD01-2378	Mg/Ca	Xu et al., 2008	-13.1	121.8	-1783
Southeast Atlantic	GeoB 1023-5	$U^{K'}_{37}$	Kim et al., 2002	-17.2	11.0	-1978
Indian Ocean	MD79257	$U^{K'}_{37}$	Bard et al., 1997	-20.4	36.3	-1260
Subtropical southeast Atlantic	ODP 1084B	Mg/Ca	Farmer et al., 2005	-25.5	13.0	-1992
Brazilian margin	KNR159-5-36GGC	Mg/Ca	Carlson et al., 2008	-27.5	-46.5	-1268
Chilean margin	GeoB 7139-2	$U^{K'}_{37}$	Kaiser et al., 2008	-30.2	-72.0	-3270
South Australia	MD03-2611	$U^{K'}_{37}$	Calvo et al., 2007	-36.7	136.7	-2420
New Zealand	MD97-2121	$U^{K'}_{37}$	Pahnke and Sachs, 2006	-40.4	178.0	-3014
Chilean margin	ODP 1233	$U^{K'}_{37}$	Lamy et al., 2007	-41.0	-74.5	-838
Southeast Atlantic	TN057-21-PC2	$U^{K'}_{37}$	Sachs et al., 2001	-41.1	7.8	-4981
Southeast Atlantic	TN057-21	Mg/Ca	Barker et al., 2009	-41.1	7.8	-4981
New Zealand	SO136-GC11	$U^{K'}_{37}$	Barrows et al., 2007	-43.5	167.9	-1556
New Zealand	MD97-2120	$U^{K'}_{37}$	Pahnke and Sachs, 2006	-45.5	174.9	-1210
Southern Ocean	MD88-770	foram assemblages	Labeyrie et al., 1996	-46.0	96.5	-3290

EDML	-	ice core $d^{18}O$	Stenni et al., 2010	-75	0	2892
Dome C, Antarctica	-	ice core $d^{18}O$	Jouzel et al., 2007	-75.1	123.4	3240
Dome Fuji, Antarctica	-	ice core $d^{18}O$, dD	Kawamura et al., 2007	-77.3	39.7	3810
Vostok, Antarctica	-	ice core dD	Petit et al., 1999	-78.5	108.0	3500

A.C References

Alley, R. B., 2000. The Younger Dryas cold interval as viewed from central Greenland. Quaternary Science Reviews 19**,** 213-226.

Arz, H. W., Pätzold, J., Müller, P. J., and Moammar, M. O. 2003. Influence of Northern Hemisphere climate and global sea level rise on the restricted Red Sea marine environment during termination I, Paleoceanography, 18, 1053, doi:10.1029/2002PA000864

Bard, E., Rostek, F., and Sonzogni, C., 1997. Interhemispheric synchrony of the last deglaciation inferred from alkenone palaeothermometry. Nature 385**,** 707-710.

Bard, E., 2002. Climate shock: Abrupt changes over millennial time scales. Physics Today 55**,** 32-38.

Barker, S., Diz, P., Vautravers, M. J., Pike, J., Knorr, G., Hall, I. R., and Broecker, W. S. 2009. Interhemispheric Atlantic seesaw response during the last deglaciation. Nature, 457, 1097-1102.

Barrows, T. T., Lehman, S. J., Fifield, L. K., and De Deckker, P., 2007. Absence of cooling in New Zealand and the adjacent Ocean during the Younger Dryas chronozone. Science 318**,** 86-89.

Benway, H. M., Mix, A. C., Haley, B. A., and Klinkhammer, G. P., 2006. Eastern Pacific warm pool paleosalinity and climate variability: 0-30 kyr. Paleoceanography 21**,** doi:10.1029/2005PA001208.

Cacho, I., Grimalt, J. O., Pelejero, C., Canals, M., Sierro, F. J., Flores, J. A., and Shackelton, N. J., 1999. Dansgaard-Oeschger and Heinrich Event imprints in Alboran Sea paleotemperatures. Paleoceanography 14**,** 698-705.

Cacho, I., Grimalt, J. O., Canals, M., Sbaffi, L., and Shackelton, N. J., 2001. Variability of the western Mediterranean Sea surface temperature during the last 25,000 years and its connection with the Northern Hemisphere climatic changes. Paleoceanography 16**,** 40-52.

Calvo, E. Villanueva, J., Grimalt, J. O., Boelaert, A., and Labeyrie, L. 2001. New insights into the glacial latitudinal temperature gradients in the North Atlantic. Results from $U^{K'}_{37}$ sea surface temperatures and terrigenous inputs. Earth and Planetary Science Letters. 188, 509–519.

Calvo, E., Pelejero, C., DeDeckker, P., and Logan, G. A. 2007. Antarctic deglacial pattern in a 30 kyr record of sea surface temperature offshore South Australia. Geophysical Research Letters, 34, L13707, doi:10.1029/2007GL029937.

Carlson, A. E., Oppo, D., Came, R. E., LeGrande, A. N., Keigwin, L., and Curry, W. B., 2008. Subtropical salinity variability and Atlantic meridional circulation during deglaciation. Geology 12, 991-994.

Castañeda, I.S., Schefub, E., Pätzold, J., Sinninghe Damsté, J.S., Weldeab, S., and Schouten, S. 2010. Millennial-scale surface temperature changes in the eastern Mediterranean (Nile River Delta region) over the last 27,000 years. Paleoceanography, 25, PA1208, doi:10.1029/2009PA001740.

deMenocal, P. B., Ortiz, J., Guilderson, T., and Sarnthein, M., 2000. Coherent high- and low-latitude climate variability during the Holocene warm period. Science 288**,** 2198-2202.

Farmer, E. C., DeMendocal, P. B., and Marchitto, T. M., 2005. Holocene and deglacial ocean temperature variability in the Benguela upwelling region: Implications for low-latitude atmospheric circulation. Paleoceanography 20**,** doi:10.1029/2004PA001049.

Flower, B. P., Hastings, D. W., Hill, H. W., and Quinn, T. M., 2004. Phasing of deglacial warming and Laurentide Ice Sheet meltwater in the Gulf of Mexico. Geology 32**,** 597-600.

Huguet, C., J.-H. Kim, J. S. S. Damste´, and S. Schouten. 2006. Reconstruction of sea surface temperature variations in the Arabian Sea over the last 23 kyr using organic proxies (TEX_{86} and $U^{K'}_{37}$). Paleoceanography, 21, PA3003, doi:10.1029/2005PA001215.

Ijiri, A., Wang, L., Oba, T., Kawahata, H., Huang, C.-Y., and Huang, C.-Y. 2005. Paleoenvironmental changes in the northern area of the East China Sea during the past 42,000 years. Palaeogeography, Palaeoclimatology, Palaeoecology, 219, 239-261.

Jaeschke, A., Rühlemann, C., Arz, H. W., Heil, G., and Lohmann, G. 2007. Coupling of millennial-scale changes in sea surface temperature and precipitation off northeastern Brazil with high-latitude climate shifts during the last glacial period. Paleoceanography, 22, PA4206, doi:10.1029/2006PA001391.

Jouzel, J., Masson-Delmotte, V., Cattani, O., Dreyfus, G., Falourd, S., Hoffmann, G., Minster, B., Nouet, J., Barnola, J. M., Chappellaz, J., Fischer, H., Gallet, J. C.,

Johnsen, S., Leuenberger, M., Loulergue, L., Luethi, D., Oerter, H., Parrenin, F., Raisbeck, G., Raynaud, D., Schilt, A., Schwander, J., Selmo, E., Souchez, R., Spahni, R., Stauffer, B., Steffensen, J.P., Stenni, B., Stocker, T. F., Tison, J. L., Werner, M., and Wolff, E. W. 2007. Orbital and millennial Antarctic climate variability over the past 800,000 Years. Science, 317, 793-796.

Kaiser, J., Lamy, F., and Hebbeln, D., 2005. A 70-kyr sea surface temperature record off southern Chile (Ocean Drilling Program Site 1233). Paleoceanography 20**,** doi:10.1029/2005PA001146.

Kawamura, K., Parrenin, F., Lisiecki, L., Uemura, R., Vimeux, F., Severinghaus, J. P., Hutterli, M. A., Nakazawa, T., Aoki, S., Jouzel, J., Raymo, M. E., Matsumoto, K., Nakata, H., Motoyama, H., Fujita, S., Goto-Azuma, K., Fujii, Y., and Watanabe, O., 2007. Northern Hemisphere forcing of climatic cycles in Antarctica over the past 360,000 years. Nature 448**,** 912-916.

Kienast, M., Kienast, S. S., Calvert, S. E., Eglinton, T. I., Mollenhauer, G., Francois, R., and Mix, A. C., 2006. Eastern Pacific cooling and Atlantic overturning circulation during the last deglaciation. Nature 443**,** 846-849.

Kim, J.-H., Schneider, R. R., Muller, P. J., and Wefer, G., 2002. Interhemispheric comparison of deglacial sea-surface temperature patterns in Atlantic eastern boundary currents. Earth and Planetary Science Letters 194**,** 383-393.

Koutavas, A., Lynch-Stieglitz, J., Marchitto, T. M., Jr., and Sachs, J. M., 2002. El Niño-like pattern in Ice Age tropical Pacific sea surface temperature. Science 297**,** 226-230.

Koutavas, A., and Sachs, J. P. 2008. Northern timing of deglaciation in the eastern equatorial Pacific from alkenone paleothermometry. Paleoceanography, 23, PA4205, doi:10.1029/2008PA001593.

Kurek, J., Cwynar, L. C., Ager, T. A., Abbott, M. B., and Edwards, M. E. 2009. Late Quaternary paleoclimate of western Alaska inferred from fossil chironomids and its relation to vegetation histories. Quaternary Science Reviews, 28, 799-811.

Labeyrie, L., Labracherie, M., Gorfti, N., Pichon, J. J., Vautravers, M., Arnold, M., Duplessy, J.-C., Paterne, M., Michel, E., Duprat, J., Caralp, M., and Turon, J.-L. 1996. Hydrographic changes of the Southern Ocean (southeast Indian sector) over the last 230 kyr. Paleoceanography, 11, 57-76.

Lamy, F., Kaiser, J., Arz, H. W., Hebbeln, D., Ninnemann, U., Timm, O., Timmermann, A., and Toggweiler, J. R., 2007. Modulation of the bipolar

seesaw in the Southeast Pacific during Termination 1. Earth and Planetary Science Letters 259**,** 400-413.

Lea, D. W., Pak, D. K., Peterson, L. C., and Hughen, K. A., 2003. Synchroneity of tropical and high-latitude Atlantic temperatures over the last glacial termination. Science 301**,** 1361-1364.

Lea, D. W., Pak, D. K., Belanger, C. L., Spero, H. J., Hall, M. A., and Shackleton, N. J., 2006. Paleoclimate history of Galápagos surface waters over the last 135,000 yr. Quaternary Science Reviews 25**,** 1152-1167.

Leduc, G., Vidal, L., Tachikawa, K., Rostek, F., Sonzogni, C., Beaufort, L., and Bard, E. 2007. Moisture transport across Central America as a positive feedback on abrupt climatic changes. Nature, 445, 908-911.

Levi, C., Labeyrie, L., Bassinot, F. C., Guichard, F., Cortijo, E., Waelbroeck, C., Caillon, N., Duprat, J., Garidel-Thoron, T., and Elderfield, H., 2007. Low-latitude hydrological cycle and rapid climate changes during the last deglaciation. Geochemistry, Geophysics, Geosystems 8**,** doi:10.1029/2006GC001514.

Minoshima, K, Kawahata, H., and Ikehara, K. 2007. Changes in biological production in the mixed water region of the northwestern North Pacific during the last 27 kyr. Palaeogeography, Palaeoclimatology, Palaeoecology, 254, 430-447.

Pahnke, K., and Sachs, J. M., 2006. Sea surface temperatures of southern midlatitudes 0–160 kyr B.P. Paleoceanography 21**,** doi:10.1029/2005PA001191.

Peck, V. L., Hall, I. R., Zahn, R., and Elderfield, H., 2008. Millennial-scale surface and subsurface paleothermometry from the northeast Atlantic, 55-8 ka BP. Paleoceanography 23, doi:10.1029/2008PA001631.

Pelejero, C., Grimalt, J. O., Heilig, S., Kienast, M., and Wang, L., 1999. High-resolution U^{k}_{37} temperature reconstructions in the South China Sea over th past 220 kyr. Paleoceanography 14**,** 224-231.

Petit, J. R., Jouzel, J., Raynaud, D., Barkov, N. I., Barnola, J.-M., Basile, I., Bender, M., Chappellaz, J., Davis, M., Delaygue, G., Delmotte, M., Kotlyakov, V. M., Legrand, M., Lipenkov, V. Y., Lorius, C., Pepin, L., Ritz, C., Saltzman, E., and Stievenard, M., 1999. Climate and atmospheric history of the past 420,000 years from the Vostok ice core, Antarctic. Nature 399**,** 429-436.

Prahl, F.G., Pisias, N. G., Sparrow, M. A., and Sabin, A. 1995. Assessment of sea-surface temperature at 42 degrees north in the California current over the last 30,000 years. Paleoceanography, 10, 763-773.

Rosenthal, Y., Oppo, D., and Linsley, B. K., 2003. The amplitude and phasing of climate change during the last deglaciation in the Sulu Sea, western equatorial Pacific. Geophysical Research Letters 30**,** doi:10.1029/2002GL016612.

Rühlemann, C., Mulitza, S., Muller, P. J., Wefer, G., and Zahn, R., 1999. Warming of the tropical Atlantic Ocean and slowdown of thermohaline circulation during the last deglaciation. Nature 402**,** 511-514.

Sachs, J. P., Anderson, R. F., and Lehman, S. J., 2001. Glacial surface temperatures of the southeast Atlantic Ocean. Science 293**,** 2077-2079.

Sagawa, T., Toyoda, K. and Oba, T. 2005. Sea surface temperature record off central Japan since the Last Glacial Maximum using planktonic foraminiferal Mg/Ca thermometry. Journal of Quaternary Science, 21, 63–73.

Schefuß, E., Schouten, S., and Schneider, R. R., 2005. Climatic controls on central African hydrology during the past 20,000 years. Nature 437**,** 1003-1006.

Schmidt, M. W., Spero, H. J., and Lea, D. W., 2004. Links between salinity variation in the Caribbean and North Atlantic thermohaline circulation. Nature 428**,** 160-163.

Steinke, S., Kienast, M., Groeneveld, J., Lin, L.-C., Chen, M.-T., and Rendle-Bühring, R. 2008. Proxy dependence of the temporal pattern of deglacial warming in the tropical South China Sea: toward resolving seasonality. Quaternary Science Reviews, 27, 688-700.

Stenni, B., Masson-Delmotte, V., Selmo, E., Oerter, H., Meyer, H., Röthlisberger, R., Jouzel, J., Cattani, O., Falourd, S., Fischer, H., Hoffmann, G., Iacumin, P., Johnsen, S. J., Minster, B., and Udisti, R. 2010. The deuterium excess records of EPICA Dome C and Dronning Maud Land ice cores (East Antarctica). Quaternary Science Reviews, 29, 146-159.

Stott, L., Timmermann, A., and Thunell, R., 2007. Southern hemisphere and deep-sea warming led deglacial atmospheric CO_2 rise and tropical warming. Science 318**,** 435-438.

Tierney, J. E., Russell, J. M., Huang, Y., Damste, J. S. S., Hopmans, E. C., and Cohen, A. S., 2008. Northern Hemisphere controls on tropical southeast African climate during the past 60,000 years. Science 322**,** 252-255.

Viau, A.E., Gajewski, K., Sawada, M. C., and Bunbury, J. 2008. Low-and high frequency climate variability in Eastern Beringia during the past 25,000 years. Canadian Journal of Earth Sciences, 45, 1435-1453.

Visser, K., Thunell, R., and Stott, L., 2003. Magnitude and timing of temperature change in the Indo-Pacific warm pool during deglaciation. Nature 421**,** 152-155.

Waelbroeck, C., Duplessy, J.-C., Michel, E., Labeyrie, L., Paillard, D., and Duprat, J. 2001. The timing of the last deglaciation in North Atlantic climate records. Nature, 412, 724-727.

Wei, G., Deng, W., Liu, Y., Li, X. 2007. High-resolution sea surface temperature records derived from foraminiferal Mg/Ca ratios during the last 260 ka in the northern South China Sea. Palaeogeography, Palaeoclimatology, Palaeoecology, 250, 126-138.

Weijers, J. W. H., Schefuss, E., Schouten, S., and Damste, J. S. S., 2007. Coupled thermal and hydrological evolution of tropical Africa over the last deglaciation. Science 315**,** 1701-1704.

Weldeab, S., Schneider, R. R., Kölling, M., and Wefer, G., 2005. Holocene African droughts relate to eastern equatorial Atlantic cooling. Geology 33**,** 981-984.

Weldeab, S., Schneider, R. R., and Kölling, M., 2006. Deglacial sea surface temperature and salinity increase in the western tropical Atlantic in synchrony with high latitude climate instabilities. Earth and Planetary Science Letters 241**,** 699-706.

Weldeab, S., Lea, D. W., Schneider, R. R., and Andersen, N., 2007. 155,000 years of West African Monsoon and ocean thermal evolution. Science 316**,** 1303-1307.

Xu, J., Holbourn, A., Kuhnt, W., Jian, Z., and Kawamura, H. 2008. Changes in the thermocline structure of the Indonesian outflow during Terminations 1 and 2. Earth and Planetary Science Letters, 273, 152-162.

Yamamoto, M., Suemune, R., and Oba, T. 2005. Equatorward shift of the subarctic boundary in the northwestern Pacific during the last deglaciation. Geophysical Research Letters, 32, L05609, doi:10.1029/2004GL021903.

Zhao, M., Beveridge, N., Shackleton, N., Sarnthein, M., and Eglington, G., 1995. Molecular stratigraphy of cores off northwest Africa: Sea surface temperature history over the last 80ka. Paleoceanography 10**,** 661-675.

Ziegler, M., Nürnberg, D., Karas, C., Tiedemann, R., Lourens, L. J. 2008. Persistent summer expansion of the Atlantic Warm Pool during glacial abrupt cold events. Nature Geoscience, 1, 601-605